The key parameters influencing the reactivity of magnesium silicate based catalysts : application to transesterification in liquid phase

Longfei Lin

Université Pierre et Marie Curie

Physico-chimie des matériaux

Laboratoire de Réactivité de Surface

The key parameters influencing the reactivity of magnesium silicate based catalysts: application to transesterification in liquid phase

Longfei Lin

PhD thesis of Chemistry

Directed by Hélène Lauron-Pernot and in collaboration with Guillaume Laugel

Présentée et soutenue publiquement le 27 septembre 2017

Devant un jury composé de:

M. Yannick Pouilloux, Professeur (Université de Poitiers)	Rapporteur
M. Jérôme Labille, Chargé de Recherche (CEREGE, Aix-en-Provences)	Rapporteur
Mme Sophie Cassaignon, Professeure (UPMC)	Examinatrice
Mme Barbara Lothenbach, Ingénieure de Recherche (EMPA, Dübendorf)	Examinatrice
Mme Claire Courson, Maître de conférences (Université de Strasbourg)	Examinatrice
Mme Maguy Jaber, Professeure (UPMC)	Examinatrice
M. Guillaume Laugel, Maître de conférences (UPMC)	Examinateur
Mme Hélène Lauron-Pernot, Professeure (UPMC)	Directrice de thèse

Titre: les paramètres clés influençant la réactivité de catalyseurs à base de silicate de magnésium: application à la transesterification en phase liquide

Résumé:

Dans le domaine de la valorisation des dérivés de la biomasse, les réactions de transestérification suscitent un grand intérêt en raison de leur importance pour transformer des molécules plateformes biobasées. L'étude des paramètres clés régissant une réaction de transestérification modèle, catalysée par des solides de type silicate de magnésium, a été menée. L'ensemble des données expérimentales (XRD, XPS, DRIFTS, RMN) a démontré qu'une phase de silicate de magnésium hydraté (MSH) est présente à la surface des catalyseurs les plus actifs. Cette phase, possédant une structure proche de celle d'une argile mais avec des défauts et présentant des propriétés acido-basiques spécifiques, est capable d'activer à la fois l'alcool (sur des sites basiques) et l'ester (sur des sites acides). Ce résultat est confirmé par l'étude cinétique qui met en évidence un mécanisme Langmuir-Hinshelwood. En outre, il a été montré que l'eau coordonnée au magnésium situé sur le bord des feuillets des particules ou dans les défauts présents à la surface des silicates engendre des sites acides particuliers.

Par ailleurs, une série de phyllosilicates de magnésium, a été testée dans la réaction de transestérification modèle. Le rôle de la taille des particules a été mis en évidence et les meilleurs résultats catalytiques ont été obtenus avec le talc et la laponite possédant des tailles de feuillet nanométriques. De plus, l'étude cinétique indique que la réaction de transestérification catalysée par la laponite, n'ayant seulement que des sites basiques, implique un mécanisme Eley-Rideal. Enfin, dans le cas de la laponite la dissociation de l'eau sur les sites basiques empoissonne la réaction.

Mots-clés : transestérification ; silicate de magnésium hydraté ; adsorption d'eau ; phyllosilicates ; nanoparticules ; mécanisme réactionnel

---

Title: the key parameters influencing the reactivity of magnesium silicate based catalysts: application to transesterification in liquid phase

Abstract:

In the field of biomass derivatives valorisation, transesterification reactions have attracted numerous interest due to its importance to transform platform molecules. A study of the parameters governing the reactivity of magnesium silicate based catalyst in a model transesterification reaction was thoroughly undertaken. The set of experimental data (XRD, XPS, DRIFTS, NMR) demonstrated that a magnesium silicate hydrate (MSH) phase is formed at the surface of the most active silicates. It is thus concluded that this active phase, presented a clay-like structure with defects and specific acido-basic properties, is able to activate together the alcohol (over base sites) and the ester (over acid sites). This result fits with the kinetic study that implies the Langmuir-Hinshelwood mechanism. Moreover, the acid sites were revealed that are created from the water coordinated to magnesium located on the edge of the clay-like particles or in the defects present in the silicate layer.

Besides, a series of phyllosilicates having the similar structure with MSH, were tested in the model transesterification reaction. The influence of the particles size was investigated and the best catalytic performances were obtained with talc and laponite with nanosheets. In addition, kinetic study indicates that the transesterification reaction on the laponite, with purely basic sites, undergoes Eley-Rideal mechanism. Finally, unlike the positive role of water on the formation of acid sites in MSH, on laponite, the dissociation of the water on basic sites poisons the reaction.

Keywords: transesterification; magnesium silicate hydrate; water adsorption; phyllosilicates; nanoparticles; reaction mechanism

Acknowledgements

This thesis was carried out at the Laboratoire de Réactivité de Surface (UMR 7197) of Université Pierre et Marie Curie (UPMC). I wish to express my sincere appreciation to those who have contributed to this thesis and supported me during this amazing PhD journey.

First of all, I am extremely grateful to my PhD supervisor at the UPMC, Prof. Hélène Lauron-Pernot, who introduced me to the field of transesterification reaction and gave me constant directions. I have appreciated so much that she gave me the opportunity to carry out my doctoral research in her laboratory. I was enlightened significantly by her wide knowledge, invaluable guidance, and useful discussions. Her deep insights helped me in various aspects during my PhD study. I have obtained invaluable comprehension and suggestions, and gained experience from her. Her enthusiasm and passion for research has made a deep impression on me. She is always so kind and very considerate of her students. She treats my future career as very important, and always does her best to provide assistance with this. I feel so lucky that I could spent the most important three years in my career with her.

I am also deeply grateful to Dr. Guillaume Laugel, who is my co-supervisor at the UPMC. I have greatly benefited from his wide knowledge and logical way of thinking. I appreciate so much the frequent discussions with him and also the significant technical support in experiments, which has greatly advanced the progress of my research. He is always so helpful, as I do not speak French, he kindly helped me to solve the problems in both research and life. He encouraged me and gave me beneficial advice when I failed in the experiments. He carefully read and corrected this thesis letter by letter. He is so generous that, when I made a mistake, he always consoled me and make me feel at ease.

My sincere thanks also goes to my Master supervisor, Prof. Yueming Liu, at the East China Normal University. I appreciate that he supported my idea to come to Paris to start my PhD study. Although I conducted my PhD in France, I should emphasize that I have learned and been trained systematically under his supervision during my master's three years, which is greatly helpful to both my PhD and future research.

The research described in this thesis could not be accomplished without a lot of people's help. I would like to thank Maguy Jaber for synthesis of phyllosilicates and her guidance on the relevant subject, Anne-Félicie Lamic-Humblot for her guidance and discussion on kinetic

study, Jean-Marc Krafft for the experiments of infrared spectroscopy, Yannick Millot and Virginie Herledan for Nuclear Magnetic Resonance (NMR) analysis, Sandra Casale for her contribution to Scanning Electron Microscopy (SEM) characterization, Christophe Calers for the X-ray Photoelectron Spectroscopy (XPS) analyses, Juliette Blanchard for the X-ray Diffraction (XRD) support, Xavier Carrier for the experiment of Thermo Gravimetric Analysis (TGA), Cyril Domingos for the N_2 sorption experiments, Damien Cornu for the scientific discussions on the subject, Maya Daou, Yohan Clement and Souleimene Ayad for the contribution to some catalytic tests, Sabine Même and Annie Mettendorff for the administrative affairs of the lab.

I would like to express my sincere gratitude to my PhD committee members Prof. Yannick Pouilloux, Prof. Jérôme Labille, Prof. Sophie Cassaignon, Dr. Barbara Lothenbach, Dr. Claire Courson, and Prof. Maguy Jaber for their their willingness to read and judge this thesis.

I would like to express my gratitude to Prof. Jacques Védrine, who forwarded my PhD application to my present supervisor Prof. Hélène Lauron-Pernot, so that I could have the chance to study in this lab. I would like to also thank my friend Dawei Zhang, who gave me numerous help for my PhD as well as postdoctoral application.

I would also like to acknowledge grants from the *China Scholarship Council* with the financial support, I could not only complete my PhD research, but also enjoy my life. Besides China and France, I have travelled to many cities and countries, such as Germany, Belgium, Luxembourg, Netherlands, Hungary, and Czech Republic which has greatly broadened my horizon and become the wealth of my life.

My time in Paris was enjoyable in large part due to the many friends and group members that took part in my life. I am grateful for the time spent with all of them, they are from all over the world, Romain, Zhao, Maya, Xiaojing, Sarah, Lu, Miao, Priyanka, Tiago, Yuiry, Diaa, Jane, Cédric, Kim, and all the members of the Laboratory. I cherish all the wonderful moments that we spent together.

Lastly, I would like to thank my family for all their love and encouragement. I have obtained constant unconditional support from my parents, my older sister and my girl friend – both emotionally and financially. Thank you!

Table of Contents

General introduction

The rapid depletion of fossil fuel reserves, the emissions of greenhouse gases and associated climate changes are driving human to exploit the alternative and sustainable sources derived from renewable feedstocks. Biomass, which is produced by micro-organisms, plants and animals, is a source of organic matter that should make it possible to no longer use fossil carbon reserves for the production of molecules of economic interest.

In order to obtain molecules from biomass, it is necessary to be able to transform easily accessible platform molecules into valuable ones by an efficient, economical and environmentally friendly way. The composition of the platform molecules obtain from biomass are mainly oxygenated molecules with alcohols, aldehydes, ketones, esters, etc[1]. Among the reactions used in the field of biomass derivatives, the transesterification reaction has been found a widely range of application both in liquid and gas phases. For example, in liquid phase, triglycerides may be transesterified to methyl esters, which may be used in addition to or in replacement of diesel[2]. In gas phase, γ-valerolactone can be converted to methyl-3-pentenoate, which could be further transformed to nylon monomers[3].

Homogeneous catalysts, such as sodium and potassium hydroxides, could achieve a high yield for the transesterification of ester[4]. However, the high cost for the purification of products make heterogeneous catalysts more attractive[5]. Basic solids have gained more attention than acidic materials due to their higher activity[6]. Catalysts with strong basic properties, such as calcium and magnesium oxides[7], zeolites[8] were reported to catalyse transesterification reactions. However, some other solids with weaker surface basicity such as Li_4SiO_4 were found to be as active as of strong base catalysts such as CaO[9]. In our lab, Damien Cornu during his PhD thesis[10] also found that magnesium silicate has higher activity even though lower basicity than MgO. Chapter 1 will illustrate the diversity of applications and catalysts associated with this reaction.

Despite the interest of solid base in this kind of reaction, the link between activity and acido-basic properties is not established and the nature of the active sites as well as the mechanism is scarcely studied. In order to develop our understanding of the relationship between acido-basic properties and reactivity for transesterification, we choose to work on a

model reaction: the conversion of ethyl acetate by methanol and to try to find the parameters that may govern magnesium silicate activity.

In chapter 2, we will study the active phase and the acido-basic properties to explain the good catalytic performance of commercial and coprecipitated magnesium silicate. Moreover, kinetic and deep characterization of the catalyst strucutre will be studied for the transesterification reaction on magnesium silicates.

Moreover, it has been established that the adsorbed water or carbonates can modify the surface properties of MgO thus influence its reactivity[11]. It is well-known that water inhibits base-catalysed transesterification reactions since it competes with the alcohol (reactant), thus lowering the conversion[7]. Nevertheless, in some case, such as CaO[12] and hydrotalcites[13], water plays a positive role on the reactivity. Chapter 3 will aim to study the role of adsorbed water on the catalytic behaviour of a commercial magnesium silicate in transesterification reaction. A link between the yield obtained in catalysis and surface properties involving adsorbed water of magnesium silicate will be developed.

Finally, chapter 4 will extend to the study of phyllosilicates which are another kind of magnesium silicate and will be devoted to study the role of edges of phyllosilicate particles on the reactivity for transesterification reaction. In addition, the reaction mechanism and the role of thermal treatment will be studied as well to compare to the results on commercial magnesium silicate.

References

[1] M. J. Climent, A. Corma, S. Iborra, *Green Chem.* **2014**, *16*, 516.

[2] G. Busca, *Chem. Rev.* **2010**, *110*, 2217–2249.

[3] P. Meessen, D. Vogt, W. Keim, *J. Organomet. Chem.* **1998**, *551*, 165–170.

[4] G. Vicente, M. Martínez, J. Aracil, *Bioresour. Technol.* **2004**, *92*, 297–305.

[5] M. Di Serio, R. Tesser, L. Pengmei, E. Santacesaria, *Energy Fuels* **2008**, *22*, 207–217.

[6] D.-W. Lee, Y.-M. Park, K.-Y. Lee, *Catal. Surv. Asia* **2009**, *13*, 63–77.

[7] D. Cornu, H. Guesmi, G. Laugel, J.-M. Krafft, H. Lauron-Pernot, *Phys Chem Chem Phys* **2015**, *17*, 14168–14176.

[8] G. Suppes, *Appl. Catal. Gen.* **2004**, *257*, 213–223.

[9] J.-X. Wang, K.-T. Chen, J.-S. Wu, P.-H. Wang, S.-T. Huang, C.-C. Chen, *Fuel Process. Technol.* **2012**, *104*, 167–173.

[10] D. Cornu, Study of the Parameters Governing the Reactivity of Weak Inorganic Bases. Towards the Transesterification Reaction., Universite Pierre et Marie Curie, **2012**.

[11] D. Cornu, H. Petitjean, G. Costentin, H. Guesmi, J.-M. Krafft, H. Lauron-Pernot, *Phys. Chem. Chem. Phys.* **2013**, *15*, 19870.

[12] M. Zabeti, W. M. A. Wan Daud, M. K. Aroua, *Fuel Process. Technol.* **2009**, *90*, 770–777.

[13] Y. Xi, R. Davis, *J. Catal.* **2008**, *254*, 190–197.

Chapter 1. Transesterification reactions

Transesterification is the process of interchange of the alkoxyl moiety between an ester and an alcohol (Figure 1.1)[1]. Another term for this reaction is alcoholysis, as the original ester is reacted with an alcohol[2]. In this thesis, we will use the term transesterification as synonymous for alcoholysis, in accordance with most of the publications in this field. Transesterification is a reversible reaction, however, the use of catalysts (typically acid or base catalysts) can accelerate the rate of the transformation to achieve equilibrium.

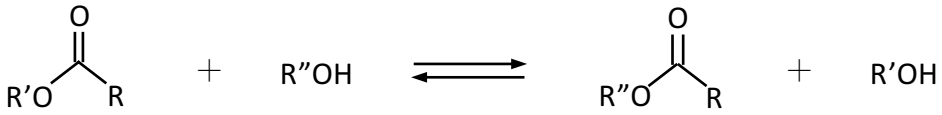

Figure 1.1: Transesterification of ester with alcohol.
R' and R'' are alkyl groups.

1.1. Application of transesterification

Transesterification reactions have found widely applications both in liquid for producing biodiesel, lubricant and poly(ethylene terephthalate) (PET), and in gas phase for producing precursor of one of the monomers of nylon 6-6 and organic carbonates.

1.1.1. Application of transesterification in liquid phase

1.1.1.1. Synthesis of biodiesel

Biodiesel is one of the main biofuels used as an alternative to fossil sources. It can be used in existing diesel engines with little to no modifications at all. As it is made from animal fats or vegetable oils, it is a renewable energy source and can be produced on demand. In addition, biodiesel provides significantly reduced emissions of carbon monoxide, particulate matter, unburned hydrocarbons, and sulfates compared to petroleum diesel fuel. As it is a renewable resource, life cycle leads to release less greenhouse gases like carbon dioxide than petroleum diesel[3].

Because of current world energy crisis and increasing environmental concerns over global climate change, the production of biodiesel has attracted a great deal of interest[4–6]. It is

mainly produced through the transesterification of oils and fats (triglyceride) with methanol (Figure 1.2)[7]. This process makes it possible to reduce the viscosity of the oils and thus to produce biodiesel that can be used in conventional diesel engines. Numerous processes are used industrially to carry out this transesterification reaction by homogeneous catalysts, such as sodium hydroxide or sodium methoxide[8,9].

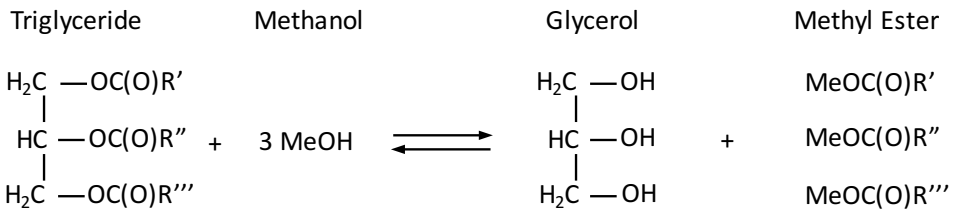

Figure 1.2: Transesterification of triglyceride with methanol.
MeOH is methanol; R', R'' and R''' are alkyl groups.

Contrary to what is required when using homogeneous catalysts, methods employing heterogeneous catalysts enable to dispense with the steps of purification and to reduce waste by catalyst recycling. This process therefore seems more promising. A pilot unit for the production of biodiesel by heterogeneous catalysis was opened in 2004 by IFP-Energies Nouvelles, using a zinc aluminate[10]. This unit currently produces 160,000 tonnes of biodiesel per year. However, biodiesel derived from edible oil has competition with food. Therefore, some inedible feedstocks such as low-grade virgin plant oils are used to produce biodiesel[11].

1.1.1.2. Synthesis of lubricants

Most of the lubricants used industrially are produced from mineral oils. Esters with sufficient molecular weight are environmental friendly substitutes of lubricants from mineral oils. Gryglewicz et al.[12] proposed the transesterification of an inexpensive ester, dimethyl adipate, with relatively heavy alcohols to produce di(2-ethylhexyl)adipate or even an oligomeric ester of neopentyl glycol whose viscosity properties and pour points make them suitable for using as lubricants. The catalysts used for this reaction are magnesium methoxide, calcium oxide, calcium alkoxides and barium hydroxide.

Glycerol, a by-product of the production of biodiesel, is a molecule produced in large quantities that can be transformed, using basic catalysis, into various molecules of economic interest[13]. For example, transesterification of glycerol with methyl esters can generate

monoglycerides and diglycerides, which can also be used as lubricants[14,15]. Basic catalysts such as lanthanum oxide, magnesium oxide[14] and guanidine derivatives[15], present good catalytic performances in this reaction. Magnesium-containing mesoporous silicas, classified as weak bases, can be used, and have significant monoglyceride selectivity due to the effect of confinements[16].

1.1.1.3. Synthesis of poly(ethylene terephthalate)

Poly(ethylene terephthalate) (PET) is an important polymer to make bottles of soft drinks or fibers for the manufacture of textiles. Two processes are commonly employed to produce this polymer: esterification of terephthalic acid with ethylene glycol followed by polycondensation, as well as transesterification of dimethyl terephthalate with ethylene glycol followed by the polycondensation of the transesterification products, bishydroxyl ethylene terephthalate and its oligomers[17]. The by-products of the reactions are methanol in the transesterification of dimethyl terephthalate and water in the case of esterification of terephthalic acid. These by-products must be removed as the reaction proceeds to shift the equilibrium in the direction of polymer formation. Methanol is more volatile, so it can be more easily removed, which is in favor of the process of transesterification.

For the moment, antimony oxide is used as catalyst in most PET plants[17]. Studies are currently being conducted to replace this oxide, as it is toxic when released from the polymer matrix. Furthermore, in view of the recycling of the polymer, preserving the catalyst in the material can improve the possibilities for the depolymerization reaction, inverse transesterification always taking place on the same catalyst. In this context, new catalysts for heterogeneous processes have been proposed: magnesium hydroxysilicates[18] and hydrotalcites[19].

1.1.2. Application of transesterification in gas phase

1.1.2.1. Ring opening of γ-valerolactone

γ-valerolactone (GVL), a sustainable platform molecule derived from lignocellulosic biomass, can be used as[20]: (1) precursor of gasoline and diesel fuels, such as C_8 alkanes, C_9-C_{18} alkanes, and valeric esters; (2) green solvents in fine chemicals synthesis and food additives; (3) as an intermediate in the synthesis of a number of value-added chemicals such as 1,4-pentanediol and methyl pentenoate.

Methyl pentenoate can be produced through transeseterification of γ-valerolactone with methanol and then dehydrated, on acidic or basic catalysts as shown in Figure 1.3. Acidic zeolites such as borosilicate zeolite, aluminosilicate zeolite, SAPO-5 were found to be active for this reaction[21]. The main product is methyl-3-pentenoate (M3P), which could be further transformed to nylon monomers[22]. It can also be catalyzed by magnesium silicate (in particular the Magnesol® produced by the company Dallas Group of America©) and base catalyst such as $CsOAc/SiO_2$[23]. However, on basic catalysts, the main product is methyl-4-pentenoate (M4P). M4P can be used to manufacture of octanedioic acid which can be used directly, or as intermediates to produce other derivatives[24].

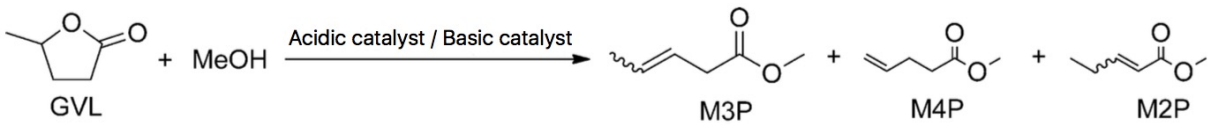

Figure 1.3: Ring opening of γ-valerolactone for producing methyl pentenoate.

1.1.2.2. Synthesis of solvents from organic carbonates

Dimethyl carbonate is a solvent with dielectric properties, which is interesting in lithium batteries. Its synthesis can be carried out in the gas phase by transesterification of ethylene carbonate with methanol, as shown in Figure 1.4[25]. This reaction is carried out on basic surfaces, such as hydrotalcites or magnesium oxide.

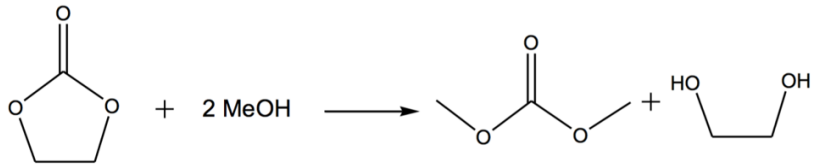

Figure 1.4: Synthesis of dimethyl carbonate from ethylene carbonate.

It is also possible to obtain other solvents from dimethyl carbonate with particular dielectric properties by transesterification in the gas phase. This will make it possible, in mixtures of organic carbonates, to adjust the overall dielectric constant of the liquid. For example, by transesterifying dimethyl carbonate with 2-propanol[26] (Figure 1.5), with phenol[27] or with ethanol[28], asymmetric organic carbonates are obtained. For this reaction, the catalysts claimed are supported titanium oxide[27], supported potassium carbonate[29], or magnesium oxide[28].

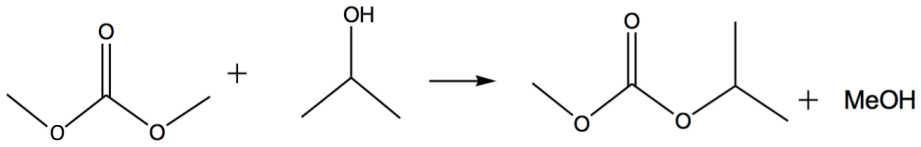

Figure 1.5: Synthesis of an asymmetric carbonate by transesterification with 2-propanol.

1.2. Catalysts for transesterification

Transesterification reaction is known to be accelerated by acid, base, and enzyme catalysts. Homogeneous catalyst shows a higher activity than heterogeneous catalysts for transesterification reaction. For instance, alkali metal hydroxides and alkoxides, that exhibit high activity, are currently used industrially for biodiesel production. However, due to the presence of free fatty acids (FFAs) and water in crude oils, soap is produced under alkaline conditions, which not only consumes the catalyst, but also causes separation challenges[11]. Accordingly, the feedstock has to be purified that increases the cost of process. In addition, homogeneous catalysts drawback is that they are hardly separated from products. In order to overcome these disadvantages, solid acid and base catalysts for transesterification reaction are widely studied.

1.2.1. Solid acid catalysts

The transesterification mechanism on homogeneous acid catalyst proposed in the literature is shown in Figure 1.6. It consists in three steps: the protonation of ester (step 1), the alcohol nucleophilic bonding (step 2), the new ester formation (step 3).

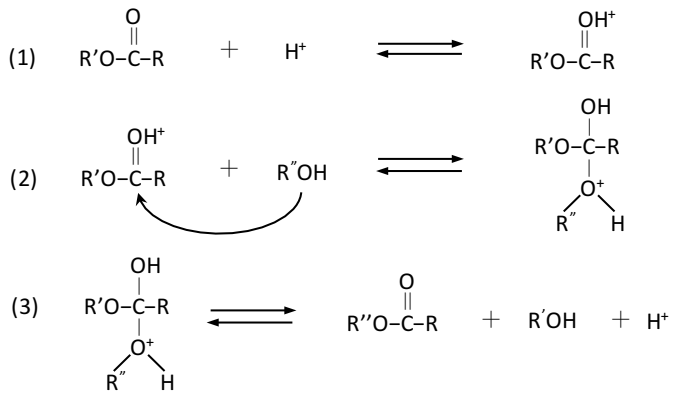

Figure 1.6: Homogeneous acid-catalyzed transesterification reaction mechanism.

The mechanism of reaction for heterogeneous catalysts is shown to be similar to that of homogeneous catalysts[30]. First, the carbonyl group of ester adsorbs on the acid sites (Figure 1.7). This increases the electrophilicity of the adjoining carbon atom, which is attacked by the nucleophilic alcohol, forming a intermediate. In the last step, the intermediate breakdowns to form products (Figure 1.7)[7].

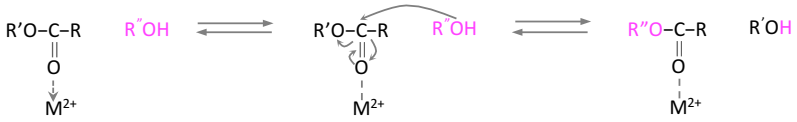

Figure 1.7: Heterogeneous acid-catalyzed transesterification reaction mechanism.

Five types of solid acid catalysts for transesterification reaction have been studied in literature: sulfated metal oxides, sulfonic acid groups, heteropolyacids (HPAs), H-form zeolites and acid phyllosilicates.

Sulfated metal oxides, *e.g.* SO_4^{2-}/ZrO_2, SO_4^{2-}/Ta_2O_5, SO_4^{2-}/Nb_2O_5 and SO_4^{2-}/TiO_2 are typical solid superacids and attract interest for transesterification[11]. These metal oxides themselves possess acidic sites, and their acidities can be enchanced through the inductive effect of SO_4^{2-} anions that increases the ability of Zr atoms to coordinate water[31]. The acidities and activities of these kinds of catalysts are similar to that of H_2SO_4[5]. Suwannakarn et al.[32] reported that the conversion of tricaprylin over SO_4^{2-}/ZrO_2 catalyst reached 85% at 120 °C and 6.8 atm for 2 h. However, the activity decreases significantly with subsequent reaction cycles, as the SO_4^{2-} species were leached out.

Sulfonic acid group such as sulfonic ion-exchange resin (Amberlyst-15 and Nafion SAC-13) can also catalyze transesterification reaction. These catalysts have a cross-linked polystyrene structure on which the active sites are the protons bonded to sulfonic groups. Around 70% conversion could be achieved in transesterification of vegetable oil with methanol at 60 °C, but it needed high methanol/vegetable oil ratio (300/1)[33].

HPAs are a class of strong solid acids made up of early transition metal (V, Nb, Mo, Ta or W)-oxygen anion clusters. In the field of acid catalysis, the most common and widely used HPAs are Keggin-type $H_3PW_{12}O_{40}$ and Wells–Dawson-type $H_6P_2W_{18}O_{62}$. For instance, Keggin-type HPAs have been applied in transesterification of rapeseed oil with methanol and ethanol, and they exhibited good catalytic activity (20% ~ 55% rapeseed oil conversion) that

was comparable to H_2SO_4 (27% rapeseed oil conversion) under the conditions of 85 °C and atmospheric pressure[34]. Nevertheless, HPAs show high solubility in polar media, and the reactions carried out homogeneously[11].

Zeolites are crystalline aluminosilicates interlinked by oxygen atoms. They possess three-dimensional framework structures with molecular pores and channels of uniform sizes[35]. When Si^{4+} is substituted byAl^{3+} in a tetrahedral zeolite framework, it produces negative charges and a cation, such as H^+ is required for compensation, which forms the Brønsted acid site[5]. However, diffusion of the reactant molecules to the active sites of zeolites can become a limiting process due to their small pore size. H-ZSM-5, H-MOR, H-BETA and H-USY show poor activity for transesterification[36] and therefore advancements in the design of zeolites with larger pores and channels are required.

Phyllosilicates were studied as catalysts in transesterification reaction. As some natural phyllosilicates such as montmorillonite[37] and kaolinite[38], showed poor activity, numerous researchers tried acid treatment to improve activities of phyllosilicates.

The works that investigated the transesterification over acid treated phyllosilicates are listed in Table 1.1. Commercial acidic treated montmorillonite such as KSF10 and K10 were tested in catalyzing transesterification of Jatropha curcas oil with methanol. At 60 °C, with an methanol/oil molar ratio 9/1, 5 wt% of catalyst and 6 h of reaction time, the fatty acid methyl ester (FAME) yields over both catalysts are still very low, below 3% (Table 1.1, entry 1)[37]. But montmorillonite K30 gave 78.4% yield of FAME in catalyzing transesterification of waste frying oil with methanol, at 90 ^oC, with a 12/1 molar ratio of methanol to waste frying oil (Table 1.1, entry 2)[39]. Saha et al.[40] also treated montmorillonite themselves with acid under reflux, and tested it in transesterification of cyclohexyl acrylate with n-butanol. 40.7% of FAME yield was achieved but at high temperature (170 °C) (Table 1.1, entry 3). From above literature, treatment with acid can improved the catalytic performance of montmorillonite in transesterification reaction. The acid treatment is expected to replace the interlayer cations by hydrated protons, improving Brønsted acidity while the structure is mostly preserved[41]. In addition, acid treatment makes the octahedral coordinated metal at the broken crystalline edges more exposed, that improve the Lewis acidity[42].

Dodecatungestophosphoric acid (TPA) was supported on montmorillonite K10 through incipient wetness method, then the supported catalyst and K10 were used in transesterification

of vegetable oils with alcohols, respectively[43]. At 170 °C, the yield of FAME over K10 is only 4.1%, but it increased to 57.6% with an 20% TPA loading (Table 1.1, entry 4). However, TPA is soluble in polar media[11], so the active sites were easily leached out.

A sulphonic acid functionalized montmorillonite was prepared through ion exchange method between sulphonic acid functionalized ionic liquid and Na^+-montmorillonite[44]. It shows high activity (95% of yield) in transesterification of ß-ketoester with octanol, at 80 °C with [TMBA] NTF_2 (trimethylbutylammonium bis(trifluoro-methylsulfonyl)imide) as solvent (Table 1.1, entry 5)[44].

Table 1.1: Catalytic performance of acid treated phyllosilicates.

Entry	Catalysts	Reaction conditions				Yield (%)
		Reactants, Alcohol/Oil	Temp. (°C)	Cata. Loading (w/w%)	Time (h)	
1[37]	KSF10, K10, montmorillonite	Jatropha curcas oil + MeOH, 9	60	5	6	<3
2[39]	Montmorillonite K30	Waste frying oil + MeOH, 12	90	3	3	78.4
3[40]	Acid/Montmorillonite	cyclohexyl acrylate + butanol, 2	160	10	5	40.7
4[43]	K10	Sunflower oil + MeOH, 15	170	5	8	4.1
	Tungstophosphoric acid/K10	Sunflower oil + MeOH, 15	170	5	8	57.6
5[44]	Montmorillonite	Ethyl ß-ketoester + octanol, 1.2	80	38.5	3	0
	Sulphonic acid/ Montmorillonite	Ethyl ß-ketoester + octanol, 1.2	80	38.5	3	95

In conclusion, sulfated metal oxides and heteropolyacids have good activities for transesterification, due to high acidity, but their stabilities are poor. Zeolites are not suitable for transesterification of bulky esters because of their small pore size. Although solid acid catalysts are insensitive to water and FFA in feedstock, the reaction rates are always low and thus need high reaction temperature. The advantages and disadvantages of solid acid catalysts are summarized in Table 1.2.

Table 1.2: Advantages and disadvantages of solid acid catalysts.

Classification	Catalysts	Advantages	Disadvantages
Sulfated metal oxides	SO_4^{2-}/ZrO_2, SO_4^{2-}/Ta_2O_5, SO_4^{2-}/Nb_2O_5 and SO_4^{2-}/TiO_2	Insensitive to water and FFA contents in feedstock	Active sites leaching out, reaction rate is low (need high temperature)
Sulfonic acid groups	Sulfonic ion-exchange resin		Reaction rate is low (need high temperature or high methanol/oil ratio)
HPAs	$H_3PW_{12}O_{40}$, $H_6P_2W_{18}O_{62}$		Soluble in alcohol, reaction rate is slow
H-form zeolites	H-ZSM-5, H-MOR, H-BETA, H-USY		Steric hindrance for bulky ester, reaction rate is slow
Acid phyllosilicates	K30		Reaction rate is low
	TPA/K10		Reaction rate is low, active sites leaching out

1.2.2. Solid base catalysts

The mechanism of transesterification on homogeneous base catalysts is shown in Figure 1.8. First, the alcohol is deprotonated by base catalyst to produce active species, RO^-. A tetrahedral intermediate is formed by nucleophilic attack on a carbonyl group in the ester. Then the tetrahedral intermediate breaks down into a new ester and an alkoxyl group. Finally it abstracted a proton from catalyst and thereby generated the catalyst[45].

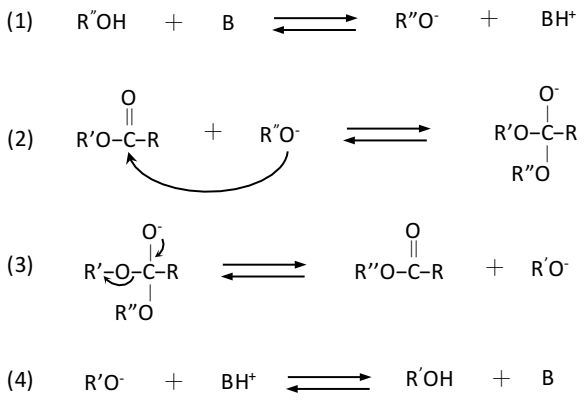

Figure 1.8: Homogeneous base-catalyzed transesterification reaction mechanism.

An heterogeneous mechanism, very similar to the homogeneous mechanism, was proposed for the transesterification of ethyl acetate with methanol on MgO by studying the conversion for this reaction with different amounts of initial reactants[46]. By comparing the experimental curves with those expected for different conventional mechanisms of heterogeneous catalysis, the authors deduced that the reaction had to take place *via* an Eley-Rideal mechanism, which starts with the adsorption of methanol at the surface. This step is followed by a reaction between the adsorbed methanol and the ester present in the liquid phase, as shown in Figure 1.9.

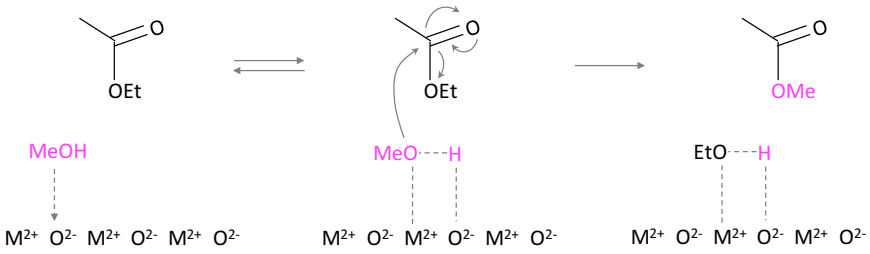

Figure 1.9: Simplified mechanism for transesterification of ethyl acetate with methanol over MgO adapted from Dossin et al.[46]

On the other hand, a Langmuir-Hinshelwood-like mechanism is observed for the transesterification of a triglyceride with methanol on a calcined hydrotalcite[47]. This model, involves the adsorption of both reactants, and implies methanol adsorption as the rate determining step, is proposed by comparing the statistical discrepancies between the theoretical and the experimental values obtained by the authors[47].

Different kinds of solid bases are able to catalyzed transesterification reaction, such as alkaline earth oxides, basic zeolites, hydrotalcites and base phyllosilicates.

Basicity in alkaline earth oxides arises from M^{2+}–O^{2-} ion pairs present in different coordination environments, with strongest base sites occurring at low coordination defect, corner and edge sites, or on high Miller index surfaces[48]. Magnesium oxide (MgO) as catalyst for transesterification in liquid phase, shows only 11% conversion at 60 °C for 8 h[49]. It is rather low compared to 100% conversion by NaOH, but better than that by solid acid catalysts (Cation-exchange resin, sulfate doped zirconium hydroxide, acidic zeolite) which only achieve <1% conversion in the same reaction conditions[49]. Some other researchers reported a high activity but at a higher temperature, *e.g.* 92% product yield at 180 °C[50].

Calcium oxide (CaO) as a catalyst for transesterification has attracted attention among researchers worldwide. Granados et al.[51] reported that 87% FAME yield was achieved in transesterification of sunflower oil with methanol at 60 °C for 2 h. However, the leaching of catalyst was evident as the solution containing the homogeneous species created by contacting the methanol and CaO for 2 h at 60 °C gave 60% FAME yield. Economic assessment was studied comparing CaO catalyst with homogeneous catalyst KOH. It showed that the manufacturing cost of biodiesel from waste cooking oil using CaO as a catalyst, manufactured in batch process, with a plant capacity of 7260 tonnes/year with hot water purification process was 584 $/tonne of biodiesel. It is slightly lower than that using KOH as catalyst (598 $/tonne of biodiesel)[52].

Alkali doped materials have also been studied for transesterification reactions. Li doped SiO_2 with 800 °C calcination resulted in a lithium orthosilicate solid base catalyst (Li_4SiO_4). It showed a similar activity than CaO for soybean transesterification, although its basic strength was lower[53]. Sodium silicate dehydrated and then calcined at 400 °C, was active for transesterification of rapeseed oil to FAME, with 98% yield for one hour at 60 °C. Although this catalyst displayed good recyclability, rapeseed oil conversions fell steadily to <60% after four reuses, attributed to water adsorption, Si–O–Si bond cleavage and sodium leaching[54]. K_2CO_3 supported over a series of support materials, such as MgO, activated carbon and SiO_2 for transesterification of soybean oil with methanol were studied[55]. The catalysts were prepared by the solid-state method (mixed two solids in a mortar and skived) and then calcined at 600 °C. They all showed high activities (90% – 99% yield) at 70 °C linked to K_2O formation during calcination, and the catalytic activity decreased little even after the catalyst had been recycled for six times[55].

A range of transition metal oxides of varying Lewis basic properties have been studied in transesterification reaction. For instance, MnO and TiO with mild basic strength were reported to have an activity for biodiesel production[56]. In addition, various transition metal oxides (TiO_2, MnO_2, Fe_2O_5, ZrO_2, CeO_2) mixed with alkaline earth oxides (MgO, CaO, BaO) were studied by Kawashima et al., and showed that only the Ca-containing catalysts having high basicities gave good catalytic activities for transesterification of rapeseed oil with methanol[57].

Hydrotalcites are another class of solid base catalysts that have attracted attention in transesterification reaction. The general formula of hydrotalcite is $[M(II)_{1-x}M(III)_x(OH)_2]^{x+}(A^{n-}$

$_{x/n})\cdot m H_2O$, where M(II) is a divalent ion, M(III) is a trivalent metal ion (usually Al^{3+}), and A^{n-} is an anion neutralizing the compound electrically. It adopts a layered double hydroxide structure with brucite-like ($Mg(OH)_2$) hydroxide sheets containing octahedrally coordinated M(II) and M(III) cations. The substitution of M(II) by trivalent cations of M(III) generates a positive charge which is neutralized by A^{n-} anions. Usually, hydrotalcites are decomposed through thermal treatment to yield a high surface area mixed oxide, which presumably exposes strong Lewis base sites[58]. Xie et al.[59] reported that the temperature of 500 °C was the optimum one for calcination of Mg-Al hydrotalcite (Mg-Al HT) and 67% conversion was achieved in transesterification of soybean oil with methanol (reaction conditions: methanol/oil molar ratio, 15/1; catalyst amount, 7.5%; reaction time, 9 h; reaction temperature, 65 °C). The reconstruction of decomposed Mg-Al HT by rehydration (HT-d-r) was reported to enhance the catalytic activity. The yield of monoesters was around 80% over HT-d-r in transesterification of tributyrin with methanol when the reaction conditions involved methanol/oil molar ratio 30:1, catalyst amount 0.5%, at 60 °C for 7 h. The high activity of HT-d-r was linked by the authors to the fact that it possessed more Brønsted base sites[60].

Some basic zeolites such as Na-mordenite, Na-beta and Na-X were tested in the transesterification of sunflower oil with methanol. Their activities were low, but could be improved with incorporation of excess Na *via* impregnation methods. Unfortunately, Na was found to have leached in the mixture, giving the reaction a homogeneous pathway[61].

Phyllosilicates treated by alkaline compounds have high activities for transesterification reaction. KOH (or NaOH), K_2CO_3 and KF were reported to be mostly employed to functionalize phyllosilicates. They were deposited into phyllosilicates through impregnation method followed by calcination. Their catalytic performances in transesterification reaction for biodiesel production are presented in Table 1.3. Soetaredjo et al.[62] studied KOH/bentonite catalysts for transesterification of palm oil with methanol. When increasing the KOH loading from 5% to 25%, the number of K_2O active sites in the catalyst also increased thus led to an increase in the yield of biodiesel. However, the conversion of soybean oil to biodiesel drops from 90.7% in the first cycle to about 52% after the third cycle (reaction time, 3 h). Dang et al.[38] studied transesterification of soybean oil with methanol using NaOH/kaolin cataslysts. Compared to raw kaolin, the conversion increased from 3% to 97% with the NaOH treated catalyst. Again, the activity drops from 97% in the first cycle to about 75% after the fourth cycle that may be due to the leaching of the active sites.

Table 1.3: Catalytic performance of base treated phyllosilicates.

Catalysts	Reaction conditions				Conv. or Yield (%)
	Reactants, Alcohol/Oil	Temp. (°C)	Cata. Loading (w/w%)	Time (h)	
KOH/bentonite[62]	Palm oil+MeOH, 6	60	3	3	90.7
NaOH/Kaolin[38]	Soybean oil+MeOH, 10	60	10	4	97
K_2CO_3/sepiolite[63]	Canola oil+MeOH, 6	65	3	2	95[a]
K_2CO_3/bentonite[64]	Canola oil+MeOH, 6	65	3	7	95
KF/smectite[65]	Soybean oil+MeOH, 6	65	15	1	99.7
KF/bentonite[66]	Soybean oil+MeOH, 9	80	15	2	95.2

[a] This value is yield, others are conversion.

Treatment of phyllosilicates with K_2CO_3 followed by calcination, also produced K_2O as active sites. Degirmenbasi et al.[63] studied the transesterification of canola oil with methanol using K_2CO_3 supported by sepiolite. With increasing the K loading, the specific surface area decreased dramatically, to only 4.1 m^2 g^{-1} for K_2CO_3(50%)/sepiolite, but it showed the highest activity. It only taked 2 h to achieve 95% yield of FAME at 65 °C. Authors ascribed the highest activity of K_2CO_3(50%)/sepiolite to its high basicity. Moreover, only a small decrease of the methyl ester yield, *i.e.*, from 98.5 ± 0.6 to 96.6 ± 0.7% was observed after 5 times of reuse of catalyst (reaction time, 8 h). Boz et al.[64] loaded the K_2CO_3 on calcium bentonite. It also performed well, and 95% yield of FAME was obtained after 7 h at 65 °C.

Alves et al.[65] investigated transesterification of soybean oil with methanol using smectite (montmorillonite and albite) modified by treatment with KF. The untreated clay showed very low activity (conversion, 3.3%), while KF-clay showed conversion of 99.7%. This achieving enhancement is linked to the improvement of the basicity of clay: the fluoride ions enhance the negative charge on oxygen atoms located in their vicinity. The presence of K^+ cations distributed around the active sites is also determining for the generation of basicity of the catalyst. These active sites seem stable, as only 2.2 % decrease of oil conversion was observed after 3 times of reuse of catalyst (reaction time, 8 h). Santos et al.[66] studied transesterification of soybean oil with methanol using bentonite treated by KF. It had excellent high activity as well, but at slight higher reaction temperature.

In conclusion, alkaline earth oxides, especially CaO shows a good activity for transesterification. The rehydration of decomposed Mg-Al HT gives a highly active sample. Alkali doped materials, *e.g.* Li_4SiO_4 despite owning weaker basicity than CaO, have higher activity. Transition metal and zeolite can catalyze transesterification, but with low activities. The alkali metal based phyllosilicates exhibit high activity. Although the active sites of KOH/phyllosilicate and NaOH/phyllosilicate are easily leached out, the K_2CO_3/phyllosilicate and KF/phyllosilicate are stable. The advantages and disadvantages of solid base catalysts are summarized in Table 1.4.

Table 1.4: Advantages and disadvantages of solid base catalysts.

Classification	**Catalysts**	**Advantages**	**Disadvantages**
Alkaline earth oxides	MgO	Good activity	
	CaO		Leaching of catalysts, sensitive to water
Alkali doped materials	Li_4SiO_4, Na_2SiO_3	Good activity	Leaching of catalysts, sensitive to water
	K_2CO_3/MgO		
Transition metal oxides	MnO, TiO		Low activity
Hydrotalcites	Mg-Al HT	High activity	
Zeolites	Na-mordenite, Na-beta, Na-X		Steric hindrance for bulky ester, reaction rate is slow
Base phyllosilicates	KOH/phyllosilicate, NaOH/phyllosilicate	High activity	Leaching of active sites
	K_2CO_3/phyllosilicate, KF/phyllosilicate,		

Numerous researches were performed in the transesterification reaction on acid and base catalysts. However, the mechanism was not so clear and active sites were not always identified. The link between acido-basic properties and reactivity is not well established. As it appears that, in some cases a link between the basic properties (strength or number of sites) and

reactivity is found (hydrotalcites[60], alkali metal base phyllosilicates[63]). Whereas in other cases moderate base (Li_4SiO_4[53]) are more active than stronger one (MgO[49]).

1.3. Preliminary work

In order to get insights on the questions, a preliminary work has been performed by Damien Cornu during his PhD thesis[67,68]. The aim was to compare gas and liquid phases reactivity in a series of Mg based catalysts and to look for the role of the acido-basic properties. A simple transesterification reaction of ethyl acetate with methanol was chosen as a model reaction. It is an ideal model reaction, as it could be processed both in gas or liquid phase. The materials to be studied were a commercial magnesium silicate (Magnesol®, provided by the Dallas Group of America©) and a series of magnesium-based materials with varying anions: oxide (O^{2-}), hydroxide (HO^-), carbonate (CO_3^{2-}), phosphate (PO_4^{3-}) and oxalate ($C_2O_4^{2-}$).

First, the surface acido-basic properties of these materials were investigated by the conversion of 3-methylbut-1-yn-3-ol (MBOH) which was proposed in 1991[69] as a tool for characterizing surface acid-base properties of solids. The decomposition reaction of MBOH presented in Figure 1.10 makes it possible to distinguish the acido-basic nature of a solid. MBOH molecule decomposes on solids following different routes depending on the presence of acidic or basic sites[69,70]. Figure 1.10 shows the two main routes followed on a large majority of solids: MBOH undergoes dehydration to yield 3-methyl-3-buten-1-yne (Mbyne) through acidic route and undergoes decomposition to give acetone and acetylene throuth basic route (The reaction conditions of MBOH test is presented in Apendix II). The results obtained in MBOH conversion are shown in Figure 1.11. With varying anions, acido-basic properties ranged widely, from strongly basic materials MgO and carbonate to weakly basic material oxalate. Phosphate shows purely acidic properties and Magnesol® shows both reactivities.

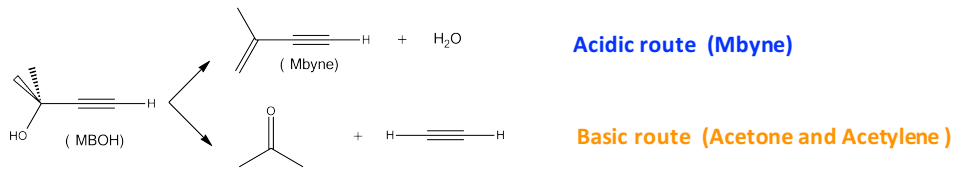

Figure 1.10: Reactivity of MBOH on various sites.[69,70]

Then, the materials are tested as catalysts in the transesterification of ethyl acetate with methanol both in liquid and gas phases (Figure 1.11). From the transesterification reaction in

gas phase, it can be seen that the conversion over purely basic materials decreased with decreasing the basicity. Moreover, the purely acidic material phosphate has no activity. It is interesting to note that Magnesol® with both reactivities of MBOH shows a moderate conversion. However, the situation in liquid phase is completely different, the most strongly basic material MgO shows a low conversion, whereas Magnesol® has the best activity.

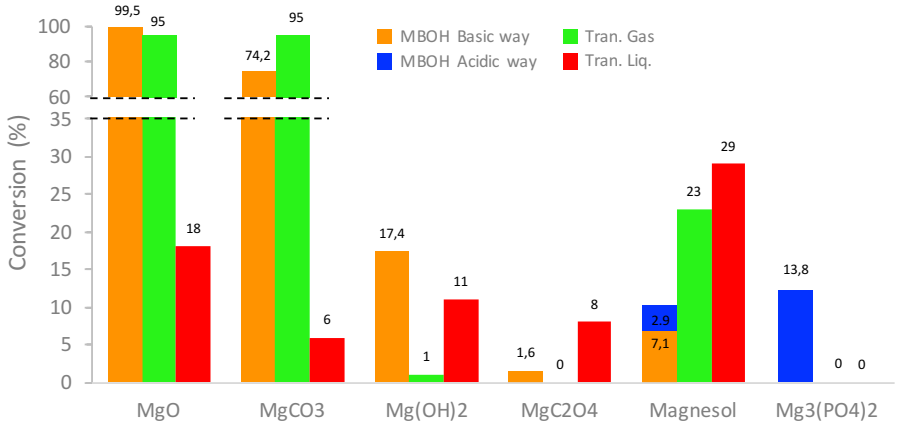

Figure 1.11: Conversion of MBOH following the acidic and basic routes. Conversions (%) for transesterification of ethyl acetate with methanol in liquid (333 K) and gas (393 K) phases.

Thus, the preliminary work[67,68] showed that a magnesium silicate called Magnesol® had high activity in transesterification in liquid phase. Besides, the magnesium silicates contain three of the eight most abundant elements in Earth's crust: oxygen (the most abundant element), silicon (the second most abundant element), and magnesium (the eighth most abundant element). So in my PhD work, I will focus on magnesium silicate based catalysts and aim to study the key parameters influencing their reactivity in transesterification reaction. First of all, I will present briefly the large family of magnesium silicate.

1.4. Magnesium silicates

Magnesium silicates family is consisted in three members: dense hydrous magnesium silicate (DHMS), magnesium phyllosilicates and amorphous magnesium silicate, reported in Table 1.5. DHMS includes so-called “alphabet phases” (phase A, B, superhydrous B, C, D, E, F and G)[71–75], 10 Å phase[76] and 3.65 Å phase[77]. It exists in earth’s mantle and subduction zones and thus its synthesis requires severe conditions (high pressure and temperature). For example, phase D (formula: $MgSi_2H_2O_6$) is synthesized at 22 GPa and 1000 °C. Its crystal structure is simple with all the Si occupying octahedral sites in a layer similar to that of brucite,

but with one of every three octahedral vacant. The MgO_6 octahedral are located above and below each vacant octahedral site. All O-H bonding occurs between SiO_6 octahedral layers[78]. Magnesium phyllosilicates, such as talc, hectorite, saponite, montmorillonite etc. are found in earth crust and they can be synthesized at moderate hydrothermal conditions[79]. DHMS and magnesium phyllosilicates are crystalline. Amorphous magnesium silicates are prepared by sol-gel[80], coprecipitation[81], or mechano-chemical method[82], and that they are known to be interesting for the transesterification reaction in liquid[83] and in gas phases[23]. For other publication, for example in the field of cements and concrete, the synthesis of these amorphous compounds has been studied, showing the formation of magnesium silicate hydrate (MSH) whose structure is identified to be similar to phyllosilicates but with defects[84].

Table 1.5: The members of magnesium silicate family.

Members	**Species**	**Structure**	**Synthesis**
DHMS	alphabet phases, 10 Å and 3.65 Å phase	crystalline	high pressure and temperature
Mg Phyllosilicates	talc, hectorite, saponite, montmorillonite etc.	crystalline	moderate hydrothermal conditions
Amorphous silicates	Magnesol®, MSH	Disorder crystal	mechano-chemical method

1.5. Aims and objectives

As shown at the beginning of introduction, in the field of biomass derivatives valorisation, transesterification reactions have found various applications in liquid phase. Currently, alkali metal hydroxides and alkoxides, are used industrially for biodiesel production, but induce saponification [11] and are hardly separated from products. Even if a heterogeneous process EsterfipH^{TM} was opened in 2004 by IFP-Energies Nouvelles[10], it requires high temperature and pressure (200 °C, 6.2 MPa)[10,85]. So numerous researchers devoted to develop more competitive heterogeneous catalysts, such as CaO[51,52], hydrotalcites[59,60].

My PhD thesis will focus on magnesium silicate based catalysts. To identify the key parameters for the transesterification reaction on magnesium silicate based catalysts, we first try to prepare magnesium silicate samples with similar Mg/Si ratio than Magnesol®, *via* coprecipitation and sol-gel methods. As these materials may exhibit quite weak basic sites and

even acidic ones, their surface acido-basic properties will be investigated by the conversion of MBOH. The link between acido-basic properties and the reactivity in the transesterification of ethyl acetate and methanol will be discussed in relation to the physico-chemical characterization (XRD, XPS, DRIFTS, ^{29}Si and ^{25}Mg NMR) of the materials. Then a kinetic study is performed and presented in chapter 2 to understand the reaction mechanism.

As it was reported that the activity of MgO can be affected by the carbonates and water adsorbed on its surface[86], then the role of adsorbed water on the catalytic behaviour of the commercial magnesium silicate will be studied. In order to link the yield obtained in catalysis to surface properties, the characterization of the catalysts is achieved by DRIFTS, IR with CO adsorption, ^{1}H NMR and calorimetry. This study will be presented in chapter 3.

Finally, in chapter 4, the study will be extended to phyllosilicates which have a similar structure than commercial magnesium silicate but more crystallized. Talc, nano talc and some species of smectite group such as montmorillonite and laponite will be tested as catalysts of transesterification reaction. The role of nano particle size on the acivity in transesterification reaction will be examined, and to understand the reaction mechanism on laponite, a kinetic study is performed. Moreover, for comparing with thermally treated commercial magnesium silicate, the role of adsorbed water on the catalytic performance of laponite will be discussed.

References

[1] U. Schuchardt, R. Sercheli, R. M. Vargas, *J. Braz. Chem. Soc.* **1998**, *9*, 199–210.

[2] J. Otera, *Chem. Rev.* **1993**, *93*, 1449–1470.

[3] J. Hill, E. Nelson, D. Tilman, S. Polasky, D. Tiffany, *Proc. Natl. Acad. Sci.* **2006**, *103*, 11206–11210.

[4] S. Semwal, A. K. Arora, R. P. Badoni, D. K. Tuli, *Bioresour. Technol.* **2011**, *102*, 2151–2161.

[5] Y. M. Sani, W. M. A. W. Daud, A. R. Abdul Aziz, *Appl. Catal. Gen.* **2014**, *470*, 140–161.

[6] A. L. de Lima, C. M. Ronconi, C. J. A. Mota, *Catal Sci Technol* **2016**, *6*, 2877–2891.

[7] M. Di Serio, R. Tesser, L. Pengmei, E. Santacesaria, *Energy Fuels* **2008**, *22*, 207–217.

[8] H. Noureddini, *System and Process for Producing Biodiesel Fuel with Reduced Viscosity and a Cloud Point below Thirty-Two (32) Degrees Fahrenheit*, **2001**, US6174501 B1.

[9] A. Martin, J. E. Flynn, H. Lange, *Biodiesel Production Method*, **2011**, US8030505 B2.

[10] L. Bournay, G. Hillion, P. Boucot, J.-A. Chodorge, C. Bronner, A. Forestiere, *Process for Producing Alkyl Esters from a Vegetable or Animal Oil and an Aliphatic Monoalcohol*, **2005**, US 6878837 B2.

[11] F. Su, Y. Guo, *Green Chem.* **2014**, *16*, 2934.

[12] S. Gryglewicz, *Appl. Catal. Gen.* **2000**, *192*, 23–28.

[13] J. Barrault, F. Jerome, *Eur. J. Lipid Sci. Technol.* **2008**, *110*, 825–830.

[14] S. Bancquart, C. Vanhove, Y. Pouilloux, J. Barrault, *Appl. Catal. Gen.* **2001**, *218*, 1–11.

[15] F. Jérôme, G. Kharchafi, I. Adam, J. Barrault, *Green Chem* **2004**, *6*, 72–74.

[16] F. Jérôme, Y. Pouilloux, J. Barrault, *ChemSusChem* **2008**, *1*, 586–613.

[17] F.-A. El-Toufaili, G. Feix, K.-H. Reichert, *J. Polym. Sci. Part Polym. Chem.* **2006**, *44*, 1049–1059.

[18] S. Habaue, Y. Takahashi, Y. Hosogoe, H. Yamashita, M. Kajiwara, *Nat. Sci.* **2010**, *2*, 557.

[19] J.-P. Wiegner, D. Runkel, V. Voerckel, G. Feix, H. Staeuber, *Catalyst Systems for Polycondensation Reactions*, **2003**, US2006/0079395A1.

[20] K. Yan, Y. Yang, J. Chai, Y. Lu, *Appl. Catal. B Environ.* **2015**, *179*, 292–304.

[21] W. Hoelderich, F. Naeumann, R. Fischer, *Preparation of Alkenecarboxylic Esters*, **1992**, US5144061 A.

[22] P. Meessen, D. Vogt, W. Keim, *J. Organomet. Chem.* **1998**, *551*, 165–170.

[23] L. E. Manzer, *Synthesis of Alkenoate Esters from Lactones and Alcohols*, **2004**, US6835849 B2.

[24] E. J. Molitor, B. D. Mullen, *Method of Manufacture of Octanedioic Acid, Precursors, and Derivatives*, **2014**, WO2014150384 A1.

[25] N. Keller, G. Rebmann, V. Keller, *J. Mol. Catal. Chem.* **2010**, *317*, 1–18.

[26] D. Yanmin, C. Xingquan, Z. Chunxiang, Z. Tiansheng, *J. Mol. Catal. Chem.* **2010**, *331*, 125–129.

[27] W. B. Kim, Y. G. Kim, J. S. Lee, *Appl. Catal. Gen.* **2000**, *194–195*, 403–414.

[28] Z. L. Shen, X. Z. Jiang, W. J. Zhao, *Catal. Lett.* **2003**, *91*, 63–67.

[29] M. Fan, P. Zhang, *Energy Fuels* **2007**, *21*, 633–635.

[30] Y. C. Sharma, B. Singh, J. Korstad, *Fuel* **2011**, *90*, 1309–1324.

[31] V. V. Strelko, *Kinet. Catal.* **2003**, *44*, 834–839.

[32] K. Suwannakarn, E. Lotero, J. Goodwinjr, C. Lu, *J. Catal.* **2008**, *255*, 279–286.

[33] S. C. M. dos Reis, E. R. Lachter, R. S. V. Nascimento, J. A. Rodrigues, M. G. Reid, *J. Am. Oil Chem. Soc.* **2005**, *82*, 661–665.

[34] P. Morin, B. Hamad, G. Sapaly, M. G. Carneiro Rocha, P. G. Pries de Oliveira, W. A. Gonzalez, E. Andrade Sales, N. Essayem, *Appl. Catal. Gen.* **2007**, *330*, 69–76.

[35] Z. Zhang, *Branched Biodiesels*, **2005**, US 2008/0045731 A1.

[36] A. A. Kiss, A. C. Dimian, G. Rothenberg, *Adv. Synth. Catal.* **2006**, *348*, 75–81.

[37] A. F. Zanette, R. A. Barella, S. B. C. Pergher, H. Treichel, D. Oliveira, M. A. Mazutti, E. A. Silva, J. V. Oliveira, *Renew. Energy* **2011**, *36*, 726–731.

[38] T. H. Dang, B.-H. Chen, D.-J. Lee, *Bioresour. Technol.* **2013**, *145*, 175–181.

[39] M. Ayoub, S. Ullah, A. Inayat, A. H. Bhat, *Procedia Eng.* **2016**, *148*, 742–749.

[40] B. Saha, M. Streat, *React. Funct. Polym.* **1999**, *40*, 13–27.

[41] L. P. Ramos, C. S. Cordeiro, M. A. F. Cesar-Oliveira, F. Wypych, S. Nakagaki, in *Bioenergy Res. Adv. Appl.*, Elsevier, **2014**, pp. 255–276.

[42] L. Zatta, L. P. Ramos, F. Wypych, *J. Oleo Sci.* **2012**, *61*, 497–504.

[43] V. V. Bokade, G. D. Yadav, *Process Saf. Environ. Prot.* **2007**, *85*, 372–377.

[44] R. Ratti, S. Kaur, M. Vaultier, V. Singh, *Catal. Commun.* **2010**, *11*, 503–507.

[45] Z. Helwani, M. R. Othman, N. Aziz, J. Kim, W. J. N. Fernando, *Appl. Catal. Gen.* **2009**, *363*, 1–10.

[46] T. F. Dossin, M.-F. Reyniers, G. B. Marin, *Appl. Catal. B Environ.* **2006**, *62*, 35–45.

[47] A. Kapil, K. Wilson, A. F. Lee, J. Sadhukhan, *Ind. Eng. Chem. Res.* **2011**, *50*, 4818–4830.

[48] H. Hattori, *Chem. Rev.* **1995**, *95*, 537–558.

[49] G. Vicente, A. Coteron, M. Martinez, J. Aracil, *Ind. Crops Prod.* **1998**, *8*, 29–35.

[50] M. Di Serio, M. Ledda, M. Cozzolino, G. Minutillo, R. Tesser, E. Santacesaria, *Ind. Eng. Chem. Res.* **2006**, *45*, 3009–3014.

[51] M. L. Granados, M. D. Z. Poves, D. M. Alonso, R. Mariscal, F. C. Galisteo, R. Moreno-Tost, J. Santamaría, J. L. G. Fierro, *Appl. Catal. B Environ.* **2007**, *73*, 317–326.

[52] T. Sakai, A. Kawashima, T. Koshikawa, *Bioresour. Technol.* **2009**, *100*, 3268–3276.

[53] J.-X. Wang, K.-T. Chen, J.-S. Wu, P.-H. Wang, S.-T. Huang, C.-C. Chen, *Fuel Process. Technol.* **2012**, *104*, 167–173.

[54] Y.-D. Long, F. Guo, Z. Fang, X.-F. Tian, L.-Q. Jiang, F. Zhang, *Bioresour. Technol.* **2011**, *102*, 6884–6886.

[55] X. Liang, S. Gao, H. Wu, J. Yang, *Fuel Process. Technol.* **2009**, *90*, 701–704.

[56] K. Gombotz, R. Parette, G. Austic, D. Kannan, J. V. Matson, *Fuel* **2012**, *92*, 9–15.

[57] A. Kawashima, K. Matsubara, K. Honda, *Bioresour. Technol.* **2008**, *99*, 3439–3443.

[58] A. Corma, S. Hamid, S. Iborra, A. Velty, *J. Catal.* **2005**, *234*, 340–347.

[59] W. Xie, H. Peng, L. Chen, *J. Mol. Catal. Chem.* **2006**, *246*, 24–32.

[60] Y. Xi, R. Davis, *J. Catal.* **2008**, *254*, 190–197.

[61] M. J. Ramos, A. Casas, L. Rodríguez, R. Romero, Á. Pérez, *Appl. Catal. Gen.* **2008**, *346*, 79–85.

[62] F. E. Soetaredjo, A. Ayucitra, S. Ismadji, A. L. Maukar, *Appl. Clay Sci.* **2011**, *53*, 341–346.

[63] N. Degirmenbasi, N. Boz, D. M. Kalyon, *Appl. Catal. B Environ.* **2014**, *150–151*, 147–156.

[64] N. Boz, N. Degirmenbasi, D. M. Kalyon, *Appl. Catal. B Environ.* **2013**, *138–139*, 236–242.

[65] H. J. Alves, A. M. da Rocha, M. R. Monteiro, C. Moretti, M. D. Cabrelon, C. A. Schwengber, M. C. Milinsk, *Appl. Clay Sci.* **2014**, *91–92*, 98–104.

[66] K. G. dos Santos, R. A. Bariccatti, E. de Rossi, L. M. S. Colpini, C. T. Eckert, G. R. dos Santos, H. J. Alves, others, *J. Food Agric. Environ.* **2015**, *13*, 250–255.

[67] D. Cornu, Study of the Parameters Governing the Reactivity of Weak Inorganic Bases. Towards the Transesterification Reaction., Universite Pierre et Marie Curie, **2012**.

[68] D. Cornu, L. Lin, M. Daou, M. Jaber, J.-M. Krafft, V. Herledan, G. Laugel, Y. Millot, H. Lauron-Pernot, *Catal. Sci. Technol.* **2017**, *7*, 1701–1712.

[69] H. Lauron-Pernot, F. Luck, J. M. Popa, *Appl. Catal.* **1991**, *78*, 213–225.

[70] H. Lauron-Pernot, *Catal. Rev.* **2006**, *48*, 315–361.

[71] A. E. Ringwood, A. Major, *Earth Planet. Sci. Lett.* **1967**, *2*, 130–133.

[72] L. Liu, *Phys. Earth Planet. Inter.* **1987**, *49*, 142–167.

[73] M. Kanzaki, *Phys. Earth Planet. Inter.* **1991**, *66*, 307–312.

[74] T. Gasparik, *J. Geophys. Res. Solid Earth* **1993**, *98*, 4287–4299.

[75] E. Ohtani, H. Mizobata, Y. Kudoh, T. Nagase, H. Arashi, H. Yurimoto, I. Miyagi, *Geophys. Res. Lett.* **1997**, *24*, 1047–1050.

[76] P. Comodi, F. Cera, L. Dubrovinsky, S. Nazzareni, *Earth Planet. Sci. Lett.* **2006**, *246*, 444–457.

[77] B. Wunder, R. Wirth, M. Koch-Müller, *Am. Mineral.* **2011**, *96*, 1207–1214.

[78] H. Yang, C. T. Prewitt, D. J. Frost, *Am. Mineral.* **1997**, *82*, 651–654.

[79] J. T. Kloprogge, S. Komarneni, J. E. Amonette, *Clays Clay Miner.* **1999**, *47*, 529–554.

[80] A. G. Kalampounias, N. Bouropoulos, K. Katerinopoulou, S. N. Yannopoulos, *J. Non-Cryst. Solids* **2008**, *354*, 749–754.

[81] D. R. M. Brew, F. P. Glasser, *Cem. Concr. Res.* **2005**, *35*, 85–98.

[82] D. Nied, K. Enemark-Rasmussen, E. L'Hopital, J. Skibsted, B. Lothenbach, *Cem. Concr. Res.* **2016**, *79*, 323–332.

[83] K. Narasimharao, T. T. Ali, S. Bawaked, S. Basahel, *Appl. Catal. Gen.* **2014**, *488*, 208–218.

[84] C. Roosz, S. Grangeon, P. Blanc, V. Montouillout, B. Lothenbach, P. Henocq, E. Giffaut, P. Vieillard, S. Gaboreau, *Cem. Concr. Res.* **2015**, *73*, 228–237.

[85] L. Bournay, D. Casanave, B. Delfort, G. Hillion, J. A. Chodorge, *Catal. Today* **2005**, *106*, 190–192.

[86] D. Cornu, H. Guesmi, J.-M. Krafft, H. Lauron-Pernot, *J. Phys. Chem. C* **2012**, *116*, 6645–6654.

Chapter 2. Role of magnesium silicate hydrate formation

2.1. Introduction

Numerous heterogeneous catalysts are claimed to catalyze the transesterification reaction. This chemical transformation is widely described for biodiesel production in liquid phase but also involved in gas phase for lactone opening or for various substrate transformation[1,2]. Among them, materials possessing basic properties have gained more attention compared to the acidic materials due to their higher reaction rate. The most common ones are the calcium and magnesium oxides. Their activities in the transesterification reaction were widely reported[3–7] and they are already used in various industrial processes[8]. Their reactivity can be enhanced or decreased by covering the surface with adsorbates (CO_2 and H_2O)[9,10]. Alkaline earth materials exhibit strong basic sites, but it has also been shown that other solids with weaker surface basicity are able to catalyze this reaction. For instance, biodiesel production can be achieved using potassium carbonate or phosphate[11,12], barium hydroxide[5], or zinc based materials[13,14] while calcium and barium acetate enable the transesterification of lactones[15]. Moreover, silicates are good catalysts for transesterification, used directly combined with magnesium[16] or as clay minerals, combined with aluminum, calcium and sodium[17–23]. The preliminary work also showed that Magnesol® with lower basicity has higher activity compared to MgO.

Magnesium silicate can be synthesized by different methods such as mechano-chemical dehydration[24–28], hydrothermal synthesis[29] and precipitation[30]. Sol-gel method was also proposed by some authors[31]. In this chapter, the properties of a commercial magnesium siliciate (Magnesol®) is compared with two laboratory made samples (by coprecipitation or by sol-gel method). Then, the materials are tested as catalysts of the transesterification of ethyl acetate with methanol in liquid phase. The link between acido-basic reactivity and the reactivity in the transesterification reaction will be discussed in relation to the physico-chemical characterization of the materials.

2.2. Choice of reaction conditions

2.2.1. Data from literature

In Chapter 1 was presented a transesterification model reaction, conversion of ethyl acetate (AcOEt) with methanol (MeOH) to form methyl acetate (AcOMe) and ethanol (EtOH). This model reaction was used to know the potential of the materials in this type of reaction carried out in liquid phase. Many procedures for liquid-phase transesterification are described in the literature. In particular, five are reported in Table 2.1 for the transesterification of ethyl acetate with methanol.

Table 2.1: Reaction conditions of transesterification of ethyl acetate with methanol reported in literature.

Entry	Reaction Temp. (^{o}C)	n_{MeOH} / n_{AcOEt}	Catalyst	Reference
1	70	12.3	NaOH/Smectites	S. Fujita[32]
2	0	1	MgO	H. Hattori[33]
3	10 to 50	0.1 to 10	MgO	T. Dossin[34]
4	65	6.2 to 24.7	Sodium silicate	Z. Yaakob[35]
5	30 to 60	1 to 10	Lewatit K1221	E. Steene[36]

The reaction temperatures range from 0 to 70 ^{o}C in literature. Considering the reaction rate and boiling point of methanol (64.7 ^{o}C), we will first choose 60 ^{o}C to perform the preliminary test.

2.2.2. Thermodynamic study

Thermodynamic equilibrium is then checked for the transesterification of AcOEt with MeOH to form AcOMe and EtOH. The position of the thermodynamic equilibrium can be determined based on the thermodynamic data in Table 2.2.

Table 2.2: The thermodynamic data of reactants and products.

Substance	$\Delta_f H_m^o(298\ K)/\ kJ \cdot mol^{-1}$	$S_m^o(298\ K)/J \cdot mol^{-1} \cdot K^{-1}$
MeOH	-239.10	130.98
AcOEt	-478.43	264.95
AcOMe	-444.53	217.39
EtOH	-286.36	159.76

First, if the reaction is written as:

MeOH + AcOEt == AcOMe + EtOH

It can be calculated that,

$$\Delta_r H_m^o(298\ K) = -13.36\ kJ \cdot mol^{-1}$$

$$\Delta_r S_m^o(298\ K) = -18.78\ J \cdot mol^{-1} \cdot K^{-1}$$

As the $\Delta_r G_m^o(T)$ can be calculated by the Eq. 2.1

$$\Delta_r G_m^o(T) = \Delta_r H_m^o(T) + T\ \Delta_r S_m^o(T) \qquad \text{Eq. 2.1}$$

Providing the T is not far from 298K, $\Delta_r G_m^o(T)$ can be calculated by the Eq. 2.2:

$$\Delta_r G_m^o(T) \approx \Delta_r H_m^o(298\ K) + T\ \Delta_r S_m^o(298\ K) \qquad \text{Eq. 2.2}$$

So the $\Delta_r G_m^o(303\ K)$, $\Delta_r G_m^o(333\ K)$ and $\Delta_r G_m^o(363\ K)$ are calculated and showed in Table 2.3.

According to the Eq. 2.3, the standard equilibrium constants (K^o) are calculated and also showed in Table 2.3. They decrease with the increase in temperature.

$$K^o = e^{-\Delta_r G_m^o(T)/RT} \qquad \text{Eq. 2.3}$$

Table 2.3: Equilibrium constants of transesterification of ethyl acetate with methanol.

T / K	$\Delta_f G_m^o(T)$ / kJ · mol^{-1}	K^o	MeOH/AcOEt	Conv. equil. / %
303	-7.66	20.92	1	82.1
			3	97.7
			12	99.6
			24.3	99.8
333	-7.10	12.98	1	78.3
			3	96.5
			12	99.3
			24.3	99.7
363	-6.54	8.72	1	74.7
			3	95.0
			12	99.0
			24.3	99.5

Then the position of the thermodynamic equilibrium can be determined from the thermodynamic constant of the reaction presented in Eq. 2.4:

$$K^o = \frac{a\ (\mathrm{AcOMe}) \times a\ (\mathrm{EtOH})}{a\ (\mathrm{AcOEt}) \times a\ (\mathrm{MeOH})} \qquad \text{Eq. 2.4}$$

a(AcOMe), *a*(EtOH), *a*(AcOEt) and *a*(EtOH) are the activity of corresponding reagents. An approximation must be made in order to calculate the equilibrium conversion of the reaction: it will be necessary to consider that all the reagents have a thermodynamic activity equal to their molar fractions.

As an example, the equilibrium conversion at 333 K, with MeOH/AcOEt ratio of 12 and without any solvent, is calculated as follow. At the initial time, there is a molar fraction of 0.07692 ethyl acetate and 0.92308 methanol.

By noting *x* the molar fraction of the two products (methyl acetate and ethanol) produced in identical proportions, it is possible to obtain the formula of the reaction quotient (RQ) in Eq. 2.5:

$$RQ = \frac{x^2}{(0.07692 - x)(0.92308 - x)} \qquad \text{Eq. 2.5}$$

The reaction reaches equilibrium when the RQ is equal to the standard equilibrium constants (K^o). The thermodynamic constant of this equilibrium is $K^o = 12.98$ at 333 K which gives a product fraction at equilibrium of x = 0.07638. This means that the conversion is equal to 99.3%.

The equilibrium conversions at other conditions are calculated in the same way and listed in Table 2.3. It is obvious that the reaction is favored in the direction of product formation, but the equilibrium constant decreases when the reaction temperature increases. This decrease can be counter balanced by a high MeOH/AcOEt ratio that displaced the equilibrium towards the products. In order to favor the kinetics, a relatively high temperature of 60 ^oC and thus a ratio >12 will be chosen. To facilitate the further kinetic study with a constant mole fraction of MeOH the highest value found in literature will be chosen and fixed to 24.3 (corresponding to volumic ratio of 10). Moreover, the ester is most often the molecule most difficult to produce in the transesterifications of industrial interest. On the contrary, the alcohol used for transesterification is very often methanol, readily obtained from natural gas by reforming methane into carbon monoxide and hydrogen, followed by synthesis itself[37]. Methanol was also produced at 100 million tonnes in 2015. This alcohol will therefore be used in excess with respect to the stoichiometry of the reaction.

It is necessary to place oneself in the reaction conditions for which the conversion is between 10% and 50%. Indeed, with these orders of magnitudes of conversion, the catalysts can be classified unambiguously. Moreover, it will be necessary to avoid being close to the thermodynamic limit to study the reactions.

2.2.3. Test with the chosen conditions

A preliminary test was carried out to determine the conversion as a function of reaction time. The catalyst used in the test shown in Figure 2.1 is Magnesol®. The temperature of the the reaction mixture is at 60 ^oC, and the mole ratio of MeOH/AcOEt is 24.3. In this study, a conversion of 32% is reached approximately 5 hours after the start of the reaction.

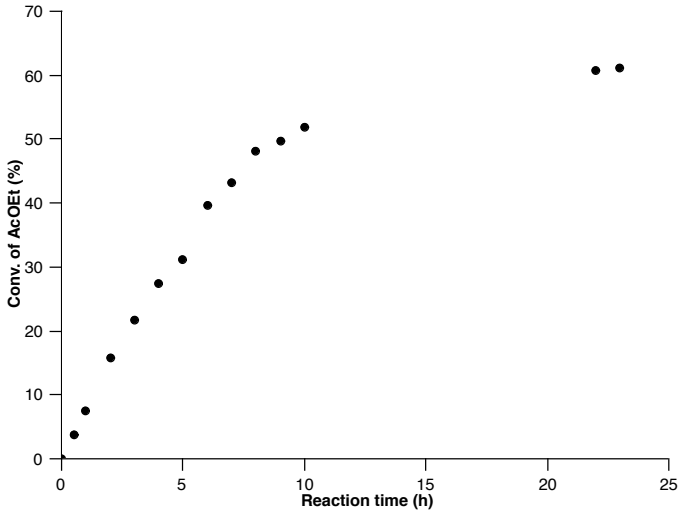

Figure 2.1: Conversion of ethyl acetate as a function of time for Magnesol®.
Reaction conditions: temperature = 60 ^{o}C, MeOH/AcOEt = 24.3, Magnesol® = 40 mg.

It must be noted that the conversion at thermodynamic equilibrium is 99.7% at 60 ^{o}C and mole ratio of MeOH/AcOEt 24.3. This indicates that a reaction with a conversion between 10% and 50% is not likely to be limited by a too rapid convergence towards the thermodynamic equilibrium of the reaction, which could level the performances of the catalysts.

In addition, it is important to perform a mass transfer test to ensure that the observed rate is the rate of the chemical reaction but not a step of diffusion of the reagents to the surface[38]. In practice, this is often the case when the conversion is over 30%. In order to exclude the effect of limitation of mass transfer, we first study the conversion of ethyl acetate as a function of the mass of Magnesol®, as shown in Figure 2.2. The conversion of AcOEt raises rapidly when the mass of catalyst increases from 0 to 20 mg. After that the limitation of mass transfer exists and the conversion of AcOEt tends to be stable even if the mass of catalyst increases to 100 mg. Therefore, we will use 18 mg of catalyst for the next study in this chapter. In conclusion, reaction conditions chosen here for a normal test are listed in Table 2.4.

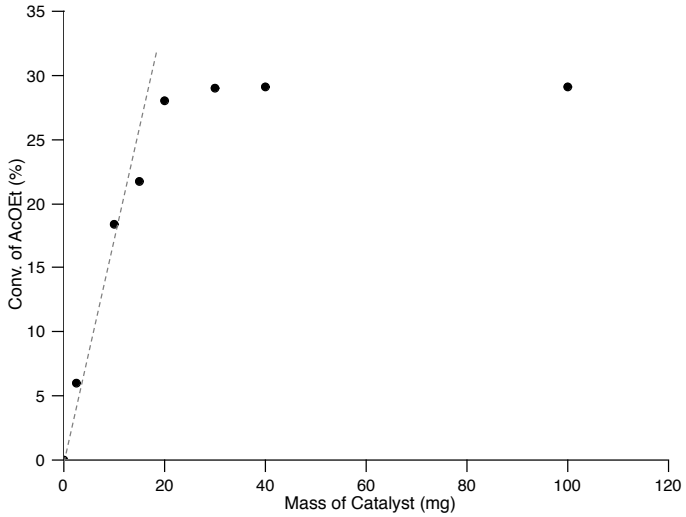

Figure 2.2: Conversion of ethyl acetate as a function of mass of Magnesol®.

Table 2.4: Standard reaction conditions for transesterification reaction.

Temp. (°C)	Catalyst (mg)	MeOH/AcOEt (mol/mol)	MeOH (mL)	AcOEt (mL)	1,4-dioxane[a] (mL)	Reaction time (h)	Stirring rate (rpm)
60	18	24.3	10	1	1	5	630

[a] 1,4-dioxane is used as internal standard.

2.2.4. Experimental setup

The transesterification of ethyl acetate with methanol was carried out in a glassware "Schlenk" which allows to control both the gas exchanges, thanks to a pipeline that can be closed by a tap, and to exchange liquid through a septum by a syringe (Figure 2.3). First, the solid catalyst is introduced in the Schlenk flask. After that, it is placed under vacuum and then filled with nitrogen at a pressure of 1 bar, prior to the addition of the reactants. The system is therefore in a closed circuit throughout the reaction time and does not exchange material with the outside. 10 mL methanol (Sigma Aldrich anhydrous 99.8%) is introduced through needles into the Schlenk. Then 1 ml of 1,4-dioxane (Sigma Aldrich anhydrous 99.8%), as standard reference, is added to the solution. 1,4-dioxane (dioxane) does not react with the molecules present in the solution and has a high boiling point, making it a reliable reference for measuring concentrations of other species. The introduction of 1 mL of ethyl acetate (Sigma Aldrich anhydrous 99.8%) determines the initial time of the reaction (t = 0).

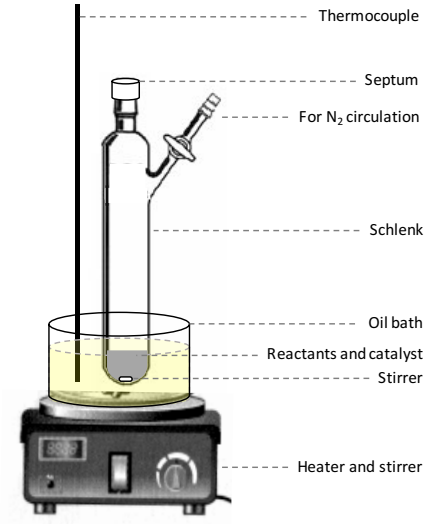

Figure 2.3: Assembly of transesterification in liquid phase.

The temperature of the reactants mixture is maintained at 60 °C. The temperature is not controlled by a thermocouple placed in direct contact with the solution, passing through the septum as perforation of the septum leads to leakage, which could be the cause of the loss of reagents and products. Thus, the temperature is controlled by the oil bath, regulated at 70 ^{o}C. For such a bath temperature, the temperature measured inside Schlenk under conditions identical to those used for the reaction is 60 °C.

Small amounts of liquid (approximatively 4 drops) are taken at the start of the reaction and after 5 hours of reaction. The collected solution is introduced into pill bottles containing about 2 mL of 1-propanol (in order to dilute the reagents so as not to saturate the chromatography detector). It is injected in an amount of 0.1 µL in gas phase chromatography (the details of gas chromatography are presented in Appendix I). The area of each of the peaks detected by gas phase chromatography is normalized by the area of dioxane. To compare the peaks belonging to different species, the relative response coefficient for each species was determined and presented in Table 2.5. The methyl acetate response coefficient is standardized to 1.

Table 2.5: Response coefficients of FID Detector.

Molecule	**AcOMe**	**AcOEt**	**MeOH**	**EtOH**	**Dioxane**
Response coefficient	1	0.6286	2.2319	1.1538	0.8083
Retention time (min)	6.18	7.68	8.73	10.38	20.88

The conversion is obtained by studying the consumption of ethyl acetate. The ratio of AcOEt/dioxane is checked at the beginning (t = 0 h) and after 5 hours of reaction (t = 5 h) by gas chromatography. Such a study is more difficult to carry out on methanol since, present in large excess, the variation of its concentration during the reaction will be smaller in proportion to the quantities. The conversion was calculated through Eq. 2.6. The only detected products are methyl acetate and ethanol, so the selectivity is always 100%.

$$\text{Conv.} = \frac{(A_{AcOEt}/A_{dioxane})_{t=0} - (A_{AcOEt}/A_{dioxane})_{t=5}}{(A_{AcOEt}/A_{dioxane})_{t=0}} \times 100\% \qquad \text{Eq. 2.6}$$

In Eq. 2.6, A_{AcOEt} and $A_{dioxane}$ is the peak area of AcOEt and dioxance, respectively, detected by FID in gas chromatography.

The analysis of the solution by sampling at room temperature is a priori more reliable because, at high temperature, there exist equilibrium with the gas phase and condensation on the walls of the schlenk, which can modify the total quantities involved, however the difference between these two analyzes remains low. The results given hereafter will emanate from the analysis of the solution samples withdrawn at ambient temperature.

Carbon balance is systematically checked by Eq. 2.7 and is always determined at values over 95%.

$$\text{Carbon balance} = \frac{[\text{carbon}]_5}{[\text{carbon}]_0} \times 100\% \qquad \text{Eq. 2.7}$$

In Eq. 2.7, the $[\text{carbon}]_0$ and $[\text{carbon}]_5$ are the total mole of carbon in t = 0 h and t = 5 h, respectively, and they are obtained by Eq. 2.8.

$$[\text{carbon}]_0 = \frac{(A_{AcOEt})_0 \times f_{AcOEt}}{(A_{dioxane})_0 \times f_{dioxane}} \times 4 + \frac{(A_{MeOH})_0 \times f_{MeOH}}{(A_{dioxane})_0 \times f_{dioxane}} \times 1$$

$$[\text{carbon}]_5 = \frac{(A_{AcOEt})_5 \times f_{AcOEt}}{(A_{dioxane})_5 \times f_{dioxane}} \times 4 + \frac{(A_{MeOH})_5 \times f_{MeOH}}{(A_{dioxane})_5 \times f_{dioxane}} \times 1 + \frac{(A_{AcOMe})_5 \times f_{AcOMe}}{(A_{dioxane})_5 \times f_{dioxane}} \times 3 + \frac{(A_{EtOH})_5 \times f_{EtOH}}{(A_{dioxane})_5 \times f_{dioxane}} \times 2 \qquad \text{Eq. 2.8}$$

In Eq. 2.8, the $(A_{AcOEt})_0$, $(A_{MeOH})_0$ and $(A_{dioxane})_0$ are the area of AcOEt, MeOH and dioxane at t = 0 h, respectively. The $(A_{AcOEt})_5$, $(A_{MeOH})_5$, $(A_{AcOMe})_5$, $(A_{EtOH})_5$, and $(A_{dioxane})_5$ are

the area of AcOEt, MeOH, AcOMe, EtOH and dioxane at t = 5 h, respectively. The f_{AcOEt}, f_{MeOH}, f_{AcOMe}, f_{EtOH}, and $f_{dioxane}$ are the response coefficients of AcOEt, MeOH, AcOMe, EtOH and dioxane, respectively (Table 2.5).

2.3. Catalysts preparation and activities tests

2.3.1. Catalysts preparation

Magnesol® catasorb and polysorb were kindly provided by the Dallas group of America©. The first one contains Cl (<0.5%) and Na (<2%) impurities, the second one, sulfate (<1.5%) impurities but they have the same specific surface area. Both have the same reactivity therefore the influence of these impurities on the catalysis can be neglected. The results for Magnesol® catasorb will be displayed with the label "Mg silicate (com)".

Two other magnesium silicate samples were synthesized using sol-gel and coprecipitation methods. The molar ratio Mg/Si is chosen to be similar to the one of Mg silicate (com), *i.e.* 0.29.

Sol-gel magnesium silicate, labelled as "Mg silicate (sg)", is obtained with a procedure adapted from Kalampounias *et al* [39]. It consists in an hydrolysis and polycondensation of tetraethyl orthosilicate (TEOS) (20 mL, Sigma-Aldrich, 99.999%) with magnesium nitrate ($Mg(NO_3)_2.6H_2O$) (9.9 g, Sigma-Aldrich, 98%) and nitric acid (HNO_3), (2N, 13.44 mL, VWR AnalaR Normapur). Nitric acid was used to catalyze the TEOS hydrolysis, using a molar ratio $\frac{H_2O+HNO_3}{TEOS} = 8$. After the addition of all reactants in a Teflon bottle, the solution was stirred for 1 h at room temperature to allow the hydrolysis and polycondensation reactions, until the formation of a viscous gel. The gel was aged, stored in the sealed Teflon bottles and kept at 60 ^oC for 3 days, then it was dried in three stages at 60 ^oC, 90 ^oC and 130 ^oC for 20 h, 24 h and 40 h, respectively and calcined by steps at 100 ^oC, 400 ^oC and 700 ^oC for 1 h, 2 h and 5 h, respectively. The temperature increase rate was 0.1 $^oC\ min^{-1}$ for all heating procedures. The Mg/Si mole ratio determined by X-ray fluorescence is 0.32.

Coprecipitated magnesium silicate, labelled as "Mg silicate (cp)", was obtained through a method adapted from Ozgul et al.[40]. A solution of magnesium chloride ($MgCl_2 \cdot 6H_2O$, 50 mL, 0.5 $mol.L^{-1}$, Sigma-Aldrich, ≥ 99%) was added dropwise into 10 ml of sodium silicate solution (10% NaOH and 27% SiO_2 wt.%, Sigma-Aldrich, reagent grade). A white precipitate

was formed immediately. After 1 h, the precipitate was filtered, washed with 3 x 200 mL of distilled water and dried overnight at 60 ^{o}C. X-ray fluorescence of the sample indicate that the Cl concentration in the solid is lower than 0.1% and lower than 1% for Na. The Mg/Si mole ratio determined by X-ray fluorescence is 0.27.

2.3.2. Catalytic performance of magnesium silicates

First of all, the potential occurrence of homogeneous catalysis by dissolution of the material in the reaction mixture was tested by removing the solid catalyst by means of centrifugation. The separated liquid phase was again used under the same reaction conditions overnight without addition of catalyst. It is confirmed that the catalytic process is purely heterogeneous on the three magnesium silicates as no additional conversion was observed in these conditions.

Catalytic tests with these three silicates are performed and the results are given in Table 2.6. It can be observed that the two more efficient are coprecipitated and commercial Mg silicates while a much lower activity is observed for the sol-gel Mg silicate. Although silicate (cp) and (com) exhibit high specific surface area, they still show high activity if the conversions are divided by specific surface area (SSA).

Table 2.6: Catalytic performance and specific surface area of the three magnesium silicates.

Samples	**Conversion (%)**	**Specific surface area ($m^2 \cdot g^{-1}$)**	**Conv./SSA ($‰ \cdot g \cdot m^{-2}$)**
Mg silicate (cp)	34	447	0.76
Mg silicate (com)	29	421	0.69
Mg silicate (sg)	8	295	0.27

2.4. Characterisation of acido-basic properties

In order to understand the key parameters influencing the activity of catalysts, the acido-basic properties of the different solids used are checked. It should be noted that “acidity” or “basicity”, usually defined by the position of an equilibrium, are thermodynamic concepts. Nevertheless, in catalysis, thermodynamic equilibria are rarely achieved for each of the elementary steps, even the proton transfer steps. The ability to react rapidly with a base or acid

site is therefore a fundamental parameter, that can be evaluated by studying the reactivity of solids in model reactions.

We employ 2-methylbut-3-yne-2-ol (MBOH) conversion test to characterize acido-basic properties of magnesium silicate catalysts (see Figure 1.10 in chapter 1). Magnesium silicates have a very interesting reactivity since products of acidic route (Mbyne) and those of basic route (acetone and acetylene) are detected together (Figure 2.4). However, the ratio of the products resulting from acidic and basic routes is not the same for all the silicates. For similar conversion, the coprecipitated silicate gives 78% selectivity on the basic route compared to 19% for the sol-gel. Moreover, the commercial magnesium silicate is slightly more active than the coprecipitated one but quite similar in terms of selectivity. Thus, among these three catalysts, the two most active in transesterification are those exhibiting the best basic selectivity in MBOH conversion, while, the sol-gel magnesium silicate, that gives 81% selectivity in Mbyne, is much less active in transesterification.

In conclusion, it should be first reminded that the results of the preliminary work given in chapter 1 show that there is no strict correlation between the catalytic activity in liquid phase and the acido-basic properties as the strongest base, MgO, is less active than magnesium silicate. Nevertheless, it can be noted that magnesium silicates exhibit both acid and base sites and that a first distinction of the less active catalyst (Mg silicate (sg)) is that it is more acidic than basic. We cannot conclude here on the mechanism of the reaction and on the required nature of the active sites but, obviously, Mg silicate (sg) exhibits different surface properties. Structural characterization, *i.e.* X-ray spectroscopies, scanning electron microscopy, ^{29}Si and ^{25}Mg NMR studies and DRIFT spectroscopy will be thus used in order to identify the differences among these materials.

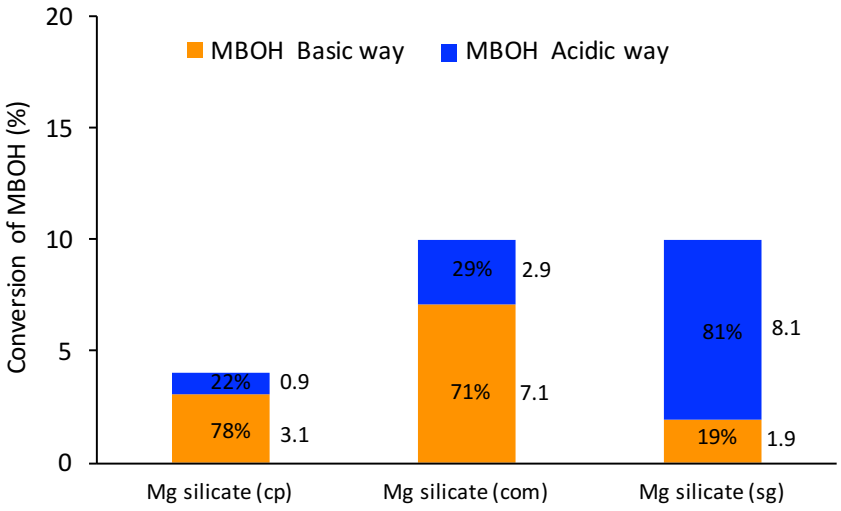

Figure 2.4: Conversion of MBOH following the acidic and basic route for the magnesium silicates.

2.5. Structural characterization of magnesium silicates samples

2.5.1. X-ray spectroscopies

The X-ray diffractrogram patterns of the three silicates are given in Figure 2.5. Only the silica broad band is visible on the Mg silicate (sg) diffractogram. On the opposite, the pattern of Mg silicates (com) shows some broad peaks at 2θ =35°, 60° and 72°. Those peaks are also present on the Mg silicate (cp), even if they are less pronounced. Literature ascribed those broad peaks together with an additional one at 2θ = 20°, which in our case disappears in the large band of amorphous silica[28,41,42], to a structure named "Magnesium Silicate Hydrate" (MSH).

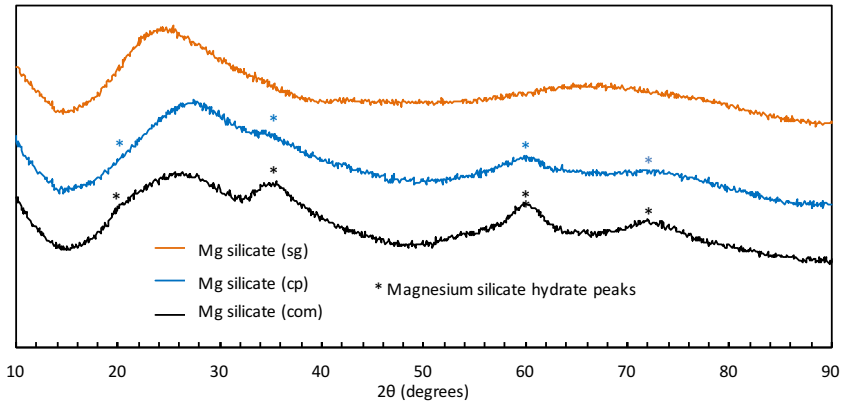

Figure 2.5: XRD patterns of the Mg silicates

MSH was described as poor crystalline phase due to the low intensity and broad XRD signals at 2θ = 20°-22°, 24°-27°, 35°-39° and 60°-62°[26–28,30,43,44]. Roosz et al.[28] synthesized two MSH samples with Mg/Si mole ratio of 0.6 (MSH0.6) and 1.2 (MSH1.2) by mixing MgO, amorphous silica and water, followed by one year's curing. They carefully clarified the crystal structure of MSH by considering results from X-ray diffraction, modeling XRD patterns and ^{29}Si MAS NMR spectroscopy. In the XRD patterns, some asymmetric peaks with an intensity rising sharply on the low-angle side and decreasing slowly on high-angle side, indicate that MSH has lamellar and turbostratic structures. A weak reflection at 2θ = 7.1° (12.45 Å) was observed in the XRD pattern of MSH1.2 but is absent in that of MSH0.6. This reflection indexed as (001) reflection is corresponding to the layer-to-layer distance. Thus it can be concluded that MSH1.2 has stacked layers, visible in TEM, but MSH0.6 consisted of isolated layers. Thanks to the XRD modeling, authors found that the ratio between the peaks at 2θ = 20° and 2θ = 35° decreases when the occupancy of silica tetrahedral decreases. Thus, MSH1.2 is shown to be more defective than MSH0.6. The XRD peak at 2θ = 25° can be linked either to amorphous silica or to MSH. ^{29}Si NMR was found to be a good tool to differentiate between both species. Moreover, according to the quantity of Q^2 and Q^3 (Q^n represents the Si atom which is bonded to four oxygen atoms and n is the number of Si neighbors) obtained by ^{29}Si NMR deconvolution, the authors proposed a schematic particle for MSH0.6, which showed a particle size similar to that obtained by XRD modeling with coherent scattering domain size of 2.4 nm along **a** axis and 1.6 nm along **b** axis. This phase appears to be structurally close to nanocrystalline turbostratic 2:1 Mg-Si phyllosilicates.

This phase is evidenced during the synthesis of talc, a 2:1 Mg-Si phyllosilicate. At early stages of talc synthesis, a MSH-like structure was observed. Its XRD pattern showed broad peaks at 2θ = 20°-22°, 24°-27°, 35°-39° and 60°-62°. After 60 days of hydrothermal treatment, these peaks became sharp and crystalline phase of talc formed. Furthermore, particles grew up from, rather fibrillar structure of around 100 nm, to regular plates of around 3 μm[45]. From the above literature, MSH can be described as a talc-like structure, consisting in magnesium surrounded by an octahedron formed by oxygen, sandwiched between two silicate layers. But this phase is poorly crystallized, with defects, *e.g.* vacant Si tetrahedral sites, numerous edges (due to smaller size than crystalline talc), bending layers or isolated layer[28]. A simple putative representation of the Si-O-Mg skeleton is given in Figure 2.6.

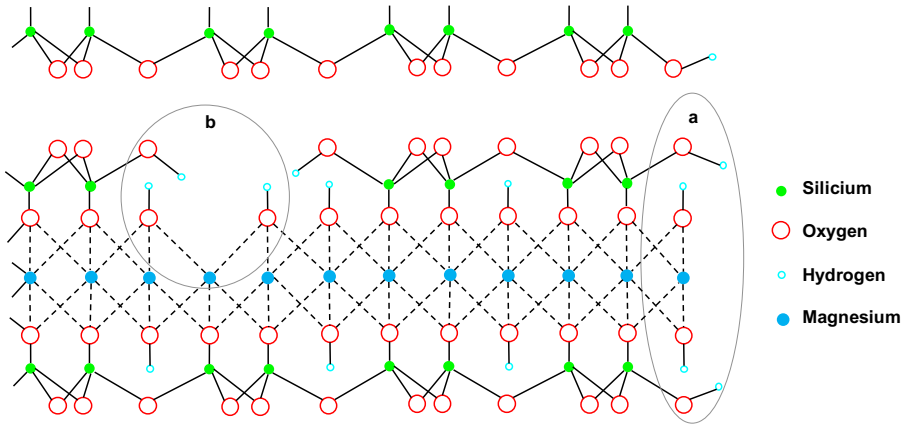

Figure 2.6: MSH structure with edges (a), and vacant Si tetrahedral sites (b).

Compared to mechanical-chemical dehydration method, MSH synthesized through coprecipitation method showed a very weak peak at $2\theta = 20°$ but a considerable broad peak at $2\theta = 25°$ and large intensity peak at $2\theta = 35°$ (Figure 2.5). Thus it contains amorphous silica and the low ratio between the peaks at $2\theta = 20°$ and $2\theta = 35°$ indicated the existence of numerous vacant Si tetrahedral sites.

Table 2.7 gathered the magnesium and silicon content of the surface (through XPS) and within the catalyst (through XRF). It can be seen from these data that sol-gel magnesium silicate presents a homogenous repartition of the magnesium with a Mg/Si ratio around 0.33 similar to the one found in the bulk, whereas commercial and coprecipitated Mg silicates show enriched magnesium content in the surface compared to the one observed on the whole solid.

The MSH phase is usually obtained for Mg/Si ratios higher than 0.5[26,28]. Therefore, the MSH structures observed by XRD in the commercial and coprecipitated catalysts are more likely to be located on the surface, as only those regions have a Mg/Si ratio high enough. In the case of the sol-gel sample no crystallized phase was detected by XRD and the composition of material seems to be more homogeneous.

Table 2.7: Mg/Si ratio of the magnesium silicates.

Samples	Mg/Si molar ratio (XRF)	Mg/Si molar ratio (XPS)
Mg silicate (cp)	0.268	0.450
Mg silicate (com)	0.290	0.485
Mg silicate (sg)	0.321	0.332

2.5.2. Scanning electron microscopy

The images in Figure 2.7 confirm the distinction observed by the X-ray techniques. Indeed, Mg silicate (sg) surface is smooth whereas the ones for the (cp) and the (com) are very corrugated. It is in line with a very homogeneous composition of the sol-gel particle and the presence of poorly crystalline phases over the surface of Mg silicate (com) and (cp). Chiang and co-workers[46] as well as Tonelli and co-workers[47] observe the same kind of structure. According to Chiang et al., the MSH forms globules of a few nanometers (the mean value of their size being 3 nm) which corresponds to what is shown for Mg silicate (com) and (cp).

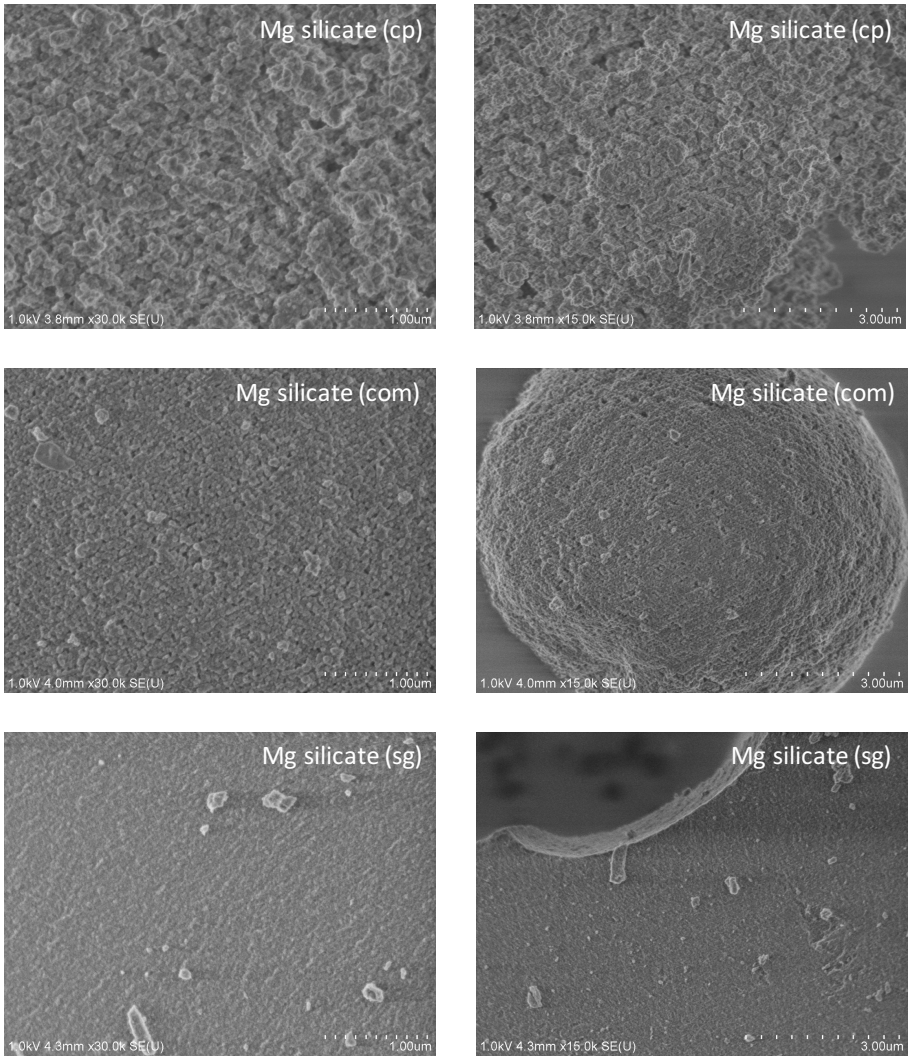

Figure 2.7: SEM images of Mg silicate (cp), (com) and (sg).

2.5.3. ^{29}Si and ^{25}Mg NMR study

To go further, $\{^{1}H - ^{29}Si\}$ direct polarization (DP) experiments, in Figure 2.8 were performed. As reported in the literature[28,47–52], the ^{29}Si MAS NMR spectra (Figure 2.8) can be

decomposed in two ranges. The resonances from -112 ppm to -99 ppm and -98 to -70 ppm are attributed respectively to silicates without direct connection to magnesium (labelled SiOSi), and silicate with at least one oxygen connected to magnesium (labelled SiOMg). In addition to this first classification, the signals recorded by ^{29}Si MAS NMR experiments can be classified into Q^n species (where Q represents the Si atom which is bonded to four oxygen atoms and n is the number of Si neighbors)[53]. For the SiOSi, the two broad peaks centered to around -110 ppm and -101 ppm are assigned to completely condensed species Q^4_{SiOSi} ($Si(OSi)_4$) and Q^3_{SiOSi} silica species ($Si(OSi)_3(OH)$), respectively[47,50,52,53]. For the SiOMg silicates, due to structural deformations, the decomposition is more difficult because each type of Q^n may consist of different contributions[28,47,49–51,54]. According to the literature[28,47,50,51], it is possible to define three zones for the SiOMg phase: from -89 to -98 ppm for Q^3_{SiOMg} species (*i.e.* $Si(OSi)_3(OMg)$), from -82 to -88 ppm for Q^2_{SiOMg} species (*i.e.* $Si(OSi)_2(OMg)(OH)$) and from -70 to -81 ppm for Q^1_{SiOMg} species (*i.e.* $Si(OSi)(OMg)(OH)_2$). ^{29}Si spectra of Mg silicates (com) and (cp) (Figure 2.8A-B), show clearly overlapping signals at around -94 ppm, which are ascribed to different Q^3_{SiOMg} sites. Moreover, one peak was identified at -85 ppm, due to Q^2_{SiOMg} site[49,50,52,54] and two peaks were found at around -80 ppm which can be attributed to different Q^1_{SiOMg} species.[47] The Mg silicate (sg) sample (Figure 2.8C) appears to have the same contributions but the two peaks at -101 ppm (Q^3_{SiOSi}) and -110 ppm (Q^4_{SiOSi}) account for larger proportion which is consistent with the XRD result that shows a broad peak of silica in Mg silicate (sg).

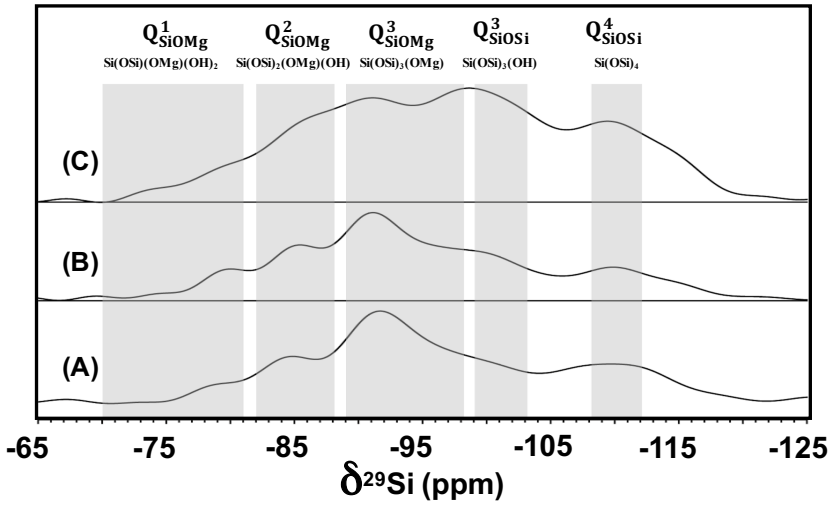

Figure 2.8: ^{29}Si DP MAS NMR spectra of (A) Mg silicate (com), (B) (cp) and (C) (sg).

Therefore, ^{29}Si MAS NMR spectra confirm the presence of silicates connected (SiOMg) and not connected (SiOSi) to magnesium in all samples. The spectra of Mg silicate (com) and Mg silicate (cp) are very similar (Figure 2.8A-B), they show that the proportion of silicates bond to magnesium phase is large. These silicates are essentially constituted by Q^3 species $Si(OSi)_3(OMg)$), branching silicate chain sites with the structural deformation expected for a MSH phase [28,47,50,51]. In the Mg silicate (sg) sample (Figure 2.8C) the silicates only connected to other silicates are more important and the contribution of silicates connected to magnesium is broader, that reflects a very disordered structure.

Due to the low natural abundance (10%), quadrupolar nature (I = 5/2) and low resonance frequency of magnesium, ^{25}Mg NMR spectra are more difficult to record and explain than ^{29}Si spectra[55,56]. The spectra of the three samples show only one peak (Figure 2.9). The broadening of the signal is induced by quadrupolar interaction and the slightly asymmetrical shape of the center band corresponds to a distribution in quadrupolar coupling parameters[57]. The lineshape simulation with Czjzek model for Mg silicate (com) gives an isotropic chemical shift, δ_{iso} = 26 ppm and a quadrupolar coupling constant, C_Q = 3.5 MHz, in good agreement with Nied et al[50]. values. The parameter values of Mg silicate (cp) are very close to those of Mg silicate (com), δ_{iso} = 26 ppm and C_Q = 3.8 MHz. But the fitted parameters for Mg silicate (sg) sample are significantly different, δ_{iso} = 31 ppm and C_Q = 6.9 MHz.

The large increase of quadrupolar coupling constant of Mg silicate (sg) (twice as large that Mg silicate (com) and Mg silicate (cp)) suggests large distortion of the local coordination[55,56]. This is in line with the formation of MSH phase only for Mg silicate (cp) and Mg silicate (com) in which the magnesium occupies octahedral positions, giving mainly Q^3 species $Si(OSi)_3(OMg)$ in ^{29}Si spectra, therefore with a small quadrupolar coupling.

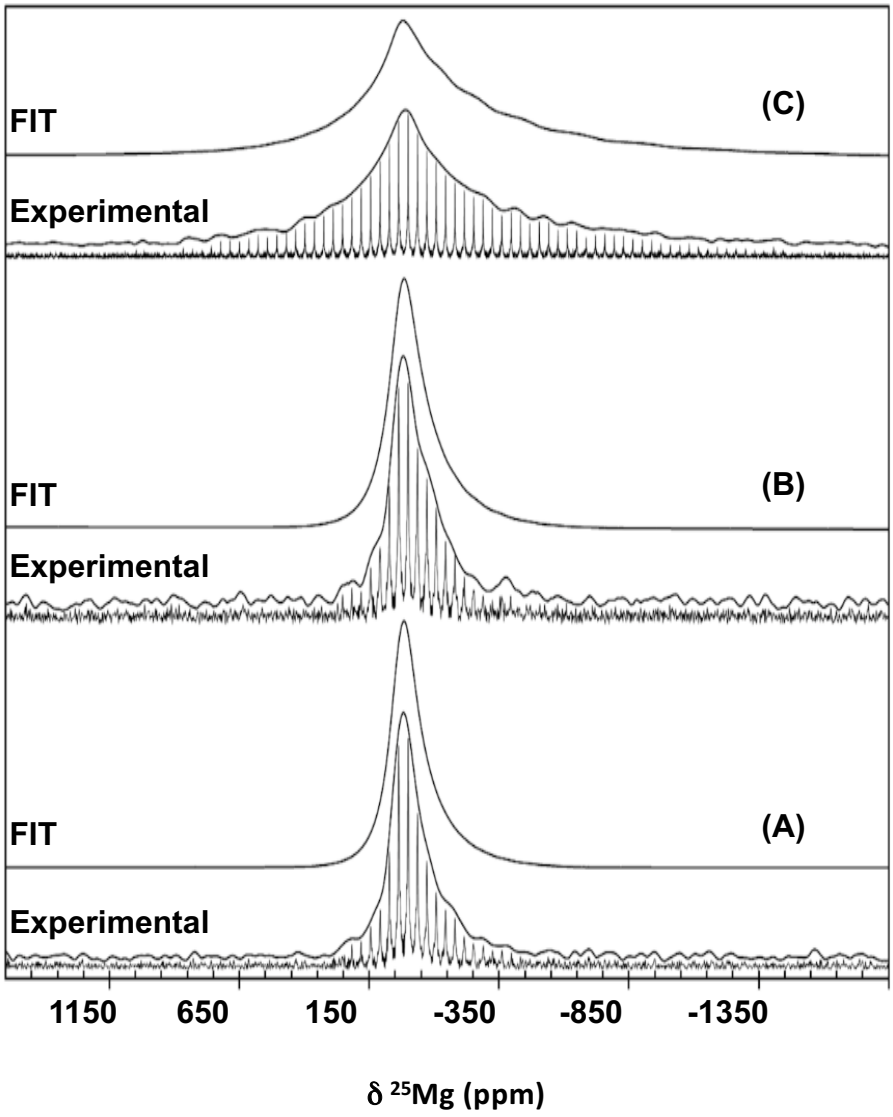

Figure 2.9: ^{25}Mg WURST-QCPMG NMR spectra of (A) Mg silicate (com), (B) (cp) and (C) (sg). Experimental spectra are composed by spikelet spectrum (bottom) and simulated spectrum (top). The spectra "FIT" are the optimum decomposition obtained with Dmfit software

2.5.4. Diffuse reflectance infrared Fourier transform spectroscopy characterization

Figure 2.10 shows the Diffuse reflectance infrared Fourier transform (DRIFT) spectra of the silicates, both taken at 140 °C, before and after a 350 °C pretreatment, respectively. After pretreatment, the contribution of adsorbed molecular water (1630 cm^{-1})[50] disappeared but a broad absorbance in the zone associated with O-H elongations (3000-3800 cm^{-1}) remains for all the samples, similar to the contribution usually found on pure silica. However, a sharp band emerges at 3737 cm^{-1} for all the samples and a second one at 3672 cm^{-1} for the Mg silicate (com) and, in a lower extend, for the Mg silicate (cp). Those two bands can also be seen on the samples pretreated only at 140 °C but were more difficult to recognize because of the presence

of residual molecular water adsorbed in these conditions. The band located at 3737 cm^{-1} is in the range observed for silanols over silica[47] and should be attributed to OH stretching of silanols species that can be in close proximity to magnesium cations. The contribution at 3672 cm^{-1} was previously assigned to OH stretching in the talc structure[58], or to similar structures[50] and is therefore compatible with the presence of MSH structure. A band at 1720 cm^{-1} appears then, that is attributed to Si-OH vibrations[47].

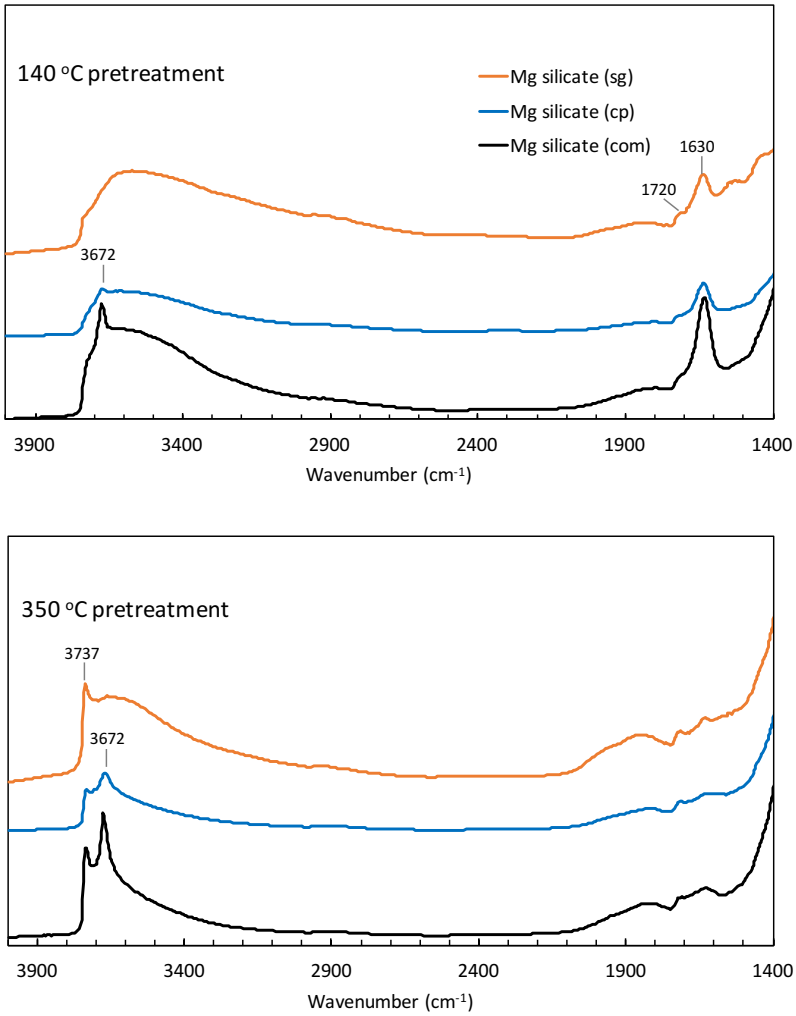

Figure 2.10: DRIFT spectra of the Mg silicates after 140 °C and 350 °C pretreatment.

2.5.5. Conclusion on the characterization of the magnesium silicates samples

These characterizations enlighten that the three magnesium silicates used in this work, exhibit different surfaces as shown by the characterization results obtained. From XPS results, it is clearly shown that Mg silicate (com) and Mg silicate (cp) surfaces are enriched in magnesium while Mg silicate (sg) exhibits on its surface the same Mg/Si ratio as in the bulk.

XRD and DRIFTS give coherent data showing the formation of MSH on Mg silicate (cp) and on Mg silicate (com), in agreement with the possibility of the presence at their surface of talc sheet with defective silicate layers. However, no MSH phase is identified in Mg silicate (sg) by XRD and DRIFTS. Moreover, ^{29}Si and ^{25}Mg NMR confirms the similarity of Mg silicate (cp) and (com) and is in line with a Mg environment more ordered than in Mg silicate (sg).

2.6. Discussion: a bifunctional catalyst

From the results shown in Figure 2.4, we can come back on the acido-basic properties of the three Mg silicates samples revealed by the selectivity of the MBOH conversion on the three magnesium silicates. The ratio of the conversion through the acidic way over the conversion through the basic route is 4.3 for the Mg silicate (sg), 0.4 for Mg silicate (com) and 0.3 for Mg silicate (cp). It is known that magnesium silicate may possess both acidic and basic sites depending on the way of synthesis[59,60]. Indeed, silanol groups over silica are mostly acidic and ionic oxygen ions in magnesium oxide are basic[61]. The repartition of the silica tetrahedrons and the magnesium, and their coverage with hydroxyl groups, carbonates or water will determine the exact acid-base nature of the surface. We find here that the samples exhibiting the MSH phase (com) and (cp) are more selective in MBOH conversion towards the basic way than the sol-gel sample. The MSH phase that was characterized in the section 2.5 is usually described as short talc sheets with defective silicon tetrahedra layers. These defects, localized at the surface of the material may give accessibility to the octahedral magnesium layer, that may generate surface basicity directly or by means of hydroxyl or carbonate groups.

This heterogeneous catalyst is thus bifunctional and offers on the same surface acidic and basic active sites. Acids and bases known to catalyse transesterification in homogeneous catalysis can cooperate on an inorganic surface: for example, when the acidic catalysis activates the ester through the oxygen of the carbonyl bond, the basic catalysis often activate the alcohol through its deprotonation. Both combined may improve the nucleophilic addition of the alcohol or of the alcoholate over the ester. Such a mechanism could occur on magnesium silicates exhibiting MSH that possess both acid and base sites. With strong base like MgO, an Eley-Rideal mechanism is operating as shown in the literature[34], but on weak bases like magnesium silicates, activation of the ester on acidic sites may be necessary. The sol-gel sample on which no MSH phase was detected, is not enough basic comparing the two other silicates that may explain its lowest activity in liquid phase transesterification.

2.7. Kinetic study

2.7.1. Deactivation behaviour of catalyst

In order to get insights on the reaction mechanism on bifunctional catalyst magnesium silicates, we will focus on Mg silicate (com) to study the kinetics of the reaction.

The deactivation of the catalyst, linked to the disappearance of active sites or to their poisoning by chemical species which adsorb on the surface of the catalyst, usually happens. It is thus necessary to check whether deactivation accurs in the operating conditions. The deactivation behavior of catalyst is then studied. As shown in Figure 2.11, the conversion of AcOEt raises with the increase in the reaction time. It is interesting to note that, during the first 5 hours, the conversion increases rapidly and linearly with the reaction time showing that the reaction rate is constant so that no significant deactivation occurs.

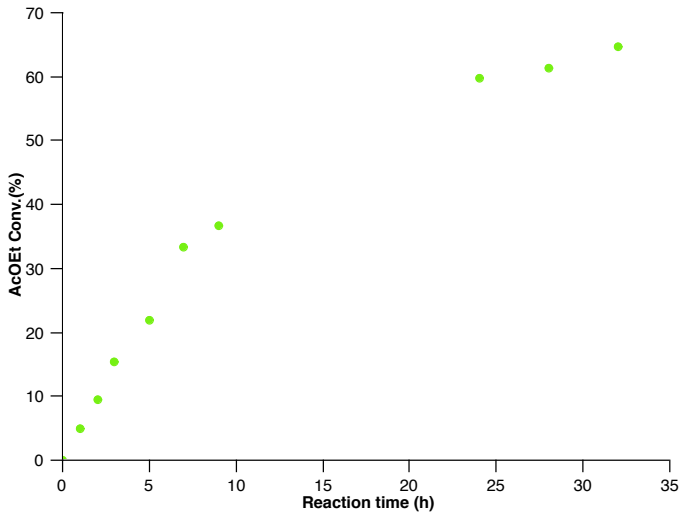

Figure 2.11: The conversion of AcOEt as a function of reaction time on Mg silicate (com).

To check the stability of the catalyst during the reaction, the catalyst after 5 hours of reaction time (spent Mg silicate (com)) is characterized by XRD and Infrared spectroscopy. Comparing the XRD patterns of fresh and spent Mg silicate (com), one can find that the structure of catalyst experiences no significant alteration during the reaction (Figure 2.12).

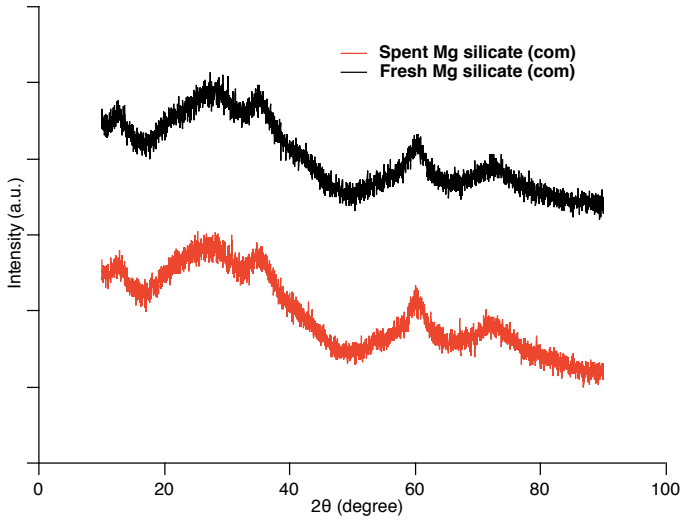

Figure 2.12: XRD patterns of fresh and spent Mg silicate (com).

Figure 2.13 shows the IR spectra of fresh and spent Mg silicate (com). The spectra were taken at 50 ^{o}C under Ar flow. In each spectrum three bands can be observed, at 3800 - 3000, 1636 and 1230 cm^{-1}. The broad band from 3800 to 3000 cm^{-1} was attributed to OH stretching[29,44]. The contribution at 1636 cm^{-1} was assigned to H-O-H bending vibrations of molecular bound water[26,27,29,44]. The band at 1230 cm^{-1} originates from Si-O stretching vibrations[26,44]. Both of the fresh and spent Mg silicate (com) show similar IR spectra. When zooming on the 4000 - 2800 cm^{-1}, two small peaks at 2850 and 2950 cm^{-1} are observed on the spent catalyst (Figure 2.14), which were ascribed to CH_3 symmetric and asymmetric stretching vibrations, respectively[62]. The CH_3 may come from methanol, which adsorbed on the surface of catalyst during the reaction.

From the XRD and IR spectroscopy, it can be concluded that, during 5 hours reaction, the structure of catalyst does not change, and little to no organics covered on the active sites. So it is reliable to directly use the first 5 hours reaction data to calculate reaction rate rather than considering the effect of deactivation.

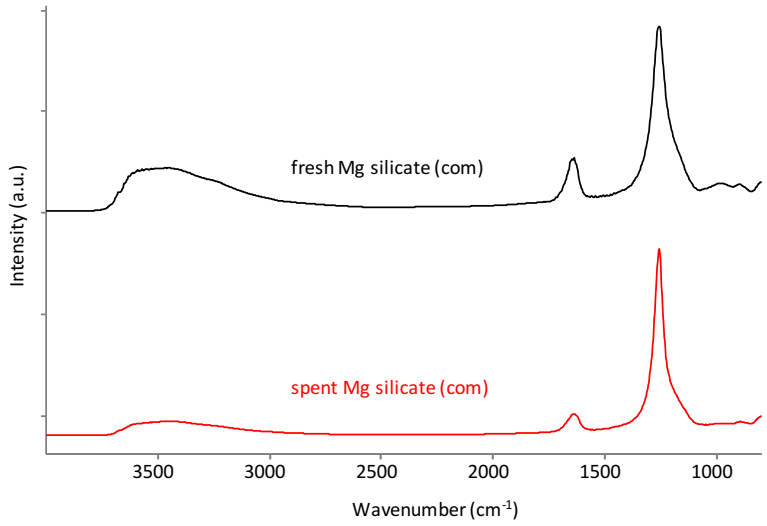

Figure 2.13: Infrared spectra of fresh and spent Mg silicate (com): 3800 - 1000 cm^{-1}.

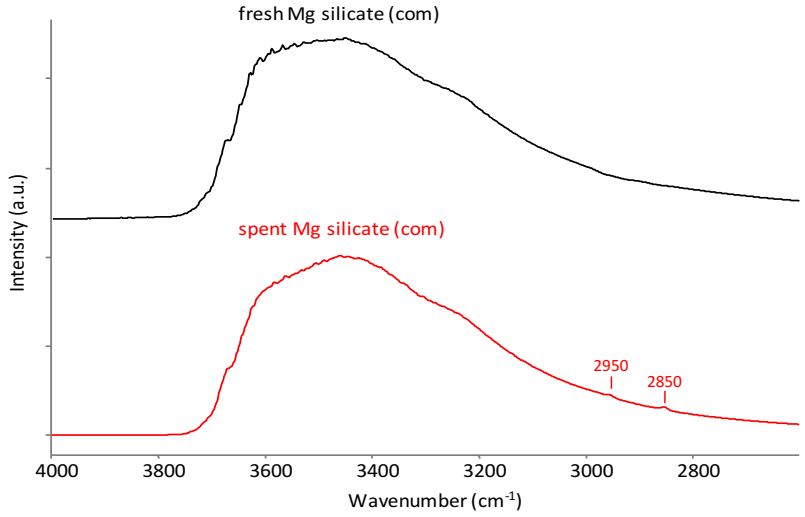

Figure 2.14: Infrared spectra of fresh and spent Mg silicate (com): 4000-2800 cm^{-1}.

2.7.2. Calculation of the order of reaction in ethyl acetate

To determine the order of the transesterification reaction in liquid phase with respect to the concentration of ethyl acetate, the kinetics will therefore be studied at a constant methanol concentration and with a variable ester concentration as indicated in Table 2.8.

Table 2.8: Volume and concentration of reactants for kinetic study.

Entry	Volume (mL)			AcOEt Concentration (mol/L)
	MeOH	AcOEt	Dioxane	
1	10	0.3	1	0.272
2	10	0.5	1	0.445
3	10	1.0	1	0.853
4	10	1.5	1	1.228

The AcOEt concentration that evolves with the reaction time, is shown in Figure 2.15. As presented in the previous section, during the first 5 hours reaction, the conversion is linear in the reaction time. So the reaction rates during the first 5 hours are very close to the initial reaction rates, which can be obtained from the slopes of the dotted lines as shown in Figure 2.15.

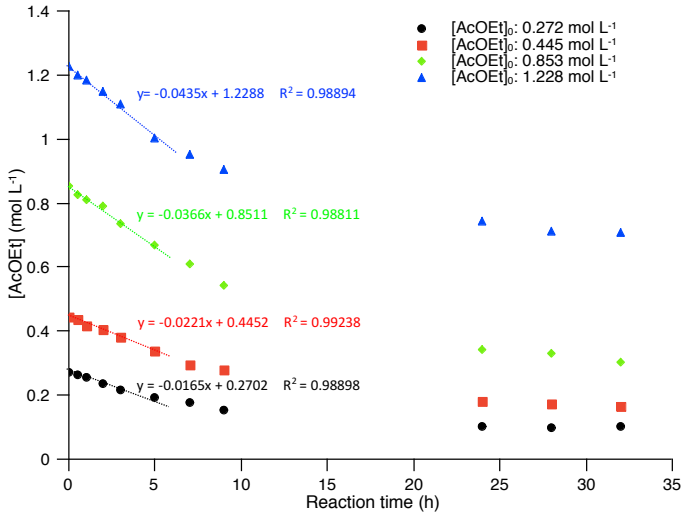

Figure 2.15: Evolution of AcOEt concentration with the reaction time on Mg silicate (com).

The reaction rate is calculated by Eq. 2.9:

$$r = \frac{-\mathrm{d[AcOEt]}}{\mathrm{dt}} = \frac{-\mathrm{d[MeOH]}}{\mathrm{dt}} = \mathrm{k\,[AcOEt]^{\alpha}[MeOH]^{\beta}} \qquad \text{Eq. 2.9}$$

k: reaction rate constant; α, β: orders of reaction.

To simplify the equation, and since the ratio MeOH/AcOEt is very high, we consider that the concentration of methanol is constant, methanol being consumed very little. This

concentration therefore does not intervene in the kinetics and the rate of the reaction depends solely on the limiting reagent which is ethyl acetate.

The reaction rate equation is then simplified to Eq. 2.10:

$$r = k'[AcOEt]^{\alpha} \qquad \text{Eq. 2.10}$$

Here, $k' = k\,[MeOH]^{\beta}$

So the initial reaction rate $r_0 = k'[AcOEt]_0{}^{\alpha}$. In order to determine the order α, it is written in the form of logarithm (Eq. 2.11).

$$\ln r_0 = \ln k' + \alpha \ln [AcOEt]_0 \qquad \text{Eq. 2.11}$$

If we plot the curve $\ln r_0 = f(\ln[AcOEt]_0)$, we should obtain a line whose slope is equal to the order of the reaction (α). Figure 2.16 shows these results based logarithmic curves with a good correlation coefficients (0.99428). The curve indicates that the reaction has a reaction order of 0.66 in ethyl acetate.

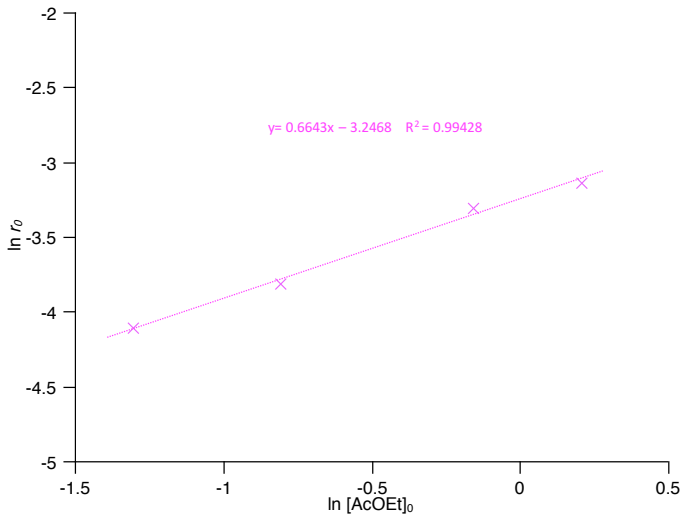

Figure 2.16: Logarithm of the initial reaction rate as a function of the logarithm of initial AcOEt concentration.

2.7.3. Interpretation of reaction order in ethyl acetate

Our objective is here to find a mechanism that may fit with the experimental data. Several models proposed in the literature will therefore be studied to observe if such order can be obtained.

2.7.3.1 Eley-Rideal mechanism with adsorption of methanol

This mechanism, assuming that methanol is adsorbed on surface sites of MgO and reacts with ethyl acetate in liquid phase was proposed by Dossin et al.[34] Here if we adopt this mechanism involving MSH, it is shown in Figure 2.17.

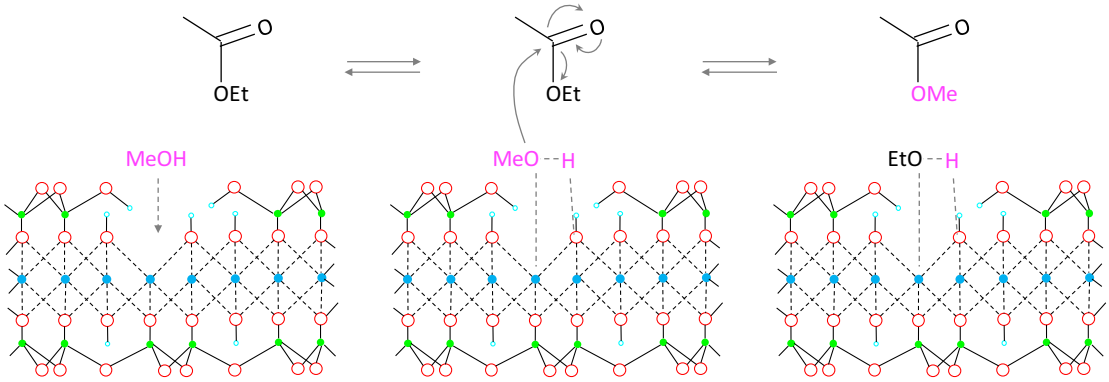

Figure 2.17: Eley-Rideal mechanism for the transesterification of ethyl acetate with methanol catalyzed by magnesium silicate.

Based on this mechanism, the overall reaction consists of three elementary reactions: (1) adsorption of MeOH, (2) reaction of adsorbed MeOH with AcOEt, (3) desorption of EtOH.

$$(1)\quad MeOH + * \underset{k_{-1}}{\overset{k_1}{\rightleftharpoons}} MeOH*$$

$$(2)\quad MeOH* + AcOEt \underset{k_{-2}}{\overset{k_2}{\rightleftharpoons}} EtOH* + AcOMe$$

$$(3)\quad EtOH* \underset{k_{-3}}{\overset{k_3}{\rightleftharpoons}} EtOH + *$$

k_1, k_{-1}, k_2, k_{-2}, k_3, k_{-3} are the reaction rate constants of corresponding elementary reactions. * is the sites that are not occupied. MeOH* is the adsorbed MeOH. EtOH* is the adsorbed EtOH.

If the elementary reaction (2) is considered as rate determining, the overall reaction rate is equal to the rate of elementary reaction (2), as shown in Eq. 2.12. Besides, the elementary reactions (1) and (3) are considered to be equilibrium state. Then [MeOH*] and [EtOH*] can be calculated by Eq. 2.13 and Eq. 2.14, repectively.

$$r = \mathrm{k}_2[\mathrm{MeOH}*][\mathrm{AcOEt}] - \mathrm{k}_{-2}[\mathrm{EtOH}*][\mathrm{AcOMe}] \qquad \text{Eq. 2.12}$$

$$[\mathrm{MeOH}*] = \mathrm{K}_1[\mathrm{MeOH}][*] \qquad \text{Eq. 2.13}$$

$$[\mathrm{EtOH}*] = [\mathrm{EtOH}][*]/\mathrm{K}_3 \qquad \text{Eq. 2.14}$$

Where K_1 and K_3 is the standard equilibrium constant of MeOH adsorption and EtOH desorption, respectively. So $K_1 = k_1/k_{-1}$, $K_3 = k_3/k_{-3}$.

If the total number of sites is L, then Eq. 2.15 is obtained.

$$\mathrm{L} = [*] + [\mathrm{MeOH}*] + [\mathrm{EtOH}*] \qquad \text{Eq. 2.15}$$

From Eq. 2.12, Eq. 2.13, Eq. 2.14 and Eq. 2.15, the reaction rate is then deduced, as shown in Eq. 2.16.

$$r = \frac{\mathrm{Lk}_2\mathrm{K}_1[\mathrm{MeOH}][\mathrm{AcOEt}] - \mathrm{L}\,(\mathrm{k}_{-2}/\mathrm{K}_3)\,[\mathrm{EtOH}][\mathrm{AcOMe}]}{1 + \mathrm{K}_1[\mathrm{MeOH}] + (1/\mathrm{K}_3)[\mathrm{EtOH}]} \qquad \text{Eq. 2.16}$$

At the initial time, the quantities of products EtOH and AcOMe are very small, so the initial reaction rate could be expressed in Eq. 2.17. Now it can be obtained that the reaction order in ethyl acetate is 1, provided following the Eley-Rideal mechanism with adsorption of methanol. However, the reaction order from experiment is 0.66 (Figure 2.16), which is not consistent with this mechanism.

$$r_0 = \frac{\mathrm{Lk}_2\mathrm{K}_1[\mathrm{MeOH}]_0[\mathrm{AcOEt}]_0}{1 + \mathrm{K}_1[\mathrm{MeOH}]_0} \qquad \text{Eq. 2.17}$$

If the adsorption of MeOH is considered as rate determining, the overall reaction rate is equal to the rate of elementary reaction (1), as shown in Eq. 2.18.

$$r = \mathrm{k_1[MeOH][*] - k_{-1}[MeOH\ *]} \qquad \text{Eq. 2.18}$$

Besides, the elementary reactions (2) and (3) are considered to be at equilibrium state. Then Eq. 2.19 and Eq. 2.20 are obtained.

$$\mathrm{K_2} = \frac{\mathrm{[EtOH\ *][Acome]}}{\mathrm{[MeOH\ *][AcOEt]}} \qquad \text{Eq. 2.19}$$

$$\mathrm{K_3} = \frac{\mathrm{[EtOH][*]}}{\mathrm{[EtOH\ *]}} \qquad \text{Eq. 2.20}$$

From Eq. 2.15, Eq. 2.18, Eq. 2.19 and Eq. 2.20, the reaction rate is then deduced, as shown in Eq. 2.21.

$$r = \frac{\mathrm{Lk_1[MeOH]} - \frac{\mathrm{Lk_{-1}}}{\mathrm{K_2K_3}}\mathrm{[AcOMe][EtOH]/[AcOEt]}}{1 + \frac{1}{\mathrm{K_2K_3}}\mathrm{[Acome][EtOH]/[AcOEt]} + \mathrm{K_3[EtOH]}} \qquad \text{Eq. 2.21}$$

At initial time, r_0 is written:

$$r_0 = \mathrm{L\,k_1[MeOH]_0} \qquad \text{Eq. 2.22}$$

From the Eq. 2.22, it can be seen that the reaction order in ethyl acetate is 0. The two cases involving in Eley-Rideal mechanism with adsorption of methanol are displayed in Table 2.9. Neither of them fits with the experimental data.

Table 2.9: Reaction rates and reaction orders based on Eley–Rideal mechanism with MeOH adsorption.

Rate determining step	**Initial reaction rate**	**Reaction order versus AcOEt**
Elementary reactions (1)	$r_0 = \mathrm{L\,k_1[MeOH]_0}$	0
Elementary reactions (2)	$r_0 = \frac{\mathrm{Lk_2K_1[MeOH]_0[AcOEt]_0}}{1 + \mathrm{K_1[MeOH]_0}}$	1

The Eley-Rideal mechanism with ethyl acetate adsorption is not considered, because it is impossible that only ethyl acetate adsorbs on magnesium silicate that has both acid and base

sites. Moreover, from the IR spectra (Figure 2.14) methanol is observed to adsorb on the surface of catalyst after reaction.

Dossin et al.[34] studied the kinetics of transesterification of ethyl acetate with methanol on MgO, a strongly basic catalyst. Their experimental results fitted well with the Eley-Rideal mechanism. Different from the mechanism on strong base as MgO[34], on moderate bases as magnesium silicates that must involve acidic sites to adsorb the ester. Thus, we have to check the Langmuir-Hinshelwood mechanism.

2.7.3.3 Langmuir-Hinshelwood mechanism

The Langmuir-Hinshelwood mechanism involves a reaction between adsorbed MeOH and adsorbed AcOEt. On magnesium silicates with acido-basic properties, we make first the hypothesis that the MeOH and AcOEt adsorption sites (* and *' respectively) are different, the first one being a basic site and the second one an acidic site, as shown in Figure 2.18.

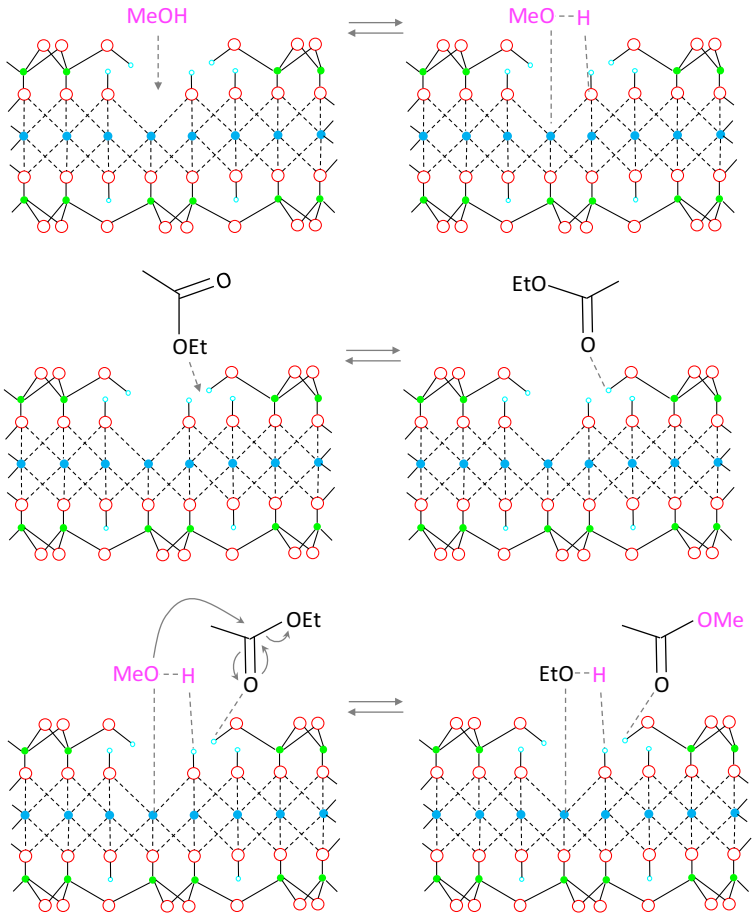

Figure 2.18: Langmuir-Hinshelwood mechanism for the transesterification of ethyl acetate with methanol catalyzed by magnesium silicate.

Based on this mechanism, the overall reaction consists of five elementary reactions: (1) adsorption of MeOH, (2) adsorption of AcOEt, (3) reaction between adsorbed MeOH and adsorbed AcOEt, (4) desorption of AcOMe, (5) desorption of EtOH.

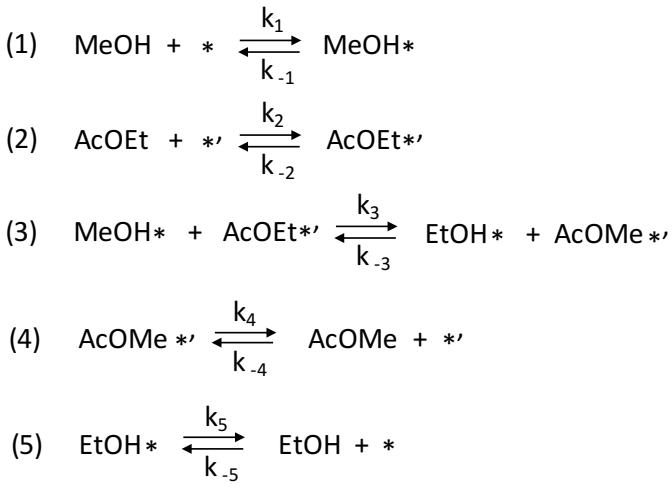

Regarding the elementary reaction (3) as rate determining, the reaction rate is written as Eq. 2.23.

$$r = k_3[\mathrm{MeOH}\,*][\mathrm{AcOEt}\,*'] - k_{-3}[\mathrm{EtOH}\,*][\mathrm{AcOMe}\,*'] \qquad \text{Eq. 2.23}$$

As at initial time, the amount of products EtOH and AcOMe are very small, so their adsorbed species EtOH∗ and AcOMe∗′ are neglected. Then the Eq. 2.23 is simplified as Eq. 2.24.

$$r = k_3[\mathrm{MeOH}\,*][\mathrm{AcOEt}\,*'] \qquad \text{Eq. 2.24}$$

Except the rate determining step, other elementary reactions are then considered to be at equilibrium state.

$$[\mathrm{MeOH}\,*] = K_1[\mathrm{MeOH}][*] \qquad \text{Eq. 2.25}$$

$$[\mathrm{AcOEt}\,*'] = K_2[\mathrm{AcOEt}][*'] \qquad \text{Eq. 2.26}$$

In addition, the total number of each site L and L’ are equal to:

$$\mathrm{L} = [*] + [\mathrm{MeOH}\ *] \qquad \text{Eq. 2.27}$$

$$\mathrm{L}' = [*'] + [\mathrm{AcOEt}\ *'] \qquad \text{Eq. 2.28}$$

Based on the Eq. 2.25, Eq. 2.26, Eq. 2.27 and Eq. 2.28, the reaction rates can be resolved and the initial reaction rate is shown in Eq. 2.29.

$$r_0 = \frac{\mathrm{k_3 L K_1 [MeOH]_0}}{1 + \mathrm{K_1 [MeOH]_0}} \cdot \frac{\mathrm{L' K_2 [AcOEt]_0}}{1 + \mathrm{K_2 [AcOEt]_0}} \qquad \text{Eq. 2.29}$$

Now it can be inferred that, from Eq. 2.29, this mechanism allows to obtain the reaction order in ethyl acetate between 0 to 1. Considering elementary reaction (1) or (2) as rate determining, the initial reaction rate are calculated as well and listed in Table 2.10.

Table 2.10: Initial reaction rates and reaction orders based on Langmuir-Hinshelwood mechanism involving two different kinds of sites.

Rate determining step	**Initial reaction rate**	**Reaction order versus AcOEt**
Elementary reactions (1)	$r_0 = \mathrm{k_1 L [MeOH]_0}$	0
Elementary reactions (2)	$r_0 = \mathrm{k_2 L' [AcOEt]_0}$	1
Elementary reactions (3)	$r_0 = \frac{\mathrm{k_3 L K_1 [MeOH]_0}}{1 + \mathrm{K_1 [MeOH]_0}} \cdot \frac{\mathrm{L' K_2 [AcOEt]_0}}{1 + \mathrm{K_2 [AcOEt]_0}}$	0-1

If MeOH and AcOEt adsorb on the same kind of sites, the initial reaction rates are determined by the same kind of calculations and listed in Table 2.11. It can be seen that when the elementary reaction (3) is considered as rate determining, it is also possible to obtain the reaction orders in ethyl acetate between 0 to 1.

Table 2.11: Initial reaction rates and reaction orders based on Langmuir-Hinshelwood mechanism involving one kind of sites.

Rate determining step	**Initial reaction rate**	**Reaction order versus AcOEt**
Elementary reactions (1)	$r_0 = \frac{\mathrm{k_1 L [MeOH]_0}}{1 + \mathrm{K_2 [AcOEt]_0}}$	< 0
Elementary reactions (2)	$r_0 = \frac{\mathrm{k_2 L [AcOEt]_0}}{1 + \mathrm{K_1 [MeOH]_0}}$	1
Elementary reactions (3)	$r_0 = \frac{\mathrm{k_3 K_1 K_2 L^2 [MeOH]_0 [AcOEt]_0}}{(1 + \mathrm{K_1 [MeOH]_0} + \mathrm{K_2 [AcOEt]_0})^2}$	0-1

From above discussion, it can be underlined that, two possibilities may fit with the experimental data in the case of Langmuir-Hinshelwood mechanism. For identification, we will try to fit the initial reaction rate equation with experimental data. Eq. 2.29 is then simplified considering the very high ratio of MeOH/AcOEt, as shown in Eq. 2.30.

$$\frac{1}{r_0} = \frac{1}{c} \cdot \frac{1}{[\mathrm{AcOEt}]_0} + \frac{\mathrm{K}_2}{c} \qquad \text{Eq. 2.30}$$

Here $c = \frac{k_3 L L' K_1 K_2 [MeOH]_0}{1 + K_1 [MeOH]_0}$

Then the curve $1/r_0$ as a function of $1/[\mathrm{AcOEt}]_0$ is plotted. As shown in Figure 2.19, $1/r_0$ is linear in $1/[\mathrm{AcOEt}]_0$ with good correlation coefficients (0.98957). It confirms that Eq. 2.29 is highly in accordance with the experimental data. The another possibility in Table 2.11 (elementary reaction (3) as rate determining), is also checked but it does not fit with the experiment data.

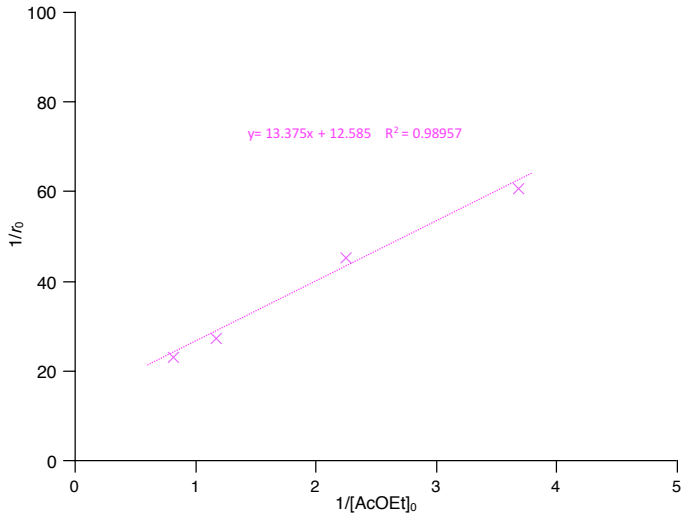

Figure 2.19: $1/r_0$ as a function of the $1/[\mathrm{AcOEt}]_0$.

In conclusion, we can reject the mechanism presented in the literature for the transesterification reaction on MgO, that only MeOH adsorbs on basic sites and reacts with AcOEt in liquid phase[34]. However, for magnesium silicate, based on the consistence of the experimental data with Langmuir-Hinshelwood mechanism, we propose that MeOH adsorbs on basic sites, meanwhile AcOEt adsorbs on acidic sites, and the reactions happen between these two adsorbed species, which is the rate determining step.

2.8. Influence of the nature of the reactants

In last section, we propose that the transesterificaction of ethyl acetate with methanol on magnesium silicate follows the Langmuir-Hinshelwood mechanism, based on the kinetic study. It would be interesting to further investigate the effect of carbon chain length of ester and alcohol on the reactivity. For this purpose, we will study the transesterification of ester such as ethyl acetate (AcOEt), ethyl butyrate (BuOEt), ethyl hexanoate (HeOEt) and ethyl laurate (LaOEt) with methanol. As shown in Table 2.12, it can be found that, similar to transesterification of AcOEt with MeOH, the activities of these three magnesium silicate catlyatsts show the same order for transesterification of BuOEt and HeOEt: Mg silicate (sg) < Mg silicate (com) < Mg silicate (cp). Moreover, for all the three catalysts, the conversions of esters decrease as the order: AcOEt > BuOEt ≈ HeOEt > LaOEt. These phenomena may confirm that the esters need to be adsorbed on the surface and react with adsorbed methanol as, if the esters in liquid phase directly react with methanol like in an Eley-Rideal mechanism, the reaction rate of different esters would show no significant distinction at the same initial concentration.

Table 2.12: Catalytic performances of magnesium silicates for transesterification of various esters with alcohols.

Catalyst	Ester + MeOH[a], Ester Conv. (%)				AcOEt + BuOH[b]
	AcOEt	BuOEt	HeOEt	LaOEt	AcOEt Conv.
Mg silicate (sg)	11	0.7	0.5	0	0
Mg silicate (com)	29	10.1	9.3	0	0
Mg silicate (cp)	38	13.9	14.8	0	0

[a] reaction conditions: temp., 60 ^{o}C; catalyst mass, 100 mg; MeOH, 0.2348 mol; ester, 0.0097 mol; reaction time, 5 h.

[b] reaction conditions: temp., 60 ^{o}C; catalyst mass, 46.5 mg; BuOH, 0.1093 mol; AcOEt, 0.0046 mol; reaction time, 5 h.

Transesterification of 1-butanol (BuOH) with ethyl acetate is studied to find out the effect of carbon chain length of alcohol. As shown in Table 2.12, the conversion of AcOEt decreases to zero when replace methanol with 1-butanol. Hattori et al. investigated the transesterification of alcohols with ethyl acetate using a variety of solid base catalysts to elucidate the activity of catalyst in relation with the type of alcohol. They found that over strong solid base catalysts, 2-propanol reacted much faster than methanol and that 2-methyl-2-

propanol only have a small reactivity. The authors interpret this behaviour considering that the abstraction of an H^+ from alcohol is easy even for 2-propanol over a strong base catalyst. But the stability of 2-propoxide anion is compared to methoxide anion, which results in the high reactivity of the 2-propoxide anion toward the adsorbed ethyl acetate. Steric hindrance of the alkoxide anion caused by bulky tertiary butoxide for attacking the adsorbed ethyl acetate may cause the low reactivity of 2-methyl-2-propanol. However, over weak solid base catalysts, methanol reacts faster than 2-propanol, and 2-methyl-2-propanol did not react with ethyl acetate. In our case, we observe the similar results that methanol is more active than 1-butanol on magnesium silicate with some weak basic sites. The steric hindrance of 1-butanol may be an important reason that the reactivity is so poor.

In conclusion, the investigation of the activity of the catalyst in relation with the type of esters and alcohols fits well with the kinetic study, and confirms that the transesterification reaction on magnesium silicate should obey the Langmuir-Hinshelwood mechanism rather than Eley-Rideal mechanism.

2.9. Conclusion

Magnesium silicate can catalyze a model reaction of transesterification using methanol and ethyl acetate in liquid phase. The highest conversions are found for coprecipitated magnesium silicate and for the commercial catalyst Magnesol®. Mg silicate (cp) and Mg silicate (com) convert MBOH towards acidic and basic ways. ^{29}Si and ^{25}Mg-NMR, IR, X-ray fluorescence and X-ray photoelectron spectroscopies, together with XRD show that those solids are covered with magnesium silicate hydrate, of which the structure is similar to talc sheet but with defective silicate layers. This phase could explain the peculiar reactivity of these bifunctional catalysts.

The kinetic study is performed and the reaction order in ethyl acetate is found to be equal to 0.66. This result implies that the transesterification reaction on the bifunctional catalysts as magnesium silicates obey to the Langmuir-Hinshelwood mechanism. A linear correlation between $1/r_0$ and $1/[AcOEt]_0$ further confirm that the reactants adsorbed on different sites. The distinct reactivities of various esters and alcohols also give an evidence that transesterification reaction on the bifunctional catalysts occur between adsorbed species.

The active MSH phase identified in the present study is highly hydroxylated. As it is known, in the case of MgO, carbonates and water adsorbed on its surface have a significant effect on its activity[63]. That is way on-going studies concerning the influence of the pretreatment of magnesium silicates before the reaction will be discussed in the next chapter.

References

[1] M. R. Avhad, J. M. Marchetti, *Catal. Rev.* **2016**, *58*, 157–208.

[2] D. M. Alonso, S. G. Wettstein, J. A. Dumesic, *Green Chem.* **2013**, *15*, 584.

[3] T. Dossin, M. Reyniers, G. Marin, *Appl. Catal. B Environ.* **2006**, *62*, 35–45.

[4] E. Leclercq, A. Finiels, C. Moreau, *J. Am. Oil Chem. Soc.* **2001**, *78*, 1161–1165.

[5] H. Hattori, M. Shima, H. Kabasjima, *Stud. Surf. Sci. Catal.* **2000**, *130D*, 3507–3512.

[6] J. I. Di Cosimo, V. K. Díez, C. Ferretti, C. R. Apesteguía, *Catalysis*, Royal Society Of Chemistry, Cambridge, **2014**.

[7] F. S. H. Simanjuntak, S. R. Lim, B. S. Ahn, H. S. Kim, H. Lee, *Appl. Catal. Gen.* **2014**, *484*, 33–38.

[8] G. Busca, *Ind. Eng. Chem. Res.* **2009**, *48*, 6486–6511.

[9] C. Xu, D. I. Enache, R. Lloyd, D. W. Knight, J. K. Bartley, G. J. Hutchings, *Catal. Lett.* **2010**, *138*, 1–7.

[10] D. Cornu, H. Guesmi, G. Laugel, J.-M. Krafft, H. Lauron-Pernot, *Phys. Chem. Chem. Phys. PCCP* **2015**, *17*, 14168–76.

[11] S. L. Britton, J. Q. Bond, T. W. Root, *Energy Fuels* **2010**, *24*, 4095–4096.

[12] S. T. Jiang, F. J. Zhang, L. J. Pan, *Braz. J. Chem. Eng.* **2010**, *27*, 137–144.

[13] D. M. Reinoso, D. E. Damiani, G. M. Tonetto, *Appl. Catal. B Environ.* **2014**, *144*, 308–316.

[14] A. Zieba, A. Pacula, A. Drelinkiewicz, *Energy Fuels* **2009**, *24*, 634–645.

[15] L. E. Manzer, *Appl. Catal. Gen.* **2004**, *272*, 249–256.

[16] L. E. Manzer, *Synthesis Of Alkenoate Esters From Lactones And Alcohols*, **2004**, WO 2004007421 A1.

[17] P. Arpino, G. Ourisson, *Anal. Chem.* **1971**, *43*, 1656–1657.

[18] T. Y. Wibowo, A. Z. Abdullah, R. Zakaria, *J. Appl. Sci.* **2011**, *11*, 3619–3624.

[19] A. F. Zanette, R. A. Barella, S. B. C. Pergher, H. Treichel, D. Oliveira, M. A. Mazutti, E. A. Silva, J. V. Oliveira, *Renew. Energy* **2011**, *36*, 726–731.

[20] V. V. Bokade, G. D. Yadav, *Ind. Eng. Chem. Res.* **2009**, *48*, 9408–9415.

[21] R. Ratti, S. Kaur, M. Vaultier, V. Singh, *Catal. Commun.* **2010**, *11*, 503–507.

[22] B. Saha, M. Streat, *React. Funct. Polym.* **1999**, *40*, 13–27.

[23] T. Issariyakul, A. K. Dalai, *Energy Fuels* **2010**, *24*, 4652–4658.

[24] J. Temuujin, K. Okada, K. J. D. MacKenzie, *J. Solid State Chem.* **1998**, *138*, 169–177.

[25] J. Temuujin, K. Okada, K. J. MacKenzie, *J. Am. Ceram. Soc.* **1998**, *81*, 754–756.

[26] D. Nied, K. Enemark-Rasmussen, E. L'Hopital, J. Skibsted, B. Lothenbach, *Cem. Concr. Res.* **2016**, *79*, 323–332.

[27] F. Jin, A. Al-Tabbaa, *Cem. Concr. Compos.* **2014**, *52*, 27–33.

[28] C. Roosz, S. Grangeon, P. Blanc, V. Montouillout, B. Lothenbach, P. Henocq, E. Giffaut, P. Vieillard, S. Gaboreau, *Cem. Concr. Res.* **2015**, *73*, 228–237.

[29] K. Narasimharao, T. T. Ali, S. Bawaked, S. Basahel, *Appl. Catal. Gen.* **2014**, *488*, 208–218.

[30] D. R. M. Brew, F. P. Glasser, *Cem. Concr. Res.* **2005**, *35*, 85–98.

[31] A. G. Kalampounias, N. Bouropoulos, K. Katerinopoulou, S. N. Yannopoulos, *J. Non-Cryst. Solids* **2008**, *354*, 749–754.

[32] S.-I. Fujita, B. M. Bhanage, D. Aoki, Y. Ochiai, N. Iwasa, M. Arai, *Appl. Catal. Gen.* **2006**, *313*, 151–159.

[33] H. Hattori, M. Shima, H. Kabashima, *Stud. Surf. Sci. Catal.* **2000**, *130*, 3507–3512.

[34] T. F. Dossin, M.-F. Reyniers, G. B. Marin, *Appl. Catal. B Environ.* **2006**, *62*, 35–45.

[35] Z. Yaakoba, S. Padikkaparambila, N. Binitha, R. Resmib, V. Surajaa, *Chem. Eng. Trans.* **2011**, *24*, 103–108.

[36] E. Van de Steene, J. De Clercq, J. W. Thybaut, *J. Mol. Catal. Chem.* **2012**, *359*, 57–68.

[37] G. A. Olah, A. Goeppert, G. K. S. Prakash, *Beyond Oil and Gas: The Methanol Economy*, John Wiley & Sons, **2011**.

[38] J. F. L. Page, *Catalyse de contact: conception, préparation et mise en œuvre des catalyseurs industriels*, Editions TECHNIP, **1978**.

[39] A. G. Kalampounias, N. Bouropoulos, K. Katerinopoulou, S. N. Yannopoulos, *J. Non-Cryst. Solids* **2008**, *354*, 749–754.

[40] O. T. Ozgul, O.-Y. Sevil, *Eur. J. Lipid Sci. Technol.* **2008**, *110*, 742–746.

[41] S. A. Walling, J. L. Provis, *Chem. Rev.* **2016**, *116*, 4170–4204.

[42] F. Jin, A. Al-Tabbaa, *Cem. Concr. Compos.* **2014**, *52*, 27–33.

[43] S. A. Walling, H. Kinoshita, S. A. Bernal, N. C. Collier, J. L. Provis, *Dalton Trans.* **2015**, *44*, 8126–8137.

[44] M. Tonelli, F. Martini, L. Calucci, E. Fratini, M. Geppi, F. Ridi, S. Borsacchi, P. Baglioni, *Dalton Trans* **2016**, *45*, 3294–3304.

[45] A. Dumas, F. Martin, C. L. Roux, P. Micoud, S. Petit, E. Ferrage, J. Brendlé, O. Grauby, M. Greenhill-Hooper, *Phys. Chem. Miner.* **2013**, *40*, 361–373.

[46] W.-S. Chiang, G. Ferraro, E. Fratini, F. Ridi, Y.-Q. Yeh, U.-S. Jeng, S.-H. Chen, P. Baglioni, *J. Mater. Chem. A* **2014**, *2*, 12991–12998.

[47] M. Tonelli, F. Martini, L. Calucci, E. Fratini, M. Geppi, F. Ridi, S. Borsacchi, P. Baglioni, *Dalton Trans* **2016**, *45*, 3294–3304.

[48] K. Narasimharao, T. T. Ali, S. Bawaked, S. Basahel, *Appl. Catal. Gen.* **2014**, *488*, 208–218.

[49] B. Lothenbach, D. Nied, E. L'Hôpital, G. Achiedo, A. Dauzères, *Cem. Concr. Res.* **2015**, *77*, 60–68.

[50] D. Nied, K. Enemark-Rasmussen, E. L'Hopital, J. Skibsted, B. Lothenbach, *Cem. Concr. Res.* **2016**, *79*, 323–332.

[51] S. A. Walling, H. Kinoshita, S. A. Bernal, N. C. Collier, J. L. Provis, *Dalton Trans* **2015**, *44*, 8126–8137.

[52] J.-B. d'Espinose de la Caillerie, M. Kermarec, O. Clause, *J. Phys. Chem.* **1995**, *99*, 17273–17281.

[53] M. Magi, E. Lippmaa, A. Samoson, G. Engelhardt, A. R. Grimmer, *J. Phys. Chem.* **1984**, *88*, 1518–1522.

[54] D. R. M. Brew, F. P. Glasser, *Cem. Concr. Res.* **2005**, *35*, 85–98.

[55] J. C. C. Freitas, M. E. Smith, in *Annu. Rep. NMR Spectrosc.*, **2012**, pp. 25–114.

[56] J. M. Griffin, A. J. Berry, S. E. Ashbrook, *Solid State Nucl. Magn. Reson.* **2011**, *40*, 91–99.

[57] J.-B. d'Espinose de Lacaillerie, C. Fretigny, D. Massiot, *J. Magn. Reson.* **2008**, *192*, 244–251.

[58] G. J. Rosasco, J. J. Blaha, *Appl. Spectrosc.* **1980**, *34*, 140–144.

[59] M. E. Llanos, T. Lopez, R. Gomez, *Langmuir* **1997**, *13*, 974–978.

[60] J. W. Kriesel, T. D. Tilley, *J. Mater. Chem.* **2001**, *11*, 1081–1085.

[61] G. Busca, *Heterog. Catal. Mater.* **2014**, 103–195.

[62] M. Falk, E. Whalley, *J. Chem. Phys.* **1961**, *34*, 1554–1568.

[63] D. Cornu, H. Guesmi, J.-M. Krafft, H. Lauron-Pernot, *J. Phys. Chem. C* **2012**, *116*, 6645–6654.

Chapter 3. Role of water on reactivity of commercial magnesium silicate

3.1. Introduction

In last chapter, we found that magnesium silicate is a bifunctional catalyst and offers on the same surface acidic and basic active sites. This bifunctional character may be a key parameter to explain the high activity. More precisely, water and other adsorbates may modify the reactivity of a surface[1]. Such a phenomenon has been evidenced, in the case of MgO[2], CaO[3] and hydrotalcites[4], in transesterification reactions[4,5].

Water has been shown to inhibit some base catalysts for transesterification reactions since it competes with the alcohol (reactant), thus lowering the conversion as observed for MgO in gas phase[2] or transforming the required transesterification reaction into ester hydrolysis, leading to the formation of free fatty acids[6,7]. This latter effect is however less pronounced in heterogeneous catalysis than in the homogeneous one[6]. Nevertheless, water has also been shown to play a positive role in different heterogeneous catalytic reactions[8]. For example, in the case of biodiesel production, Zabeti et al.[3] noted that the presence of little amounts of water in the reaction medium can enhance the catalytic activity of calcium oxide (CaO). Their conclusion is that water is necessary to form hydroxide ions, which will be an homogeneous catalyst in the reaction.

Greenwell et al.[4] used *ab initio* plane-wave density functional theory to investigate mechanism of transesterification of methylacetoacetate with prop-2-en-1-ol catalyzed by MgAl-layered double hydroxides (LDH) intercalated with *tertiary*-butoxide (*t*-butoxide) anions, involving the participation of water (Figure 3.1). Firstly, *t*-butoxide would deprotonate any interlayer water, resulting in the formation of *t*-butoxide alcohol, and hydroxide anions as charge balancing anion in the LDH. Then prop-2-en-1-ol was deprotonated by hydroxide anions to generate prop-2-en-1-oxide which was H-bonded over a Mg-OH. At second stage, the nucleophilic attack occurred involving the ester carbonyl group coordinated to the Al-hydroxyl groups, with the deprotonated prop-2-en-ol located in the vicinity. At third stage, the water molecule, itself polarized by the Al-hydroxyl groups in the adjacent layer and by the *t*-butyl alcohol, acting as a Brønsted acid, was small enough to approach the methoxy oxygen closely and polarize the C-O bond *via* hydrogen bonding to facilitate abstraction of the methoxy group.

This study shows that the presence of interlayer water, facilitates interactions between the LDH host and the guest species by transferring the Brønsted acidity.

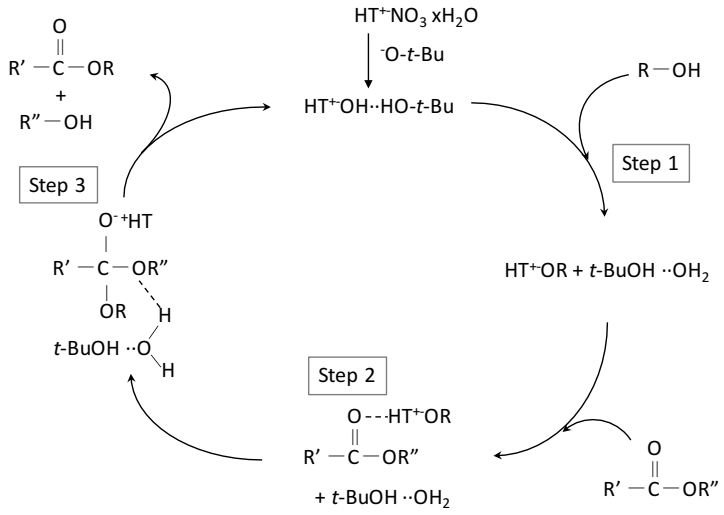

Figure 3.1: Mechanism for transesterification of methylacetoacetate with prop-2-en-1-ol proposed by Greenwell et al.[4].

R'COOR" is methylacetoacetate, R-OH is prop-2-en-1-ol.

The aim of this chapter is to study the role of adsorbed water on the catalytic behaviour of the commercial magnesium silicate (in Chapter 2, this sample is labelled as Mg silicate (com), in this chapter, it is simply labelled as COM) in the model reaction of transesterification of ethyl acetate by methanol. In order to link the yield obtained in catalysis to surface properties, the characterization of the catalysts is achieved by infrared and ^{1}H Nuclear Magnetic Resonance spectroscopies.

3.2. Role of thermal pretreatment

3.2.1. Experimental procedure

To vary the water coverage, we perform thermal pretreatment that releases water from catalyst. The catalyst used in this chapter for transesterification reaction is still Magnesol® catasorb provided by the Dallas group of America© (COM). The COM was thermally treated at 70, 90, 110, 140 °C respectively for 2 h after heating at a rate of 5 °C min^{-1} in 20 mL min^{-1} of flowing N_2, then cooled down to room temperature. The obtained samples are denoted as

COM-70, COM-90, COM-110 and COM-140, respectively. After pretreatment, the samples were transferred to the schlenk reaction quickly to avoid rehydration. For TGA analysis, the pretreated samples transferred to the oven in the same conditions and it showed very little rehydration (less than 0.3%).

In order to understand the reversibility of thermal treatment, COM-140 is put in a dessicator with water at bottom for rehydration. Then the samples are noted as COM-140-Rt with t the time of rehydration (hour).

We use the same apparatus (Figure 2.3) and operating conditions (Table 2.4) as for transesterification in liquid phase as chapter 2.

3.2.2. Catalytic performances and TGA analysis

Table 3.1 indicates the conversion of ethyl acetate (AcOEt) for magnesium silicate with (COM-X) and without (COM) pretreatment (X being the pretreatment temperature in °C). Conversion of ethyl acetate decreases for increasing pretreatment temperatures, especially for pretreatment temperatures higher than 70 °C. Figure 3.2 shows the results from thermogravimetric analysis (TGA) and differential thermogravimetric analysis (DTA) of COM and COM-X. DTA curves (Figure 3.2B) show a main weight loss feature, occurring below 200 °C that can be attributed to the removal of water[9]. Water adsorbed on catalysts is released step by step (Figure 3.2A) and the maximum for DTA curve shifts towards higher temperatures (Figure 3.2B) for increasing pretreatment temperatures. The data are listed in Table 3.1 to compare with catalytic performances. The quite significant decrease of conversion does not occur for the important weight loss under 70°C, attributed to water weakly bonded to the surface, but when more strongly adsorbed water molecules are desorbed. Similar results were also found by Xi et al.[5,10] for the activity of rehydrated hydrotalcites in the transesterification reaction of tributyrin with methanol. This effect was ascribed to the loss of OH^- base sites that were produced by dissociating interlayer water[5,10,11].

Table 3.1: Conversions and TGA/DTG measurements for COM and COM-X.

Samples	AcOEt Conv. (%)[a]	TGA/DTA Measurement	
		Weight loss (%)	Temp. for maximum desorp. (°C)
COM	22.8	16.5	71
COM-70	22.0	5.4	128
COM-90	15.2	4.5	136
COM-110	14.5	3.4	145
COM-140	13.8	1.8	148

[a] The mass of catalysts added in schlenk flask is around 15 -18 mg, and thus pure mass of catalyst (excluding water) is 15 mg.

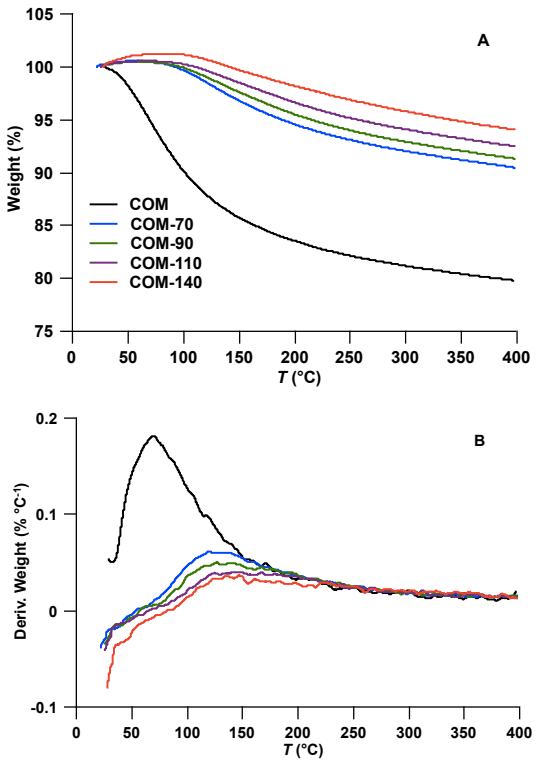

Figure 3.2: (A) Thermogravimetric analysis (TGA), (B) differential thermogravimetric analysis (DTA) for COM depending on pretreatment temperature. Little rehydration in the oven is responsible for the slight weight increase at low temperature.

Rehydration experiments were performed in water saturated atmosphere on the sample COM-140. As shown in Table 3.2 and Figure 3.3, 0.4 h exposure is enough to fully recover the global water content of the sample COM, with similar desorption pattern. Longer exposure

times increase slowly the water content of the sample, reaching 51.8% after 425 h. Catalytic tests of rehydrated samples show that the activity can be fully recovered after 0.4 h rehydration period (Table 3.2). It indicates that the catalyst is not irreversibly modified upon drying and that the decrease of the reactivity upon dehydration cannot be explained by a structure modification. Besides, XRD shows that the structure is kept unchanged and N_2 sorption analysis confirms that there is no decrease of specific surface area of COM at 140 ^oC pretreatment (data are not presented; before measurement, the samples are degassed at 60 ^oC for 22.5 h). However, excessive rehydration is harmful to the reactivity, leading to some decrease of the conversion (Table 3.2). The effect of this excessive water in the catalyst is similar to the one observed with direct introduction in the reactant mixture of liquid water. Indeed, when 0.1 mL of water is added into the schlenk together with the reactants, the conversion decreases to 4.7%, compared to 22.8% initially. This can be due to the deactivation caused by the hydrolysis of the ester molecules over the catalyst as mentioned by Xi et al. on hydrotalcites catalyst[10].

Table 3.2: Results of catalysis tests and TGA/DTG measurements as a function of rehydration time for COM-140.

Samples	**AcOEt Conv. (%)[a]**	**Conv./Mass (% g^{-1})[b]**	**TGA/DTA Measurement**	
			Weight loss (%)	**Temp. for maximum desorp. (°C)**
COM	22.8	1.52	16.5	69
COM-140	13.8	0.88	1.8	148
COM-140-R0.4	22.0	1.47	17.1	69
COM-140-R2.5	16.1	1.21	26.2	64
COM-140-R24	16.1	1.26	29.0	61
COM-140-R425	11.2	1.29	51.8	70

[a] The mass of catalysts added in schlenk flask is 18 mg (except for COM-140 that is 16 mg).
[b] Conversion of ethyl acetate divided by pure mass of catalyst (excluding water).

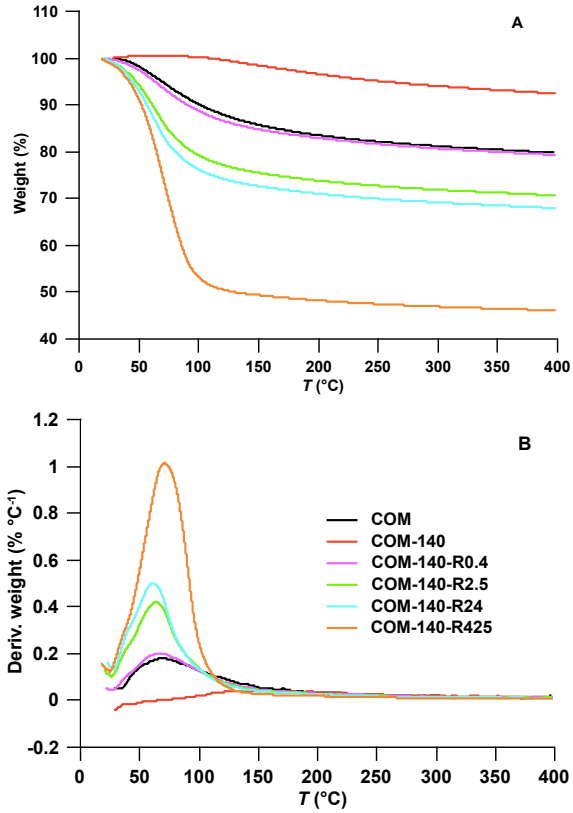

Figure 3.3: (A) Thermogravimetric analysis (TGA), (B) differential thermogravimetric analysis (DTA) for COM-140 depending on time of rehydration (RX, with X being the rehydration time in h).

3.3. Characterizations of the pretreated magnesium silicate

3.3.1. DRIFTS analysis

Figure 3.4 gathers DRIFT spectra of COM and COM-X. Only wavenumbers from 4000 to 1500 cm^{-1} are shown because they provide information on hydroxyl groups and water stretching and bending. In each spectrum four bands can be observed, at 3740 - 3720, 3672, 3620 - 3200, and 1636 cm^{-1}. The band observed here at 3740 to 3720 cm^{-1} is assigned to OH stretching of silanols species, that is located at 3737 cm^{-1} for the stretching of silanols over silica [12] and at 3720 cm^{-1} on sepiolite[13,14]. The band at 3672 cm^{-1} has been ascribed to hydroxyls coordinated to the magnesium (Mg-OH stretching)[9], as what is observed in sepiolite, antigorites and talc[13,15]. The broad band from 3620 to 3200 cm^{-1} was attributed to OH stretching of adsorbed water [12,16]. The contribution at 1636 cm^{-1} was assigned to H-O-H bending vibrations of molecular bound water[9,12,16,17]. More precise assignments are made by

comparison with the IR spectra of sepiolite, a magnesium silicate clay with ordered cavities filled with water molecules, as shown in Table 3.3.

Table 3.3: Assignments of Infrared absorption bands of COM comparing with that of sepiolite given in the literature (wavenumber in cm^{-1}).

COM	**Sepiolite**[13,14,18,19]	**Suggested assignments**[13,14,18,19]
3740 - 3720	3720	Si-OH hydroxyl stretch
3672	3680	Internal Mg-OH stretch
3620 - 3200	3620	Mg-OH stretch
	3565[13]/3599[18]/3532[18]	OH-stretch of water coordinated to Mg
	3430	Water OH-stretch
	3230	Water OH-stretch
1717	1710	Eventually a bending mode of water with strong hydrogen bonding
1684	1660 - 1670	Bending of water coordinated to Mg
1651	1656	Bending of zeolite-like water (2 H-bonded)
1632	1630	Bending of zeolite-like water (1 H-bonded)
1613	1616	Bending of water weakly H-bonded

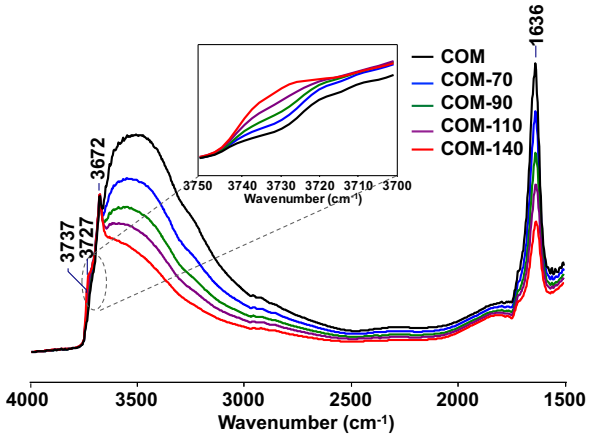

Figure 3.4: DRIFT spectra of COM after each pretreatment step. They are taken at the pretreatment temperature.

It can be seen in Figure 3.4 that, when increasing the pretreatment temperature, the intensity of the band at 1636 cm^{-1} and that of the broad band at 3620 to 3200 cm^{-1} decrease significantly, which is well consistent with the water loss observed with TGA results. As the catalytic performances (Table 3.1), show a significant decrease in conversion by pretreating the sample from 70 to 140 °C, the spectrum of COM-140 is compared to the one of COM-70, with the curve log(COM-140/COM-70) (Figure 3.5). A sharp band appears at 3732 cm^{-1}, which means that the intensity at 3732 cm^{-1} increases for COM-140 compared to COM-70. However, the band at 3672 cm^{-1} is quasi not altered.

Thus, accompanying the release of adsorbed water, the intensity of silanol bands (3740 to 3720 cm^{-1}) arises, whereas the intensity of Mg-OH stretching band is not changed, although the bands are revealed and become more apparent.

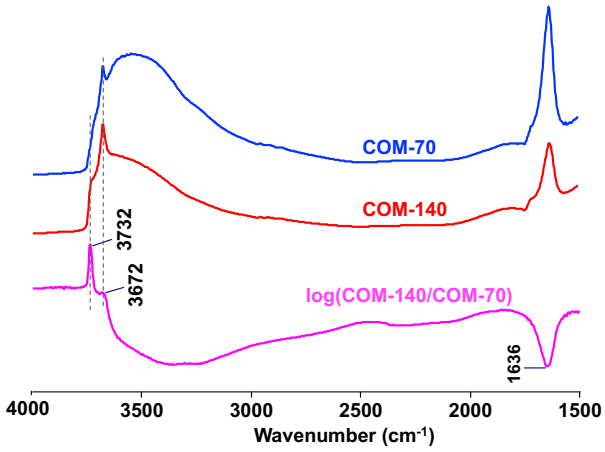

Figure 3.5: DRIFT spectra of COM-70 and COM-140, and their subtraction curve.

More precise assignments can be obtained from comparison with the IR spectra of crystalline magnesium silicates: chrysotile, talc, sepiolite. Chrysotile is a 1:1 layered silicate, in which an octahedral brucite-like sheet is covered up by a SiO_4 tetrahedral sheet [20]. Hence, there are two kinds of Mg-OH, one is at the top of the brucite-like sheet (external Mg-OH) with a stretching frequency of 3695 cm^{-1}, and the other one is at the bottom of the brucite-like sheet next to the silicate one (internal Mg-OH) with a frequency of 3649 cm^{-1} [21]. Only external Mg-OH is accessible to water. On the opposite, talc, is a 2:1 layered silicate. The brucite-like sheet is thus sandwiched between two silicate sheets. The talc is therefore centrosymmetric and exhibits only internal OH with a stretching mode at 3677 cm^{-1}[22]. For our COM sample, the intensity of the band at 3672 cm^{-1} is not altered while releasing water, this band should therefore be ascribed to internal Mg-OH as the band at 3680 cm^{-1} in sepiolite (Table 3.3).

The bands at 3620 - 3200 cm^{-1} were deconvoluted by Frost et al.[13] on sepiolite, into four bands at 3620, 3565, 3430 and 3230 cm^{-1} for more precise assignment. By comparing near-infrared with mid-infrared spectroscopy, Frost et al.[13] assigned the band at 3620 cm^{-1} to OH stretching for hydroxyl group adsorbed on Mg, the one at 3565 cm^{-1} to the OH stretching of water also coordinated to Mg cation, and bands at 3430 and 3230 cm^{-1} were assigned to water OH-stretching weakly coordinated to the surface. Cannings et al.[18] ascribed the bands at 3599 and 3532 cm^{-1} to antisymmetric and symmetric stretching modes of molecular water coordinated to Mg cation at the edges of the channels in sepiolite. Water molecule could be absorbed and dissociated on Mg^{2+}-O^{2-} pairs to form two OH groups associated by H-bonding[23,24], and these OH groups contribute in a stretching band around 3583 and 3515 cm^{-1}[25,26]. As MSH is a structure defective in silicate groups, Mg located at the edge or close to the defects of the silicate layer are probably able to adsorb water or exhibit OH groups. The broad bands at 3620 - 3200 cm^{-1} are hardly deconvoluted here, but may result from different contributions such as the stretching of Mg-OH at edge or defects of layer, water OH-stretch linked to magnesium, water OH-stretch adsorbed on Mg-OH or silanols.

Upon dehydration, the band corresponding to water desorption can contain different species (Table 3.3), thus experimental bands of water bending modes around 1636 cm^{-1} are decomposed and fitted with five bands at 1717, 1684, 1651, 1632, and 1613 cm^{-1} using Gaussian line shape functions (Figure 3.6). The areas for each band evolve with pretreatment temperature (in Figure 3.7). For sepiolite, the band at 1710 cm^{-1} is difficult to attribute, as Frost et al., states that it is not sure that this absorption is linked to water molecule. The band at 1660 - 1670 cm^{-1}

[1] is assigned to water strongly bonded to magnesium cation in sepiolite. Famer et al.[27] assigned the bands at 1656 and 1630 cm^{-1} to two distinct water molecules in sepiolite: the former has two OH groups involved in hydrogen bonding, the later only one [19]. Prost et al.[19] reported that when sepiolite was dehydrated, a band at 1616 cm^{-1} appeared. They attributed this band to water molecules connected with weak hydrogen bonds[19] in agreement with physical considerations showing that the wavenumber of water bending vibration should decrease with a decrease in the strength of hydrogen bonding[28]. Nevertheless, an inverse relationship was observed by Kolesov et al. and a low wavenumber at around 1590 cm^{-1} was ascribed to the bending of water adsorbed on cation and strongly H-bond to structural oxide[29].

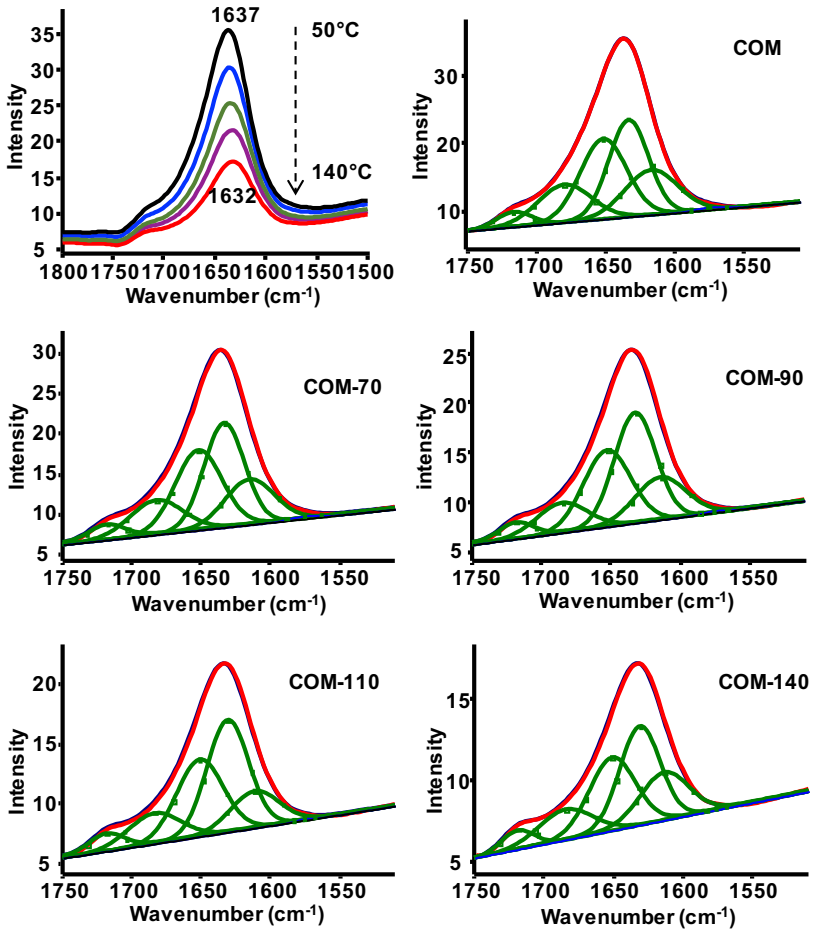

Figure 3.6: Deconvoluted DRIFT spectra of COM and COM-X at the region of 1800–1500 cm^{-1}.

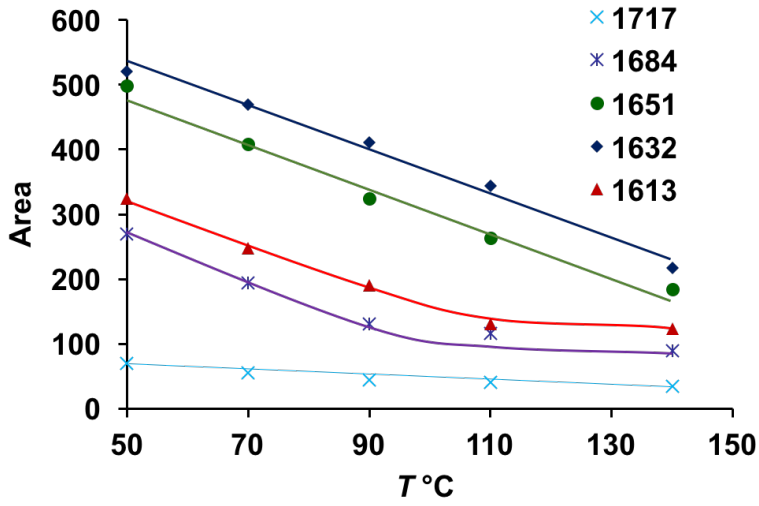

Figure 3.7: Areas of deconvoluted DRIFT spectra at the region of 1800 – 1500 cm^{-1} evolved with pretreatment temperature.

As can be shown from Figure 3.7, up to 90 °C, the bands at 1684, 1651, 1632 and 1613 cm^{-1} decrease substantially in the same way. Then, beyond 90 °C, the band located at 1684 cm^{-1} does not seem to evolve. The band at 1613 cm^{-1} is not modified for pretreatment temperatures higher than 110 °C. It is possible that the bands at 1651, 1632 and 1613 cm^{-1} characterize the water interacting with other water molecules or silanols and that the band at 1684 cm^{-1} characterizes the water molecules interacting with magnesium, therefore more rigid than the one in the H bond network. The evolution of the intensities of this band with pretreatment temperature (Figure 3.7) can be understood considering two kinds of magnesium presented on Figure 3.8: the one located on the edge of the clay-like particles and the other one in the defects of the silicate layer, respectively **a** and **b** on the scheme proposed Figure 3.8. Please note that in each site, water molecule can also interact through H-bond with Mg-OH or Si-OH groups but for sake of clarity, these H-bonds are not shown on Figure 3.8. One of these species may be released up to 90 °C while the other one, more strongly bounded is stable up to 140 °C.

The evolution of the band located at 1613 cm^{-1} is more difficult to comment due to controversial assignment in literature. Again two different species must be involved in this contribution, both adsorbed on the H-bond network formed on sites **a** or **b** Figure 3.8 (not represented). The first one is weakly bonded and desorbed at low temperature. The second one is stable above 110 °C and must be linked to water more strongly bonded.

To identify the sites more precisely, the transmission FTIR spectroscopy with carbon monoxide (CO) adsorption will be performed.

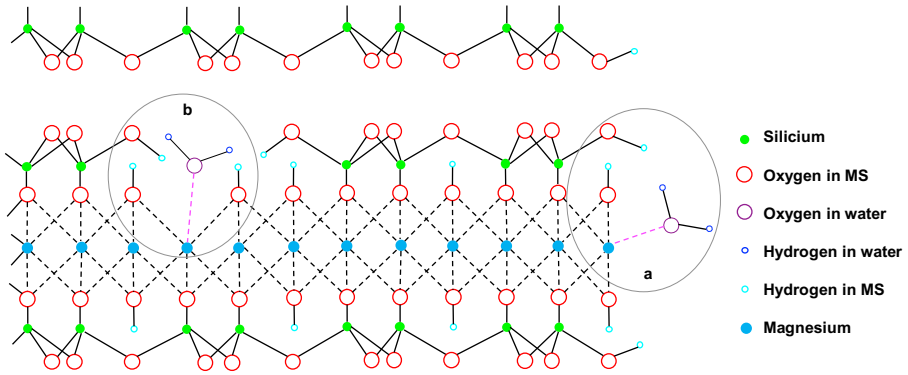

Figure 3.8: Two dominant modes of adsorption of water on magnesium: (a) adsorption of water on magnesium located at the edge of layer, (b) adsorption of water on magnesium located in defects.

3.3.2. The transmission FTIR spectra of adsorbed CO

It has been demonstrated that the interaction of water occuring on the surface of the amorphous aluminosilicate, can lead to the formation of strong Brønsted sites[30]. It would thus be interesting to study the evolution of acidity with the release of water on COM. The MBOH test is helpless to characterize the evolution of acidity in this situation, as the interesting pretreatment temperature for COM is between 70 and 140 °C, that is lower than the reaction temperature. The transmission FTIR spectra of adsorbed (CO) is a powerful technique to characterise the acidities of solids. The probe molecule CO has small size, softness (in terms of basicity), non-reactivity (at low temperature) and sensitivity to acid sites, which makes it ideal for the investigation of samples with acidity.

The sample COM was successively treated at 70, 90, 140 and 350 °C for 2 hours under an Ar stream (20 mL min^{-1}) and analyzed at the temperature of liquid nitrogen before and after adsorbing CO (at a pressure of 1 Torr CO). As the IR spectra (Figure 3.9) are obtained by subtracting the spectra of the initial samples from those registered after adsorption, negative bands will correspond to species adsorbing CO and the positive ones, to the species formed upon adsorption. Three spectral regions will be considered: 3800 - 3400, 2220 - 2100 and 1650 - 1550 cm^{-1}. 3800 - 3400 cm^{-1} relative to OH stretching region, 2220 - 2100 cm^{-1} ascribed to the stretching vibration of CO[30,31], and 1650 - 1550 cm^{-1} for the water contribution.

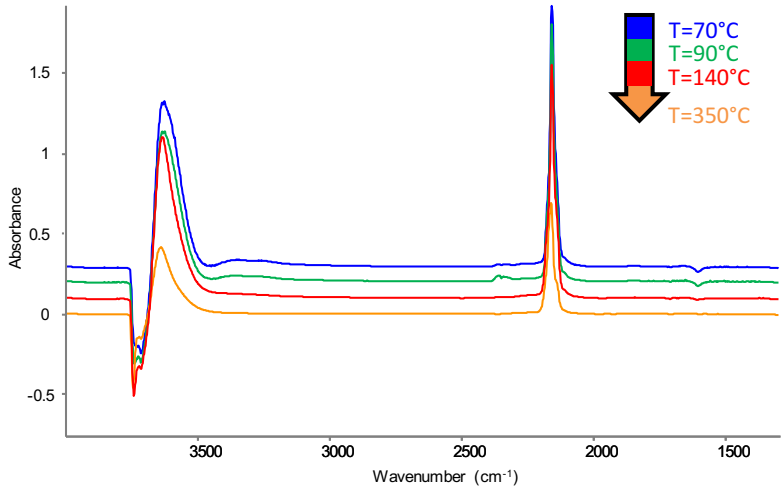

Figure 3.9: IR difference spectra after CO adsorption on COM treated at 70, 90 140 and 350 °C.

Figure 3.10 shows the IR spectra region of CO vibration, located between 2200 and 2100 cm^{-1}. The band at 2142 cm^{-1}, assigned to physisorbed CO, is observed for all the samples, and indicates the saturation of all sites for CO adsorption. The main band is identified at 2158 cm^{-1}, with side bands at 2172 and 2181 cm^{-1}. The band at 2158 cm^{-1} can be assigned to the interaction of CO with weak acid sites and it is obviously noted that the increase of pretreatment temperature leads to a remarkable decrease of weak acid sites. Specifically, for the 350 °C pretreatment, a shift from 2158 to 2161 cm^{-1} is observed. Then focusing on the higher wavenumbers, Blanchard et al.[30] ascribed 2169 cm^{-1} and 2180 cm^{-1} to υ(CO) on mild and strong Brønsted sites formed by adsorption of H_2O on Lewis sites (possibly silanols in close proximity with Lewis Al) on amorphous aluminosilicates, respectively. Similarly, these two kinds of band are found as well in COM and the one at 2172 cm^{-1} may be caused by υ(CO) on mild Brønsted sites formed with the coordination of H_2O on Mg in close proximity with silanols, like on amorphous aluminosilicates. Furthermore the one at 2181 cm^{-1} should be linked to the υ(CO) on strong Brønsted sites (Figure 3.10). Crepeau et al. also reported that the band at 2178 cm^{-1} corresponds to the υ(CO) of CO adsorbed on the acid sites of amorphous aluminosilicate whose acidic strength is as strong as that present in H-beta zeolite[32]. From Figure 3.10, it can be noted that, the side band located at 2172 cm^{-1}, decrease with the increase of pretreatment temperature to 140 °C, while the band located at 2181 cm^{-1} seems to be stable but decreases dramatically up to 350 °C. It means that the mild acid sites could be removed upon dehydration at moderate pretreatment temperature. Then, with further increasing the

temperature to 350 °C, the strong acid sites are removed upon release of the strong adsorbed water.

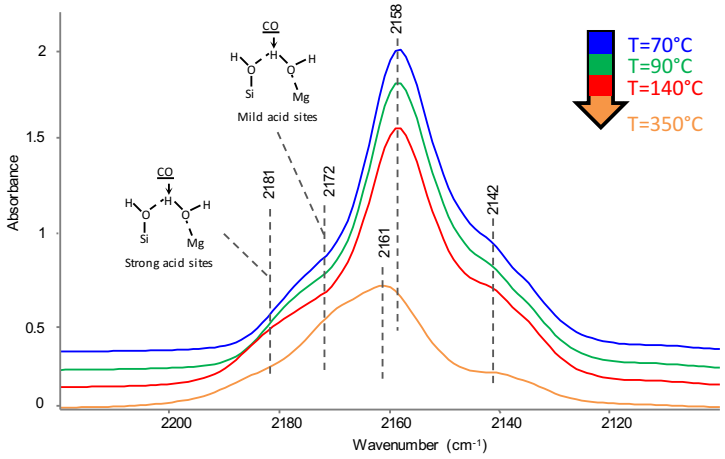

Figure 3.10: IR difference spectra after CO adsorption on COM treated at 70, 90 140 and 350 °C: 2220 -2100 cm^{-1}.

In Figure 3.11, the part of the spectra corresponding to the OH vibration is shown. At least two types of OH negative peaks at 3742 and 3713 cm^{-1}can be distinguished. No significant difference is found between the spectra of COM-70 and COM-90. However, the COM-140 shows a more intensive band at 3742 cm^{-1} (υ(Si-OH)) that may be linked to the reveal of Si-OH upon dehydration at 140 °C. Up to 350 °C, the intensity of the band at 3742 cm^{-1} decreases and the correspondingly positive band at 3635 cm^{-1} (υ(Si-OH···CO)) also experiences a decrease and shifts to 3643 cm^{-1}, showing the dehydroxylation of the surface. Another kind of Si-OH band is observed at 3713 cm^{-1}. Blanchard et al. ascribed a band at 3718 cm^{-1} to υ(OH) of mild Brønsted acid sites (possibly silanols in close proximity with Lewis Al) in amorphous aluminosilicate [30]. In COM, we suggest the assignment of 3713 cm^{-1} to silanols close to the mild Brønsted acid sites formed *via* the coordination of water to Mg (Figure 3.10). It can be seen that, the negative bands at 3713 cm^{-1} of COM-140 is less intense than those of COM-90 and COM-70. It means that the COM-140 possesses less mild Brønsted acid sites, which should be due to the removal of water at 140 °C. The corresponding positive band at 3580 cm^{-1} also shows a lower intensity at 140 °C pretreatment. It fits with the observation from the CO vibration in Figure 3.10.

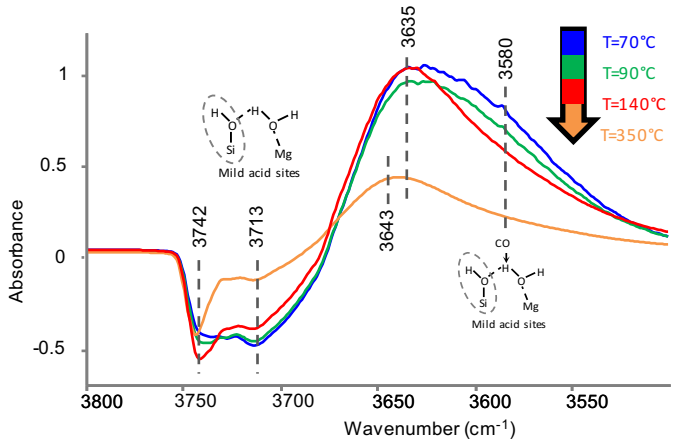

Figure 3.11: IR difference spectra after CO adsorption on COM treated at 70, 90 140 and 350 °C: 3800 -3100 cm^{-1}.

In the region of water vibration, a negative band at 1605 cm^{-1} is observed (Figure 3.12). In the DRIFTS analysis, we did not precise the assignment of the band at 1613 cm^{-1} due to controversial assignment in literature[19,29]. However, a similar negative band at 1606 cm^{-1} was also observed on amorphous aluminosilicate by Blanchard et al[30]. They attributed this band to the bending vibration of water interacting with Al Lewis acid sites. For COM, we may also link the band at 1605 cm^{-1} to the water in interaction with Mg Lewis acid sites. The adsorption of CO on ($H_2O\cdots Mg$) should lead, in the range of water bending vibration, not only to the negative band at 1605 cm^{-1} but also to a positive band (corresponding to the bending mode of H-O-H···CO). However, a corresponding positive band is hardly observed in the spectra in Figure 3.12. Blanchard et al.[30] observed the same phenomenon and they demonstrated that the absence of a corresponding band is due to its weak extinction coefficients and close to the water bending vibration. From the negative band at 1605 cm^{-1}, it can be seen that, the intensity of this band decreases significantly with the increase of pretreatment temperature to 140 °C, in agreement with the evolution of band at 1613 cm^{-1} (Figure 3.8). These results again indicate that the mild acid sites could be removed upon release of water at moderate temperature. The attributions of the FTIR bands discussed in this section have been summed up in Table 3.4.

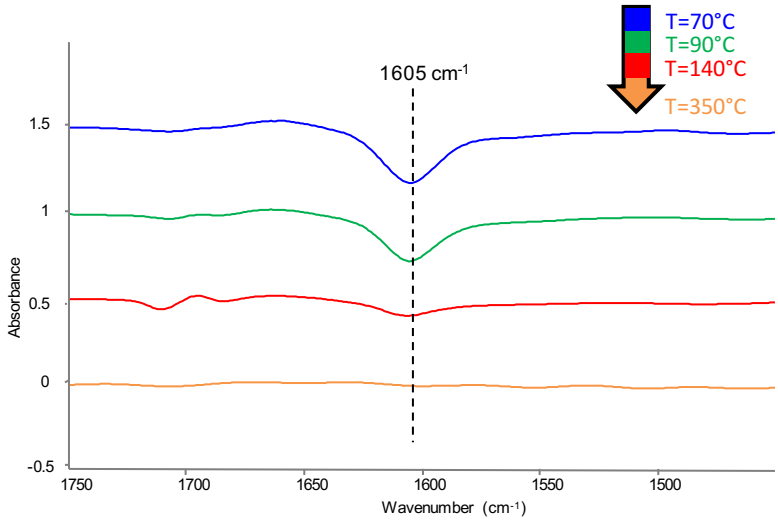

Figure 3.12: IR difference spectra after CO adsorption on COM treated at 70, 90 140 and 350 °C: 1650 - 1550 cm^{-1}.

The evidences of the mild and strong acid sites from FTIR with CO adsorption, are coherent with the hypothesis (Figure 3.8) proposed, based on the DRIFTS analysis, and the strength of acid sites is dependent on their chemical environment, i.e. located at defects or at edges of particle layers.

Table 3.4: Proposed assignment of the FTIR bands associated with the adsorption of CO.

υ(OH)	υ(OH···CO)	υ(CO)	Assignment
3742	3635	2158	Weak acid sites (Si-OH)
3713	3580	2172	Mild Brønsted sites (formed by the coordination of H_2O on Mg in close proximity with silanols)
		2181	Strong acid sites (formed with the coordination of H_2O on Mg in close proximity with silanols)
		2142	Physisorbed CO
1605			Water linked to Mg

To complete this study, ^{1}H NMR will be performed as it is a useful technique that can give structural information on water, Mg-OH and Si-OH which are involved in the formation of active sites.

3.3.3. ^{1}H NMR analysis

^{1}H NMR spectra are obtained for COM and COM-X and shown in Figure 3.13. For sake of comparison, the spectrum of fully dehydrated sample, thus pretreated at 350°C, is also given. Three resonance regions are observed. The broad resonance at 5 ppm can be assigned to adsorbed water[9,12,33]. The resonance at 1.8 ppm can be attributed to silanol[12], and the resonance in the range 0 - 1 ppm can be assigned to Mg-OH[9].

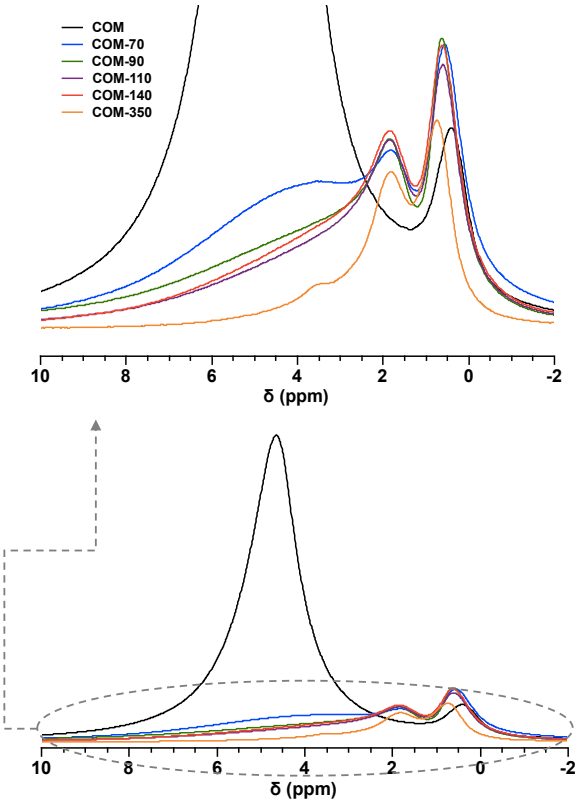

Figure 3.13: ^{1}H NMR spectra of COM and COM-X.

When increasing pretreatment temperature, the band at 5 ppm decreases dramatically and the maximum shifts to lower value. Yesinowski et al. found that, for water in mineral, ^{1}H isotropic chemical shifts of oxygen-bound hydrogen depend linearly on the O-H··O distance. For instance, two structurally distinct water molecules were observed in nepheline (a silica-undersaturated aluminosilicate, $(Na,K)AlSiO_4$), located at 4.6 and 3.4 ppm, corresponding to O-H··O distances of 2.92 and 2.97 Å, respectively. Furthermore, the band at 5 ppm is assigned to highly mobile water molecules found in fluid inclusions and the broad band at around 4 ppm is ascribed to a structurally isolated water group[34]. In our experiments, the highly mobile water molecules are released at low pretreatment temperatures. This desorption leads to higher O-H··O distances, thus the band is shifted to lower values. Confronting these results to catalytic

performances, we can note that the activity of catalyst is not affected by removal of the highly mobile water below 70°C, but the activity decreases significantly for pretreatment temperatures higher than 90°C pretreatment when the structurally isolated water molecules at 4 ppm are released.

The silanol resonance at 1.8 ppm appears after the pretreatment at 70 °C and does not shift upon further dehydratation. On the reverse, the Mg-OH contribution at 0-1 ppm is shifted upon the pretreatements. In the fully hydrated sample, the centre of Mg-OH resonance is located at 0.4 ppm. A moderate thermal treatment releases the highly mobile water and reveals the structurally isolated water molecules that are adsorbed on Mg-OH, shifting the resonance to 0.6 ppm. Then further thermal treatment at 350 °C removes the isolated water molecules and leaves bare Mg-OH, causing a further shift to 0.8 ppm. This is also observed by Nied et al. for the position of the Mg-OH peak which shifts from 0.57 to 0.74 ppm as the amount of water in MSH decreases[9]. In addition, on COM-350, a new contribution appears at 3.6 ppm that can be related to bridging OH groups formed upon dehydroxylation, as in the case of Si-(OH)-Al in zeolite[35,36].

The appearance of the silanol resonance at 1.8 ppm upon drying at 70 °C is in agreement with DRIFTS experiments showing that the silanol contribution at 3732 cm^{-1} grows for higher pretreatment temperatures. Concerning the Mg-OH contribution, DRIFT spectroscopy shows clearly that internal Mg-OH (3672 cm^{-1}) are not affected by water adsorption but cannot conclude about the interaction between external Mg-OH and water as the contribution is located in the 3620 – 3200 cm^{-1} large band. By ^{1}H NMR, the shift of the Mg-OH band upon dehydration clearly evidences that water desorbs from sites implying Mg-OH groups. Two successive shifts are evidenced at moderated temperature and at 350 °C, that can be related to the successive desorption of water from sites **a** and **b** (Figure 3.8) in which it may interact with Mg-OH groups by H-bonding. This hypothesis is in line with the evolution of water adsorbed IR bands located 1684 and 1613 cm^{-1} that is discussed above. From the FTIR with CO adsorption, it is identified that the water adsorbed on Mg, may interact with adjacent Si-OH groups. From the ^{1}H NMR, it is confirmed that the adsorbed water also interacts with the Mg-OH located at defects or edges, which is accessible to water.

3.3.4. Calorimetry analysis

Figure 3.14 shows the adsorption of ethyl acetate on COM and COM-X by calorimetry measurement. The experiments were conducted in solid-liquid phase at 30°C, measuring the heat released by contacting 0.37 mL of ethyl acetate with 0.15 g of the sample. The overall heat of adsorption is thus obtained by integration after reaching equilibrium (8 h). Heats of adsorption increase with the pretreatment temperature up to 90 °C. A further increase of pretreatment temperature no longer improves it. There are two dominant modes of adsorption of ester on the surface of MSH, either *via* its electronegative oxygen in carbonyl group to surface cation[37] or through a hydrogen bond to OH group[4]. Similarly, water can also adsorb on surface cation through its nucleophilic properties[37] or on OH group *via* hydrogen bond[38]. Clausen et al. studied the adsorption of ethyl acetate and water on the dry surface of a smectite clay through density functional theory and they showed that adsorption energy of ethyl acetate on sodium cation is close to the one of water [37]. Even if our system is different, a competition between the adsorption of ethyl acetate and water exists. This may explain the increase of heat of adsorption of ethyl acetate when releasing water.

The fact that the mean heat of ester adsorption is constant for pretreatment temperature over 90 °C can be understood considering the two sites proposed from IR results for water coordination on Mg cations (**a** and **b** on Figure 3.8). At room temperature, both sites are hydrated leading to a low value of heat of adsorption. Up to 90 °C, water is desorbed from one of the sites leading to the decrease of the IR band located at 1613 and 1684 cm^{-1} and to a more efficient adsorption of the ester. Over 90 °C no more water is released from these sites as seen by DRIFTS, in agreement with a constant value of the mean heat adsorption measured by calorimetry. However, the calorimetry results are not link to the catalytic results. Probably, upon release of water, the Brønsted acid sites transfer to Lewis acid sites (Mg cation) which are favored in the adsorption of ethyl acetate but do not act as the sites to activate the ethyl acetate. Moreover, ethyl acetate is pure for the calorimetry analysis, but during reaction it may exist the adsorption competition between ethyl acetate and methanol.

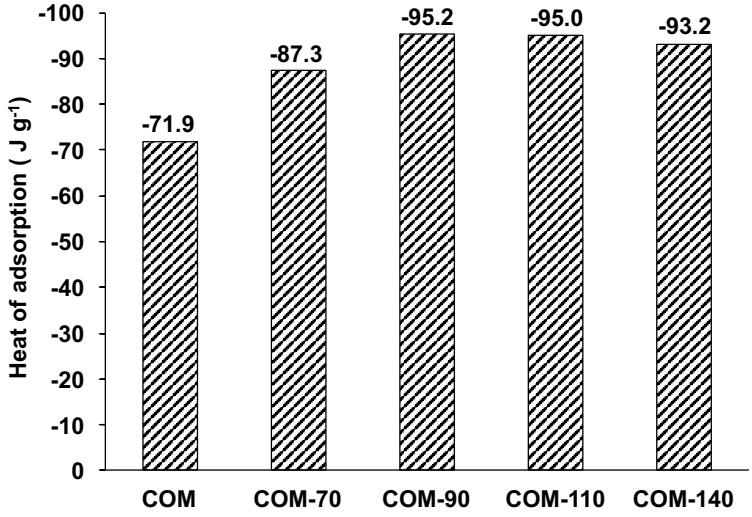

Figure 3.14: Adsorption heats of ethyl acetate on COM and COM-X. The unit J g^{-1} of pure mass of catalyst (excluding water).

3.4. Discussion of the structural characterizations and role of water

Combining the analyses of DRIFTS, FTIR with CO adsorption, ^{1}H NMR and calorimetry, various types of adsorption of water molecules over MSH surface are evidenced.

- Water molecules adsorbed on silanol groups (the ones not close to mild or strong acid sites) *via* hydrogen bonding can easily be desorbed, and the uncovered silanol groups are evidenced by DRIFTS (band at 3737 cm^{-1}), FTIR with CO adsorption (band at 3742 cm^{-1}), and ^{1}H NMR (peak at 1.8 ppm).
- Although internal Mg-OH cannot be accessed directly and are, therefore, not perturbed during dehydration, water molecules can interact with Mg-OH and/or Mg cations located on the edge of the clay-like particles or in the defects present in the silicate layer. Specifically, the two modes of the water molecules linked to Mg cations (Figure 3.8 **a** and **b**) can be released at different temperatures. The band at 1684 cm^{-1} in DRIFTS shows that one species can be released up to 90 °C while the other one, is stable up to 140 °C. This observation is consistent with the evolution of the peak at 4 ppm in ^{1}H NMR (ascribed to isolated water) that decreases up to 90 °C and is stable up to 140 °C. These isolated water molecules are also identified by FTIR with CO adsorption (band at 1605 cm^{-1}) showing that one species can be released at low temperature while the other one needs relatively high temperature to be removed. The adsorption of these two kinds of water molecules competes with that of ethyl acetate on the surface of MSH.

The evolution of the mean heat adsorption of ethyl acetate measured by calorimetry as a function of pretreatment temperature exhibits a comparable shape: it increases up to 90 °C and is stable up to 140 °C, in agreement with a two steps water releasing.

Water is known to inhibit the activity of basic catalysts in some publications[2,6,7]. Nevertheless, on magnesium silicates with acido-basic properties, the above results show that water molecules are beneficial to this reaction. From literature analysis we can formulated three hypothesis to explain the specific role of water in our systems.

- It was reported that in amorphous aluminosilicate, water molecules adsorbed on aluminium atoms and interacting with neighbouring silanols can easily be deprotonated and therefore are Brønsted acidic sites[30,39]. In MSH, magnesium may polarize adsorbed water and form mild and strong Brønsted acidic sites (Figure 3.8 **a** and **b**) as identified by FTIR with CO adsorption, which could stabilise the methoxide molecule, or activate ester, directly by bonding to the carbonyl group, or indirectly, favouring the departure of the alkoxyl group as reported by Greenwell et al. for adsorbed water on MgAl-layered double hydroxides [4].
- Besides, water may also act as an inhibitor of too strong acidic sites that retain too strongly the reactants, especially the ester as shown by calorimetry.
- Moreover, water contained in catalyst can facilitate the migration of methanol due to the high miscibility between water and methanol, as mentioned by several researchers[5,16]. The removal of this positive water may also affect the conversion of ethyl acetate.

In Chapter 2, the Langmuir–Hinshelwood mechanism is proposed for the transesterification reaction on magnesium silicate with acido-basic properties. We demonstrate here that adsorbed water generates mild Brønsted acids sites that enhance the reactivity, probably by activating the ester.

3.5. Conclusions

Magnesium silicate was thermally treated to remove water adsorbed, and the catalytic performance of this solid before and after pretreatments was tested in the transesterification of ethyl acetate with methanol. Based on DRIFT spectra and ^{1}H NMR results, the effect of water adsorbed on COM on the conversion in transesterification reaction is the following: highly mobile water molecules released for pretreatment temperature lower than 70 °C have no effect on the reactivity. Then, for pretreatment temperatures between 70 to 90 °C, water molecules

that are believed to be bonded to magnesium from their DRIFT spectra and ^{1}H NMR characteristics are lost, and the conversion for the transesterification reaction decreases strongly. Further increase of the pretreatment temperature only led to a small decrease of the conversion as the number of water molecules bonded to magnesium tends to be stable. Two kinds of water adsorption sites are therefore proposed: the magnesium cations located on the edge of the clay-like particles or in the defects present in the silicate layer. From FTIR with CO adsorption results, it is shown that water coordination on these Mg cations in close proximity with OH groups gives mild and strong Brønsted sites which can either stabilise methanol deprotonated by basic Mg-OH groups, activate ester or help the departure of the alkoxyl moiety. Upon water removal, the adsorption energy of ethyl acetate over the catalyst increases, which mean that the ester can be directly connected to the magnesium ion. A too strong adsorption energy of the ester is therefore bad for its reactivity. As a Langmuir-Hinshelwood mechanism has been proposed for the reaction, that involves ester adsorption, it may be inferred that the main role of water on these systems is to help ester adsorption thus enhancing the reactivity.

References

[1] H. Petitjean, H. Guesmi, H. Lauron-Pernot, G. Costentin, D. Loffreda, P. Sautet, F. Delbecq, *ACS Catal.* **2014**, *4*, 4004–4014.

[2] D. Cornu, H. Guesmi, G. Laugel, J.-M. Krafft, H. Lauron-Pernot, *Phys Chem Chem Phys* **2015**, *17*, 14168–14176.

[3] M. Zabeti, W. M. A. Wan Daud, M. K. Aroua, *Fuel Process. Technol.* **2009**, *90*, 770–777.

[4] H. C. Greenwell, S. Stackhouse, P. V. Coveney, W. Jones, *J. Phys. Chem. B* **2003**, *107*, 3476–3485.

[5] Y. Xi, R. Davis, *J. Catal.* **2008**, *254*, 190–197.

[6] I. M. Atadashi, M. K. Aroua, A. R. Abdul Aziz, N. M. N. Sulaiman, *Renew. Sustain. Energy Rev.* **2012**, *16*, 3456–3470.

[7] A. F. Lee, J. A. Bennett, J. C. Manayil, K. Wilson, *Chem Soc Rev* **2014**, *43*, 7887–7916.

[8] C.-R. Chang, Z.-Q. Huang, J. Li, *Wiley Interdiscip. Rev. Comput. Mol. Sci.* **2016**, *6*, 679–693.

[9] D. Nied, K. Enemark-Rasmussen, E. L'Hopital, J. Skibsted, B. Lothenbach, *Cem. Concr. Res.* **2016**, *79*, 323–332.

[10] Y. Xi, R. J. Davis, *J. Catal.* **2009**, *268*, 307–317.

[11] M. J. Kim, S. M. Park, D. R. Chang, G. Seo, *Fuel Process. Technol.* **2010**, *91*, 618–624.

[12] M. Tonelli, F. Martini, L. Calucci, E. Fratini, M. Geppi, F. Ridi, S. Borsacchi, P. Baglioni, *Dalton Trans* **2016**, *45*, 3294–3304.

[13] R. L. Frost, O. B. Locos, H. Ruan, J. T. Kloprogge, *Vib. Spectrosc.* **2001**, *27*, 1–13.

[14] R. L. Frost, E. Mendelovici, *J. Colloid Interface Sci.* **2006**, *294*, 47–52.

[15] V. C. (Victor C. Farmer, *Infrared Spectra of Minerals*, Mineralogical Society, **1974**.

[16] K. Narasimharao, T. T. Ali, S. Bawaked, S. Basahel, *Appl. Catal. Gen.* **2014**, *488*, 208–218.

[17] F. Jin, A. Al-Tabbaa, *Cem. Concr. Compos.* **2014**, *52*, 27–33.

[18] F. R. Cannings, *J. Phys. Chem.* **1968**, *72*, 1072–1074.

[19] R. Prost, *Spectrochim. Acta Part Mol. Spectrosc.* **1975**, *31*, 1497–1499.

[20] J. T. Kloprogge, R. L. Frost, L. Rintoul, *Phys. Chem. Chem. Phys.* **1999**, *1*, 2559–2564.

[21] M. K. Titulaer, *Porous Structure and Particle Size of Silica and Hydrotalcite Catalyst Precursors: A Thermoporometric Study*, Faculteit Aardwetenschappen Der Rijksuniversiteit Te Utrecht], [Utrecht, **1993**.

[22] G. J. Rosasco, J. J. Blaha, *Appl. Spectrosc.* **1980**, *34*, 140–144.

[23] E. Knözinger, K.-H. Jacob, S. Singh, P. Hofmann, *Surf. Sci.* **1993**, *290*, 388–402.

[24] C. Chizallet, G. Costentin, M. Che, F. Delbecq, P. Sautet, *J. Am. Chem. Soc.* **2007**, *129*, 6442–6452.

[25] M. Bailly, C. Chizallet, G. Costentin, J. Krafft, H. Lauronpernot, M. Che, *J. Catal.* **2005**, *235*, 413–422.

[26] S. Coluccia, L. Marchese, S. Lavagnino, M. Anpo, *Spectrochim. Acta Part Mol. Spectrosc.* **1987**, *43*, 1573–1576.

[27] V. C. Farmer, *Infrared Spectra of Minerals*, Mineralogical Society, London, **1974**.

[28] M. Falk, *Spectrochim. Acta Part Mol. Spectrosc.* **1984**, *40*, 43–48.

[29] B. A. Kolesov, *Am. Mineral.* **2006**, *91*, 1039–1048.

[30] J. Blanchard, J.-M. Krafft, C. Dupont, C. Sayag, T. Takahashi, H. Yasuda, *Catal. Today* **2014**, *226*, 89–96.

[31] E. Garrone, B. Onida, B. Bonelli, C. Busco, P. Ugliengo, *J. Phys. Chem. B* **2006**, *110*, 19087–19092.

[32] G. Crépeau, V. Montouillout, A. Vimont, L. Mariey, T. Cseri, F. Maugé, *J. Phys. Chem. B* **2006**, *110*, 15172–15185.

[33] B. L. Phillips, P. C. Burnley, K. Worminghaus, A. Navrotsky, *Phys. Chem. Miner.* **1997**, *24*, 179–190.

[34] J. P. Yesinowski, H. Eckert, G. R. Rossman, *J. Am. Chem. Soc.* **1988**, *110*, 1367–1375.

[35] J. Jiao, S. Altwasser, W. Wang, J. Weitkamp, M. Hunger, *J. Phys. Chem. B* **2004**, *108*, 14305–14310.

[36] Y. Jiang, J. Huang, W. Dai, M. Hunger, *Solid State Nucl. Magn. Reson.* **2011**, *39*, 116–141.

[37] P. Clausen, W. Andreoni, A. Curioni, E. Hughes, C. J. G. Plummer, *J. Phys. Chem. C* **2009**, *113*, 12293–12300.

[38] A. Krysztafkiewicz, R. Werner, L. K. Lipska, T. Jesionowski, *Colloids Surf. Physicochem. Eng. Asp.* **2001**, *182*, 65–81.

[39] F. Leydier, C. Chizallet, A. Chaumonnot, M. Digne, E. Soyer, A.-A. Quoineaud, D. Costa, P. Raybaud, *J. Catal.* **2011**, *284*, 215–229.

Chapter 4. Phyllosilicates

4.1. Introduction

In last chapter, the role of water adsorbed on Mg located at defects or edges on the activity of MSH was clarified. As the MSH has a similar structure than phyllosilicates, such as talc, it would be interesting to investigate the reactivity of phyllosilicates for transesterification reaction. Phyllosilicates have been widely studied as catalysts in transesterification reaction as presented in chapter 1, showing that natural clay minerals such as montmorillonite and kaolin have no activity in transesterification reaction, and that, acidic or basic treatment are required to improve their catalytic performance. In this chapter, we will study some natural phyllosilicates such as talc, montmorillonite, and some synthesized ones, *i.e.* nano talc and laponite for transesterification of ethyl acetate with methanol in liquid phase. First, the classification of phyllosilicates and their structures will be presented.

4.1.1. Classification of phyllosilicates

Silicate minerals are classified as seven subclasses based on the number of Si tetrahedrons linked together by oxygen: nesosilicate, sorosilicate, cyclosilicate, inosilicate-single chain, inosilicate-double chain, phyllosilicates and tectosilicates (Figure 4.1)[1]. Their structures, except phyllosilicates which will be described later, are displayed in Figure 4.2[1]. They all present the tetrahedral unit SiO_4^{4-} consisting of one Si^{4+} surrounded by four O^{2-}. In the subclass nesosilicate, no oxygen of one SiO_4^{4-} tetrahedron is shared with other SiO_4^{4-} tetrahedra, but they are shared with octahedral groups that contain cations like Mg^{2+} or Ca^{2+}. The common species are olivines, garnets, sphene etc. If one oxygen of one tetrahedron is shared with another tetrahedron, it forms sorosilicate, the basic structural unit is $Si_2O_7^{6-}$. In cyclosilicates, two oxygens of each tetrahedron are shared with two adjacent tetrahedra, and the linked tetrahedra are arranged in a ring. The ring may be formed by linking of 3, 4, 5 or 6 tetrahedra, forming the structural units $Si_3O_9^{6-}$, $Si_4O_{12}^{8-}$, $Si_5O_{15}^{10-}$ and $Si_6O_{18}^{12-}$, respectively. In inosilicate-single chain, two oxygens of each SiO_4^{4-} tetrahedron are shared in a way to form a long single chain of linked tetrahedra. The elementary structural unit of inosilicate-single chain is $Si_2O_6^{4-}$. Two parallel chains linked together form insolicate-double chain, with an elementary structural group $Si_4O_{11}^{6-}$. In tectosilicates, each SiO_4^{4-} tetrahedron is linked to four adjacent tetrahedra to form framework, for example, quartz, cristobalite etc.[1]. In phyllosilicates, three

oxygens of each SiO_4^{4-} tetrahedron are shared with adjacent tetrahedra to form an infinite sheet of tetrahedra, having the elementary structural unit $Si_2O_5^{3-}$, which will be described in detail later.

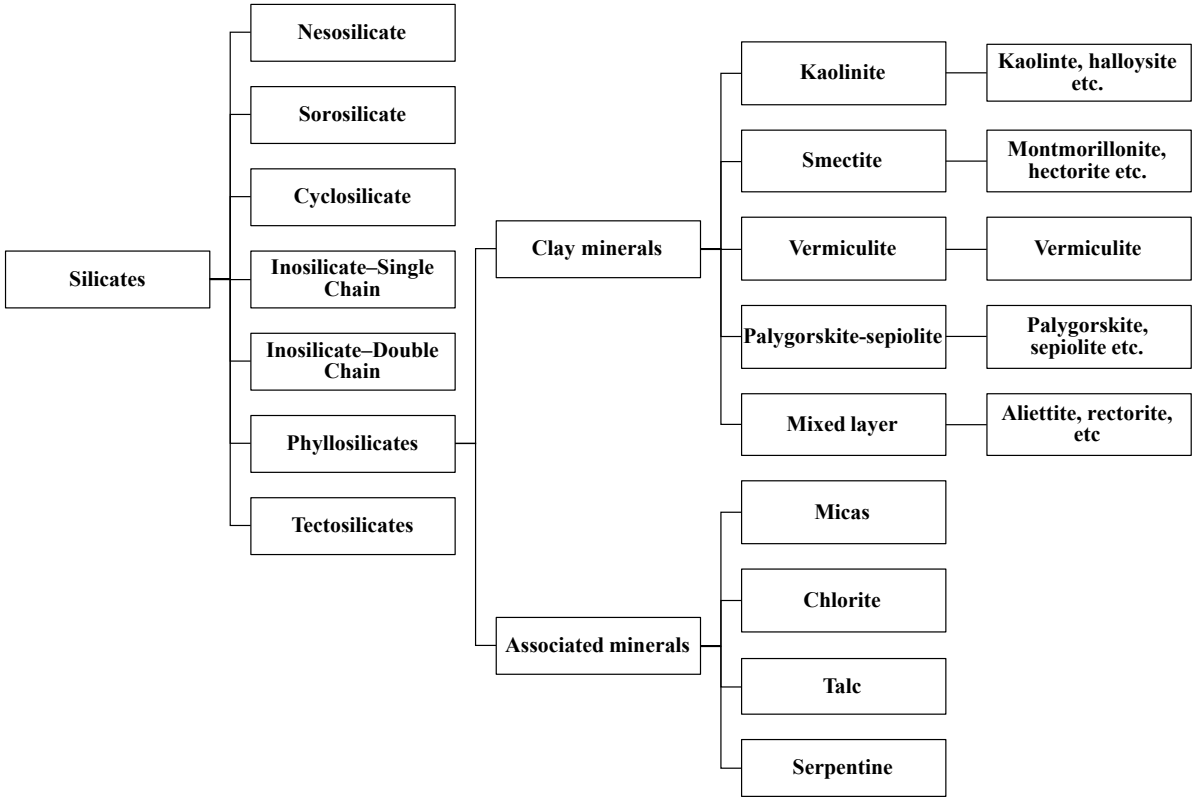

Figure 4.1: Classification of silicate minerals[1].

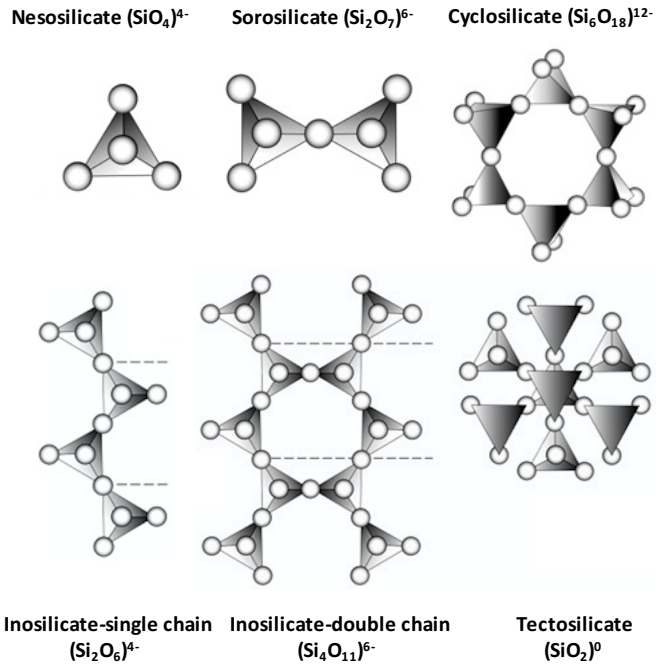

Figure 4.2: Structures of silicates[1].

Phyllosilicates are the object of the study in this section. They are the main constituents of clay, so we first define what clay is. The Joint Nomenclature Committee (JNC) gives the definition of clay: "the term 'clay' refers to a naturally occurring material composed primarily of fine-grained minerals, which is generally plastic at appropriate water contents and will harden when dried or fired." In nature, clay contains mineral constituents and associated phases (amorphous like allophone, imogolite etc., and organic matters like peat, muck etc.). Then, the mineral constituents are divided into two types: clay minerals and associated minerals[2] (Figure 4.1). The former type includes five groups: kaolinite, smectite, vermiculite, palygorskite-sepiolite and mixed layer group. While the later one includes four groups: micas, chlorite, talc and serpentine group (Figure 4.1)[1].

4.1.2. Structure of phyllosilicates

Two elementary units are important to build the phyllosilicates, *i.e.* tetrahedric silicon species (SiO_4^{4-}) and divalent or trivalent metals coordinated octahedrically to hydroxyl groups ($M^{2+}/M^{3+}(OH)_6$). The silicon tetrahedra share the three basal oxygens with other silicon tetrahedra to build a hexagonal two-dimensional pattern, the tetrahedral sheet (T-sheet), and the remained apical oxygens point toward the same direction to link to octahedric cation. The octahedra share edges to form a two-dimensional unit, the so-called octahedral sheet (O-sheet). If the octahedron is centered with M^{2+}, all octahedral sites are occupied like in the structure of brucite ($Mg(OH)_2$) and the sheet is called trioctahedral. If the cation is trivalent (M^{3+}), then only 2/3 of the octahedral sites are occupied and the resulting two-dimensional unit resembles the structure of gibbsite $Al(OH)_3$; in this case, the sheet is named dioctahedral[3].

In the ideal condition, the apical oxygen of the tetrahedral sheets can be linked to one octahedral, building the T-O structure (1:1 structure). On one side, the basal plane consists in O^{2-} of the T-sheet, on the other side there is a plane of OH^-. Between them, an anionic plane consists of the apical oxygens of the T-sheets and the unshared OH^- of the octahedra[3]. So the chemical formulas of phyllosilicates with dioctahedral or trioctahedral T-O structure are written as $M_2(OH)_4Si_2O_5$ and $M_3(OH)_4Si_2O_5$ respectively, for example kaolinite ($Al_2(OH)_4Si_2O_5$).

As both sides of the octahedral have hydroxyls to share, one octahedral can be sandwiched by two tetrahedral sheets, originating the T-O-T structure (2:1 structure). Again, the chemical formulas of phyllosicates with dioctahedral or trioctahedral T-O-T structure are $M_2(OH)_2Si_4O_{10}$ and $M_3(OH)_2Si_4O_{10}$ respectively, for example talc ($Mg_3(OH)_2Si_4O_{10}$).

In nature, phyllosilicates are formed under weathering process, through which many different isomorphic substitutions occur either in the tetrahedral (Si by Al or Fe) or in the octahedral sheets (Al or Mg by Fe, Li, Ti, V, Cr, Mn, Co, Ni, Cu and Zn)[4]. The isomorphic substitution generates an excess of negative charge into the layers, which needs to be compensated by corresponding cations located between two T-O-T layers. An interlayer cation is surrounded by 12 oxygens: six basal oxygens from each T-O-T layer in its opposite sides. So its position is known as the 12-fold coordination site[3].

Depending on the structure and chemical nature of the clay minerals, four main groups will be described below[3]:

- The kaolinite group have dioctahedral T-O structure and the general chemical formula is $Al_2(OH)_4Si_2O_5$, as shown in Figure 4.3[5].

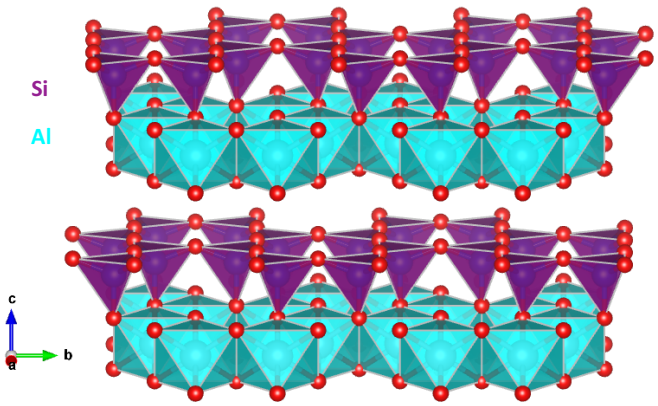

Figure 4.3: Structure of kaolinite. Database_code_amcsd 0017947.[5]

- The smectite group has trioctahedral or dioctahedral T-O-T structure. The tetrahedral and/or octahedral cations are substituted by cations in low degree. The charge imbalance thus produced is neutralised by a small number of interlayer cations like Ca^{2+} or Na^{+}, but they don't occupy all the available vacant sites between two T-O-T layers. The general chemical formula is $(Ca,Na,Cs)_{0.2\text{-}0.3}(Al,Mg,Fe)_{2\text{-}3}(OH)_2[(Si,Al)_4O_{10}]\cdot nH_2O$. Representatives of this group are hectorite, laponite (a synthesized phyllosilicate that has similar structure than hectorite, but shorter sheets), saponite, montmorillonite, etc. The structure of hectorite-Cs is shown in Figure 4.4[6].

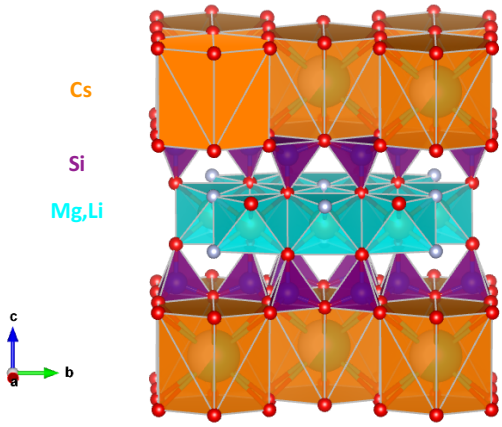

Figure 4.4: Structure of hectorite. Database_code_amcsd 0015819.[6]

- The vermiculite group also has trioctahedral or dioctahedral T-O-T structure, but the substituted degree is higher than that of smectite group, and the most common interlayer cation in vermiculites is Mg^{2+}; others are Ca^{2+} and Na^{+}. The general chemical formula is $(Mg,Ca,Na)_{0.6\text{-}0.9}(Mg,Fe^{3+}Al)_6(OH)_4[(Si,Al)_8O_{20}]\cdot nH_2O$.

- The palygorskite-sepiolite group are finely fibrous minerals. They have T-sheets like the other phyllosilicates, but the cationic octahedra are linked together to form chains or ribbons, not O-sheets like other phyllosilicates. These octahedral chains are attached to the T-sheets, with much vacant spaces left in between them. Those vacant channels can accommodate water molecules and also organic molecules. The chemical formula of sepiolite is $Mg_4(OH)_2Si_6O_{15}\cdot nH_2O$ and the structure is shown in Figure 4.5[7].

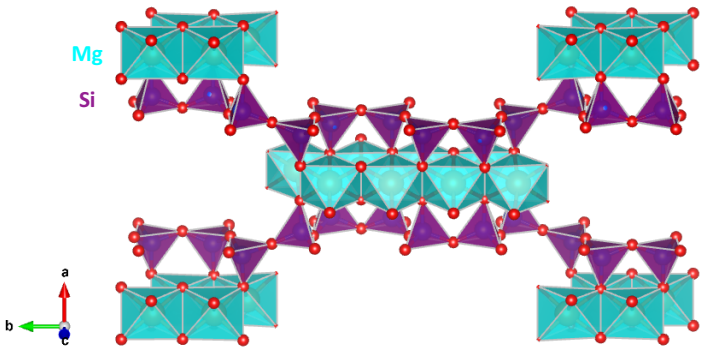

Figure 4.5: Structure of sepiolite. Database_code_amcsd 0004269.[7]

In our study, talc, nano talc, laponite and montmorillonite were studied. The choice of these phyllosilicates is based on the fact that, talc has a similar structure than MSH. To study the role of particle edges, nano talc and laponite, with small particle size were synthesized. Finally, the montmorillonite is also tested as it was reported numerously in literature for transesterification reaction, even if not very active when not treated with acids.

Montmorillonite has dioctahedral T-O-T structure and small amounts of aluminium octahedra are substituted by magnesium octahedra. Talc has trioctahedral T-O-T structure, consisting in magnesium surrounded by an octahedron formed by oxygen, sandwiched between tetrahedral silicate sheets. Nano talc has the similar structure and chemical formula but its particle sizes are smaller. Laponite with nanoparticle sizes, has trioctahedral T-O-T structure, and small amounts of Mg octahedra are substituted by Li octahedra. The chemical formulas of these phyllosilicates are given in Table 4.1.

Table 4.1: Chemical formulas of phyllosilicates.

Phyllosilicates	**Chemical Formula**
Montmorillonite	$(Na,Ca)_{0.33}(Al,Mg)_2(OH)_2\ (Si_4O_{10})\cdot nH_2O$
Talc	$Mg_3(OH)_2\ (Si_4O_{10})\cdot nH_2O$
Nano talc	$Mg_3(OH)_2\ (Si_4O_{10})\cdot nH_2O$
Laponite	$Na_{0,55}(Mg_{5,45}Li_{0,55})\ (Si_8O_{20})(OH)_4\cdot nH_2O$

4.2. Preparation of catalysts

Montmorillonite (Gonzales County, Texas, USA) is purchased from University of Missouri-Columbia, Source Clay Minerals Repository.

Talc was purchased from Sigma-Aldrich (243604-500G, CAS: 14807-96-6), whose average grain size is 10 µm. For synthesis of nano talc, the starting materials for the experiment were magnesium acetate tetrahydrate ($(CH_3COO)_2Mg\_4H_2O$), sodium metasilicate pentahydrated ($Na_2SiO_3\_5H_2O$), sodium acetate trihydrate ($CH_3COONa\_3H_2O$), and acetic acid. All reagents were purchased from Aldrich and used without any further purification. A 1N solution of acetic acid was prepared using deionized water. Samples of synthetic talc were prepared using the new process describes in a recent patent by Dumas et al.[8]. Synthetic talc preparation, whatever the process, requires at least two steps: (1) the preparation of a talc

precursor at room temperature that respects the Mg/Si talc ratio and (2) the hydrothermal treatment. (by Maguy Jaber)

In the synthesis of laponite, sodium silicate (metasilicate pentahydrated (Na_2SiO_3_$5H_2O$),) is reacted with magnesium, sodium and lithium salts (acetate salts from sigma Aldrich) in presence of acetic acid forming an amorphous product. The amorphous product is transformed in a less ordered material by hydrothermal reaction at around 220°C. (by Maguy Jaber)

4.3. Characterisation of the phyllosilicates

4.3.1. X-ray spectroscopy analysis

The structure of talc is monoclinic, having two structural layers per unit[9]. XRD patterns of talc and nano talc are displayed in Figure 4.6. The peaks profile of talc fit well with the PDF 00-013-0558, the data of which was provided and identified to the feature reflections of talc by Stemple et al.[10]. It can be seen from the Figure 4.6 that, the nano talc is highly disordered, and apart from the basal reflections, few clear reflections remain. Furthermore, the $(\bar{1}32)$ and (132) reflections are broadened into a single broad peak. The (004), $(\bar{1}11)$, (006), (0010) and (060) reflections, usually strong, are broadened and their intensities decrease.

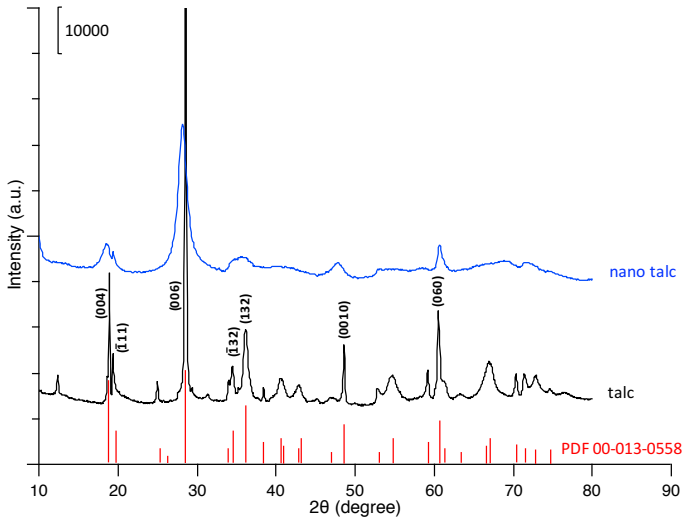

Figure 4.6: XRD patterns of talc and nano talc.

XRD patterns of laponite are shown in Figure 4.7. For comparing, the profiles of PDF 00-009-0031 which was identified as hectorite[11], is also displayed in Figure 4.13. Laponite

exhibits a somewhat broad XRD pattern indicating low crystallinity and small particle size. The (100), (005) and (300) reflections are broad and the (110) and (112), (211) and (212), (220) and (222) reflections are broadened into a single broad peak, respectively.

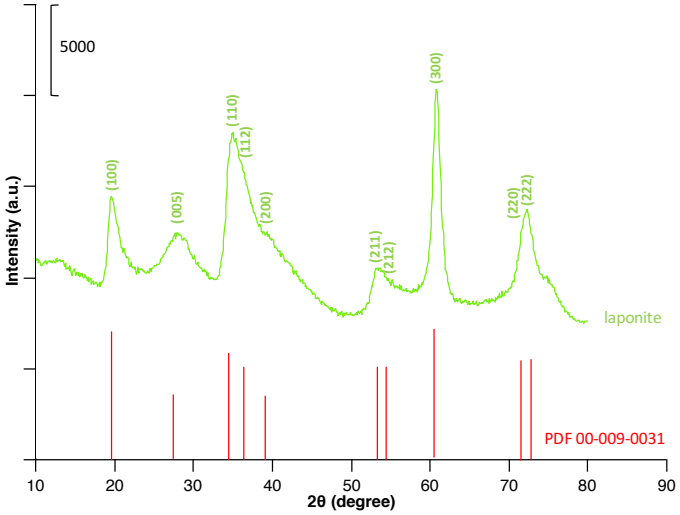

Figure 4.7: XRD patterns of laponite

The broadening of a peak in a diffraction pattern is related to the size of sub-micrometer particles, which can be determined by the Scherrer equation (Equation 4.1)[12,13].

$$\tau = \frac{K\lambda}{\beta \cos\theta}$$

Equation 4.1

In this equation, τ is the mean size of the ordered (crystalline) domains, which may be smaller or equal to the grain size; K is a dimensionless shape factor, with a value close to unity. The shape factor has a typical value of about 0.9, but varies with the actual shape of the crystallite; λ is the X-ray wavelength; β is the line broadening at half the maximum intensity (FWHM), after subtracting the instrumental line broadening (in radians); θ is the Bragg angle (in degrees).

From the Equation 4.1, one can deduce that the increase of the broadening of peak, could be caused by the decrease of the size of sub-micrometer particles. We will use the Equation 4.1, to calculate the crystallite size of talc, nano talc and laponite (Table 4.2). The talc is purchased

from Sigma Aldrich, whose grain is 10 μm, but the crystallite size calculated based on the reflection is 45 nm. Dellisanti et al.[14] also reported a commercial talc with a grain size of around 20 μm, but its crystallite diameter is calculated to be 60 nm from XRD reflection. The crystallite diameter of nano talc is around 6 nm based on the reflection at 2θ = 28.18˚. The crystallite diameter of laponite is slightly higher, with a calculated value of 8 nm based on the reflection 2θ = 60.84˚. In conclusion, the nano talc and laponite are successfully synthesized with small particle sizes.

Table 4.2: Calculating particle sizes of talc, nano talc and laponite.

Sample	**2θ (degree)**	**FWHM (degree)**	**Size (nm)**
Talc	28.58	0.18	45
Nano talc	28.18	1.29	6
Laponite	60.84	1.10	8

Thanks to the X-ray fluorescence measurement, the compositions of studied talc, nano talc and laponite are revealed and shown in Table 4.3. Only elements whose atomic numbers are higher than 11 are given here. All samples present the main elements Mg and Si, with negligible impurities Ca, Al, K and Cl. As expected the talc and nano talc have the same mole ratio of Mg/Si.

Table 4.3: Compositions of phyllosilicates by X-ray fluorescence measurement.

Sample	**Mg (wt%)**	**Si (wt%)**	**Ca (wt%)**	**Al (wt%)**	**K (wt%)**	**Cl (wt%)**	**Mg/Si (mol/mol)**
talc	16.94	31.41	0.14	0.56	0.07	0.25	0.62
nano talc	17.36	32.68	0	0.03	0.06	0.28	0.61
laponite	14.75	34.56	0.09	0.05	0.09	0.40	0.49

4.3.2. Nitrogen sorption analysis

Nitrogen sorption measurements are performed to examine the porous nature of the talc, nano talc and laponite. Figure 4.8 shows the N_2 adsorption-desorption isotherms of the samples. The N_2 isotherm of talc corresponds to a type II isotherm in IUPAC classification[15]. Reversible Type II isotherms are given by the physisorption of most gases on nonporous or macroporous

adsorbents. The shape is the result of unrestricted monolayer-multilayer adsorption up to high P/P_0. At low P/P_0, the small increase section usually corresponds to the completion of monolayer coverage, after that, the multilayer adsorption occurs. The thickness of the adsorbed multilayer generally appears to increase without limit when $P/P_0 = 1$. Using the BJH method and the desorption branch of the nitrogen isotherm, the calculated pore-size distribution indicates that the talc contains no pores (Figure 4.9) and the BET specific surface area is only 14 $m^2 g^{-1}$ (Table 4.4). Dellisanti et al.[14] also reported a very low specific surface area (5 $m^2 g^{-1}$) of a commercial talc.

The shape of adsorption branch of nano talc resembles that of talc. But adsorption/desorption isotherms of nano talc exhibit a type IV isotherm with a hysteresis loop, demonstrating its mesoporous characteristics. According to the IUPAC classification[15], the loop observed is ascribed to type H_3, which is given by non-rigid aggregates of plate-like particles. The pore size calculated using the BJH method is 3.7 nm (Figure 4.9). The BET specific surface area of nano talc is calculated from N_2 isotherms, and is found to be as much as about 140 $m^2 g^{-1}$, which is remarkably higher than that of talc (Table 4.4). The total volume of pores is 0.14 $cm^{-3} g^{-1}$ (Table 4.4). The extremely high BET surface area and large total pore volume strongly support the fact that the nanoparticles have a porous structure.

Isotherms of the laponite are identified as type IV, which is characteristic of mesoporous materials. According to the IUPAC classification[15], the wide triangular loop at medium relative pressures is ascribed to type H_2 hysteresis. The H_2 hysteresis is characteristic of ink-bottle-like pores (internal porosity). In addition, the same narrow pore size distribution, derived from desorption data and calculated from the isotherm using the BJH model, was observed with an average pore diameter at 3.7 nm (Figure 4.9). The BET specific surface areas are calculated as shown in Table 4.4, that is as high as 390 $m^2 g^{-1}$. From the BET gas sorption measurements, we can conclude that the laponite has a more developed porous nature than nano talc, and both of them shows a remarkable higher specific surface area than talc, which fits well with the particle sizes calculated from the XRD reflections.

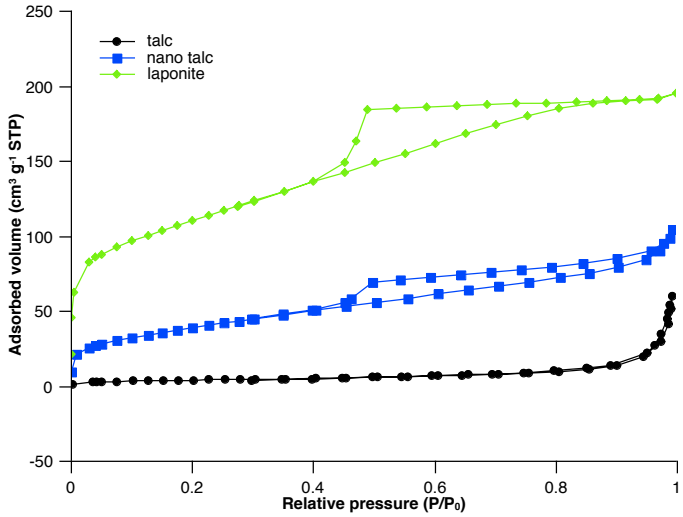

Figure 4.8: N_2 adsorption-desorption isotherms patterns of phyllosilicates.

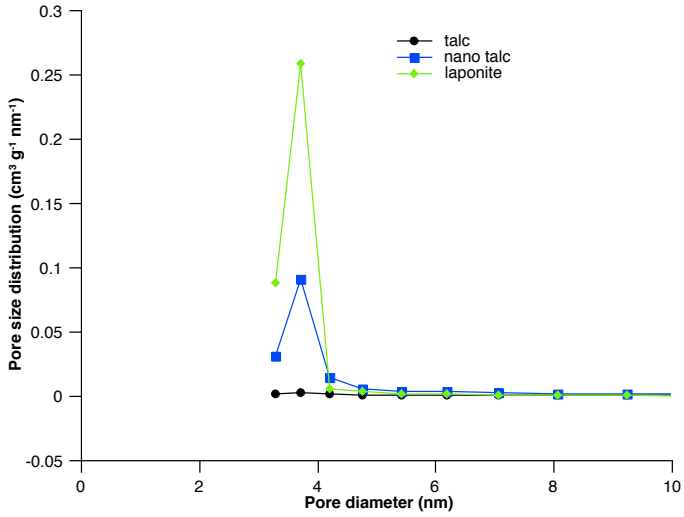

Figure 4.9: BJH pore size distributions for phyllosilicates.

Table 4.4: Specific surface area and pore volume of phyllosilicates.

Sample	**talc**	**nano talc**	**laponite**
Specific surface area (m^2 g^{-1})	14	140	390
Pore volume (cm^3 g^{-1})	0.05	0.14	0.30

4.4. Catalytic test of phyllosilicates

We use the same operation conditions for transesterification in liquid phase as described in chapter 2 (Figure 2.3). The limitation of mass transfer is checked with the laponite sample.

As shown in Figure 4.10, the conversion of AcOEt increases rapidly linearly with the mass of laponite below 15 mg. Then the limitation of mass transfer exists beyond 15 mg of catalyst. Thus, we will use 15 mg of catalyst for the next study.

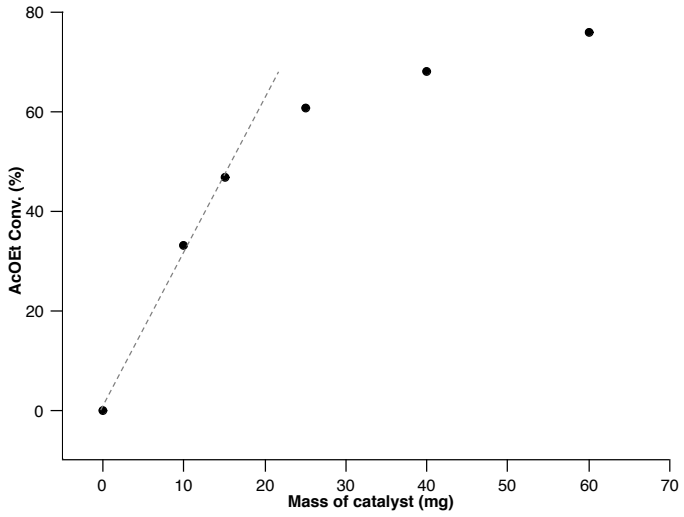

Figure 4.10: Conversion of AcOEt as a function of mass of laponite after 5 hours of reaction.

The reaction conditions for the next study are resumed: temperature = 60 ^{o}C; catalyst = 15 mg; mole ratio of MeOH/AcOEt = 24.3; MeOH = 10 mL; AcOEt = 1 mL; dioxane = 1 mL; stirring rate = 630 rpm; reaction time = 5 hours.

The catalytic performances of talc, nano talc and laponite are studied in the transesterification of ethyl acetate. Moreover, these will be compared to those obtain with the montmorillonite, which is already used in the literature as catalyst in transesterification reaction. As shown in Figure 4.11, no conversion of ethyl acetate is observed on montmorillonite, similar to the result reported by Zanette et al.[16]. Ratti et al.[17] also tested montmorillonite to catalyze transesterification of ß-ketoester with octanol, and no activity was observed as well. Talc shows only 3% conversion of ethyl acetate. However, the nano talc with smaller particle size shows a good activity. Moreover, laponite with higher specific surface area, shows around twice activity than that of nano talc (Figure 4.11). The catalytic results indicate that the phyllosilicates catalysts with small particle size, thus having high specific surface and abounding border OH, are promising for transesterification reaction. It can be inferred that the active sites should be located at the edges of particle layers.

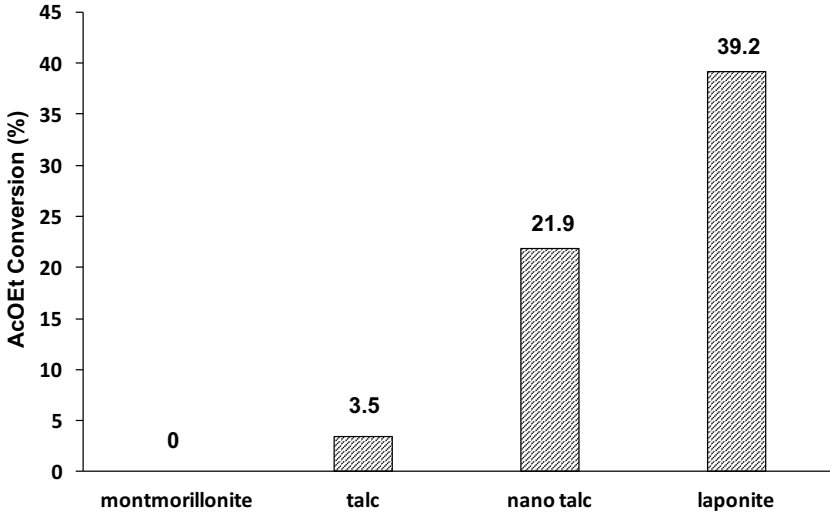

Figure 4.11: Conversion of ethyl acetate on a series of phyllosilicates catalysts.

To go further, it would be very interesting to focus on laponite to understand why the laponite is so active and to reveal the active sites. First of all, the potential occurrence of homogeneous catalysis is checked by removing the solid catalyst by means of centrifugation at high speed (20000 rpm). As shown in Figure 4.12, the conversion of ethyl acetate evolves little after removing the solid laponite. It means that the homogeneous reaction is limited.

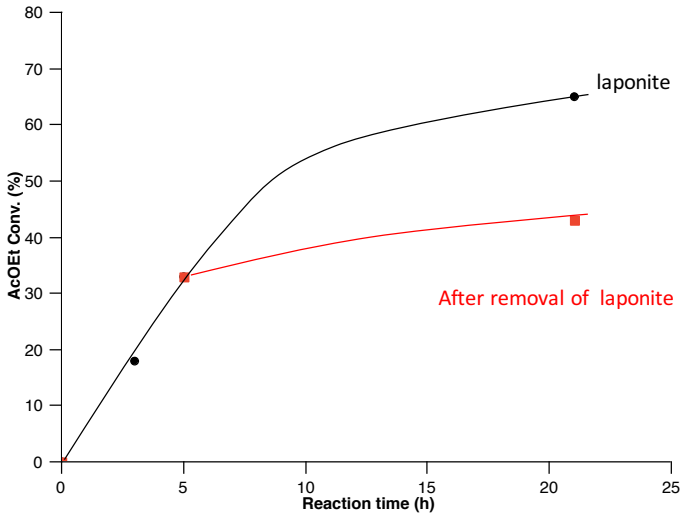

Figure 4.12: Evolution of ethyl acetate conversion before and after removal of laponite.

As the particle size of laponite is small, a low speed of centrifugation may be unable to remove all laponite, which means that some smaller particles may remain in the liquid. This idea stimulates us to obtain these smaller particles to test whether they are more active or not. As shown in Table 4.5, first, after 5 h reaction, the solid is separated from the reactant mixture

by centrifugation at 7000 rpm (labelled as laponite spent). The laponite spent is reused and it encounters a significant decrease of activity (Entry 2). Then, we just treat the laponite with methanol at 60 ^{o}C for 5h (the treatment conditions is the same as reaction conditions) and separate the solids by centrifugation at 7000 rpm (labelled as laponite treated). The laponite treated shows a similar activity than laponite spent. (Entry 3 *vs* Entry 2). These experiments indicate that a speed of 7000 rpm of centrifugation is not enough to separate all laponite solids from liquid phase, smaller particles can form colloids in methanol at 60 oc that are hardly separated at 7000 rpm and contribute significantly to the total conversion. We find that these smaller particles can forms colloid in methanol at 60 ^{o}C that is hardly separated through centrifugation at 7000 rpm. So we obtain these small amount of the smaller particle (labelled as laponite AS) by evaporating the liquid phase: 2 g laponite was treated by 200 mL methanol at 60 ^{o}C for 5h, then after centrifugation at 7000 rpm, we obtained the liquid phase and evaporate the methanol, the laponite AS was then obtained. As shown in Table 4.5, Entry 4, it is interesting to note that, laponite AS with smaller particle sizes exhibits excellent catalytic performances.

Table 4.5: Reactivity of laponite based catalysts.

Entry[a]	**Catalyst**	**AcOEt Conv. (%)**	**Reaction time (h)**	**Catalyst mass (mg)**
1	laponite	39.2	5	15
2	laponite spent	23.9	5	15
3	laponite treated	25.7	5	15
4	laponite AS	94.9 (78.4)[b]	5	15

[a] Entry 1: standard reacition, reaction conditions: laponite, 15 mg; temp, 60 ^{o}C; MeOH, 10 mL; AcOEt,1 mL.

Entry 2: after a standard reaction, solid was separated from reaction mixture by centrifugation at 7000 rpm, then solid was put in oven at 60 ^{o}C overnigth. It is labelled in laponite spent.

Entry 3: 2 g laponite was treated by 200 mL MeOH at 60 ^{o}C for 5h, then after centrifugation at 7000 rpm, solid was obtained and dry in oven at 60 ^{o}C overnigth. It is labelled laponite treated.

Entry 4: 2 g laponite was treated by 200 mL MeOH at 60 ^{o}C for 5h, then after centrifugation, the MeOH was obtained (colloidal sol), after evaporation, solid was obtained. It is labelled in laponite AS.

[b] The data in the parenthesis is the conversion after 1 h reaction time.

Laponite AS is then characterized by XRD to identify the very active phase. As shown in Figure 4.13, the XRD pattern of laponite AS indicates that it consists of laponite and carbonates ($Na_3H(CO_3)_2$ $2H_2O$, PDF 00-029-1447, a mixture of $NaHCO_3$ and Na_2CO_3). We try to used methanol to wash away the carbonate crystalline phase (the washed sample is labelled as laponite ASW) but it does not seem to be soluble (Figure 4.14).

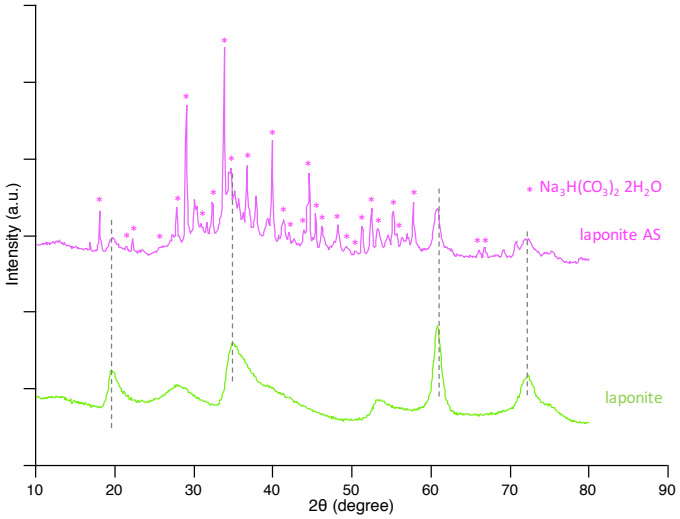

Figure 4.13: XRD patterns of laponite, laponite treated and laponite AS.

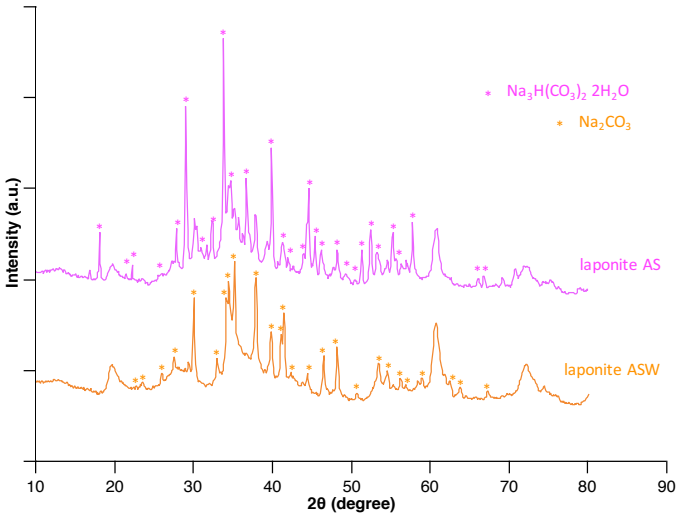

Figure 4.14: XRD patterns of laponite AS and laponite ASW.

Thus we may ask whether the high catalytic activity of laponite AS is due to laponite or the carbonates. To try to answer this question, we test $NaHCO_3$ (15 mg) for transesterification reaction. As shown in Figure 4.15, $NaHCO_3$ is able to catalyse the transesterification of ethyl acetate with methanol. However, the active of laponite AS is 8 times higher that that of

$NaHCO_3$. So we can conclude that the main activity of laponite AS does not come from the carbonates, but due to the smaller particle size of laponite.

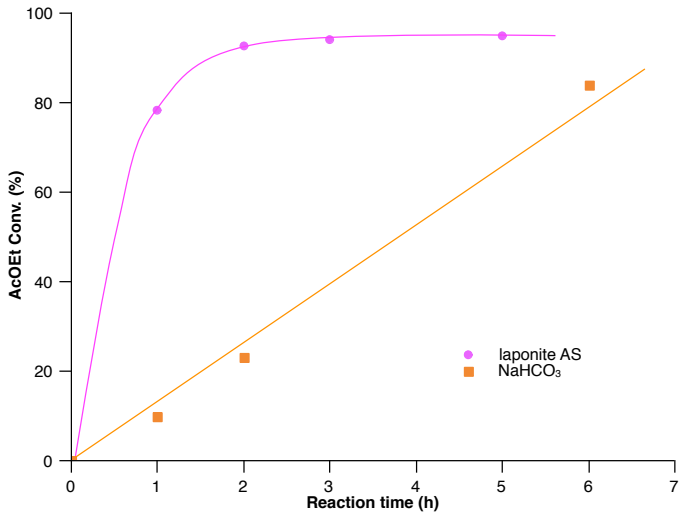

Figure 4.15: Activity of laponite AS and $NaHCO_3$ for transesterification reaction.

In conclusion, a series of phyllosilicates are studied for transesterification reaction, and nano talc and laponite with nanoparticle sizes show promising catalytic performance. Moreover, depending on the speed of centrifugation, laponite with smaller particle size can be obtained, that give an excellent activity. Thus, it further confirm that the edges of particles with abounding OH play a key role on the activity. To understand the reaction mechanism on laponite, the kinetic study will be performed.

4.5. Kinetic study

4.5.1. Deactivation behaviour of catalyst

The evolution of AcOEt conversion during 32 hours is displayed in Figure 4.16. In the first 7 h, the conversion increases linearly, but after that, it increases more slowly. This phenomenon implies that at the beginning of the reaction, deactivation occurs insignificantly. So we can directly calculate the reaction rate at the beginning of reaction without considering the deactivation of catalyst.

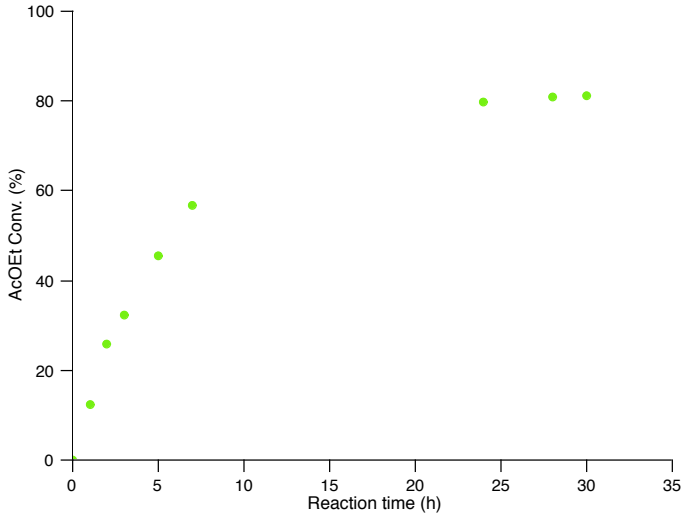

Figure 4.16: The conversion of AcOEt as a function of reaction time on laponite.

4.5.2. Calculation of the order of reaction in ethyl acetate

In order to calculate the order of reaction in ethyl acetate, the kinetics study will therefore be carried out at a constant methanol concentration and with a variable ester concentration (Table 2.8). The evolution of AcOEt concentration as a function of reaction time is given in Figure 4.17. As there is no significant deactivation at the beginning of reaction, the initial reaction rates are obtained from the slopes of the dotted lines (Figure 4.17). Then, the intial concentrations of AcOEt and initial reaction rates are plotted with the logarithm of these two quantities, which gives access to $\ln r_0 = \ln k' + \alpha \ln[\mathrm{AcOEt}]_0$. The slope obtained should be the order of the reaction in ethyl acetate (Figure 4.18). The curve seems to have points aligned on two straight lines with good correlation coefficients (0.99977), which indicates that the order of the reaction for AcOEt is 0.97 for a concentration lower than 0.85 mol L^{-1} (MeOH/AcOEt > 24.3). For higher concentration, it seems that the order of the reaction decreases even if the number of experiments is not sufficient to conclude.

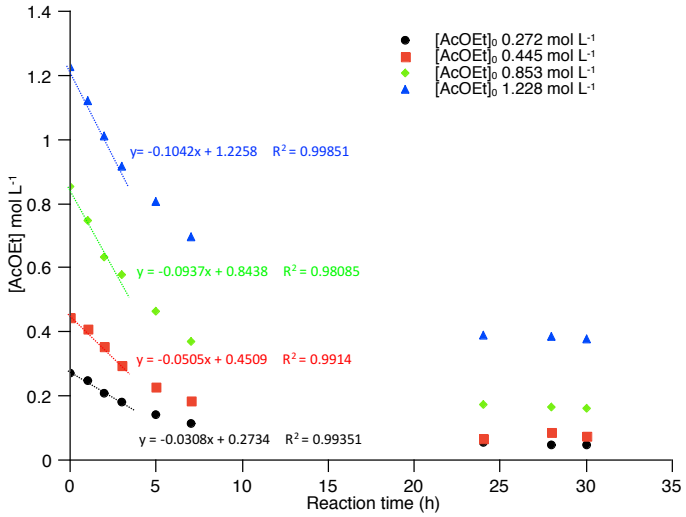

Figure 4.17: The evolution of AcOEt concentration with the reaction time on laponite.

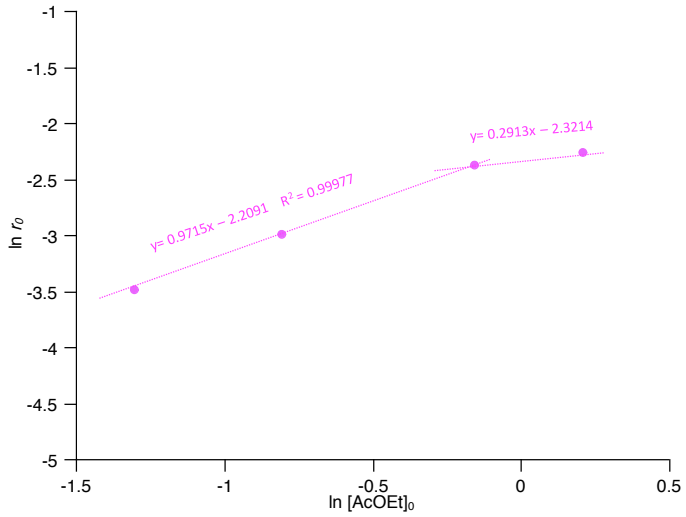

Figure 4.18: Logarithm of the initial reaction rate as a function of the logarithm of initial AcOEt concentration.

As discussed in section 2.7, several mechanisms allow us to find an order equal to 1: (1) Eley-Rideal mechanism assuming the reaction of adsorbed methanol with ethyl acetate in liquid phase as rate determining; (2) Eley-Rideal mechanism with the ethyl acetate adsorption as rate determining. (3) Langmuir-Hinshelwood mechanism involving two different kinds of sites, and considering the adsorption of ethyl acetate as rate determining; (4) Langmuir-Hinshelwood mechanism involving one kind of sites, and considering the adsorption of ethyl acetate as rate determining.

In Chapter 2, from the kinetic study, we concluded that transesterification reaction on magnesium silicate with acido-basic properties, obeys to the Langmuir-Hinshelwood mechanism. For laponite, in order to identify the most plausible mechanism among the four discussed above, the acido-basic properties of laponite are studied and compared with that of Mg silicate (com). From Figure 4.19, it can be seen that, laponite shows almost purely basic properties that is completely different from Mg silicate (com). It is thus reasonable to propose that, the laponite that exhibits mainly basic route in MBOH conversion (like MgO[18]), reacts following a mechanism in which MeOH adsorbs on basic sites but does not involve the ester adsorption on acidic sites. So we can reject the later three mechanisms that involve the adsorption of ester and proposed that the transesterification reaction on laponite with mainly basic sites obey the Eley-Rideal mechanism considering the reaction of adsorbed methanol with ethyl acetate in liquid phase as rate determining.

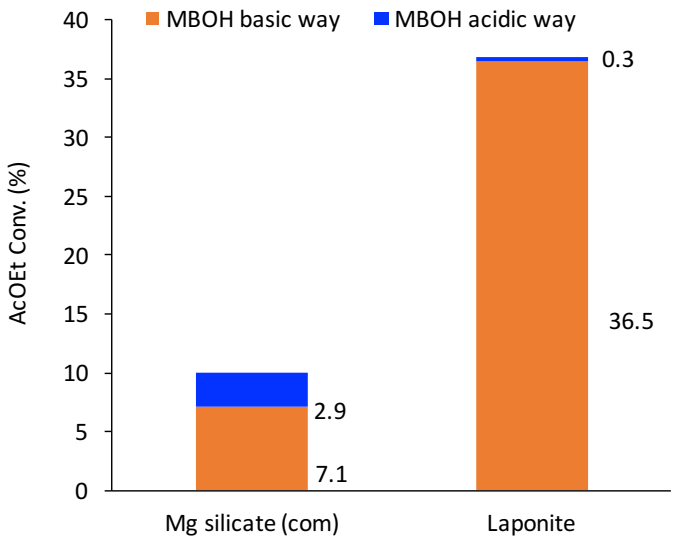

Figure 4.19: Conversion of MBOH following the acidic and basic route for the COM and laponite.

From the results of kinetic study, laponite shows very distinct acido-basic property compared to Mg silicate (com), thus obey a different mechanism for transesterification reaction. In chapter 3, the role of water on the reactivity of COM was clarified. It would be interesting to investigate the effect of thermal treatment on the reactivity of laponite to see if this difference in the mechanism leads to a different behaviour upon when adsortion.

4.6. Role of thermal treatment

4.6.1. Catalytic performance and TGA measurement

In last chapter, it has been found that the adsorbed water on COM plays a positive role on the reactivity. Here we also want to see if on the laponite we have the same effects. So the laponite were thermally treated at 70, 200, 280, 350, 430 and 500 °C, respectively for 2 h after heating at a rate of 5 °C min^{-1} under 20 mL min^{-1} of flowing N_2. These samples are denoted as laponite-X (X being the pretreatment temperature in °C).

Transesterification of ethyl acetate with methanol on laponite with thermal pretreatment was studied and the AcOEt converison as a function of the pretreatment temperature are given in Figure 4.20. At low pretreatment temperature, the conversions show a slight increase below 200 °C and then improves rapidly as the pretreatment temperature increases. A maximum of reactivity is observed for intermediate pretreatment temperature (around 350 °C). Then a further increase in pretreatment temperature leads to the decrease of conversion.

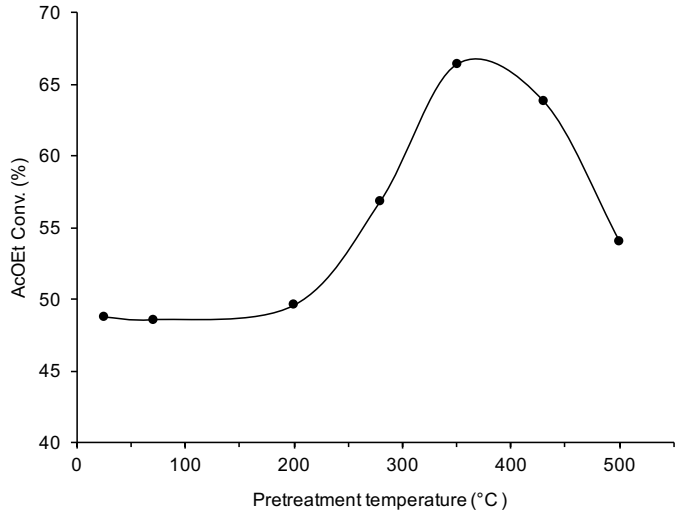

Figure 4.20: Conversion of ethyl acetate on laponite as a function of pretreatment temperature.

Kim et al.[19] studied the transesterification of triacetin and tributyrin with methanol over rehydrated hydrotalcites followed by thermal treatment. They found that when increasing pretreatment temperature until 300 °C, the activity decreased, however, with further increase of the temperature, the activity then increased. The authors proposed that at low pretreatment temperature, water participates to the formation of OH^- basic sites on the rehydrated

hydrotalcites (HT-reh), which were more active than O^{2-} basic sites. On the other hand, the pretreatment at high temperatures above 300 °C effectively removed the water and carbon dioxide contained in the HT-reh, producing strong basic sites on their surface.

Xi et al.[20] also used thermally-decomposed and rehydrated Mg-Al hydrotalcites (HT-d-r) to catalyze the transesterification of tributyrin with methanol. They performed the pretreatment at various temperature to remove water in HT-d-r sample. Removing the physisorbed molecular water of HT-d-r by heating to 60 °C for 1 h did not significantly alter the catalytic activity. However, upon removal of interlayer water at temperatures above 60 °C, the catalytic activity decreased substantially. Heating HT-d-r to 200 °C apparently removed all the interlayer water and resulted in a significant loss of basicity, as illustrated by the very poor catalytic activity of this sample. Again, authors ascribed the role of water to the formation of OH^- base sites as charge-balancing anions. In the transesterfication of ethyl acetate with methanol on magnesium silicate hydrate, we also observed that the conversion decreases with the increase of the pretreatment temperature to 140 °C[21]. However for laponite, the thermal pretreatment below 200 °C has little effect on the activity, and from 200 to 500 °C the reactivity behaviors are opposite to the rehydrated hydrotalcites[19]. On the reverse, the activity trend as a function of pretreatment temperature is similar to that of MgO[22]. Cornu et al.[22] reported that in the transesterification of ethyl acetate with methanol on MgO with natural surface, at low pretreatment temperature, the conversion increased with an increase in pretreatment temperature, while at high temperature, the conversion decreased. A link between basicity and activity was found.

In order to understand what occurs during the thermal treatment that could influence the activity of laponite, thermogravimetric analysis (TGA) is performed as shown in Figure 4.21 and Figure 4.22. TGA curves (Figure 4.21) present three weight losses in the range of 50-200 °C, 200-650 °C and 650-800 °C. The first weight loss, occurring below 200 °C can be attributed to the removal of water[23]. The water can be removed sharply, which is associated to an endothermic phenomenon (Figure 4.22). The weight loss between 200 and 650 °C corresponds to dehydroxylation. The dehydroxylation occurs slowly and is accompanied by an exothermic phenomenon as a broad heat flow peak appears between 200 and 650 °C (Figure 4.22). The last weight loss is observed in the 650–800 °C temperature range which corresponds to the phase transition from laponite to enstatite[24].

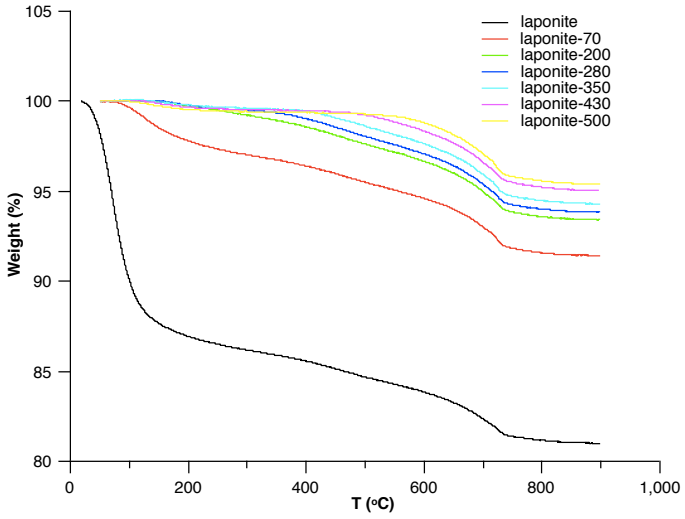

Figure 4.21: Thermogravimetric analysis (TGA) for laponite and laponite-X.

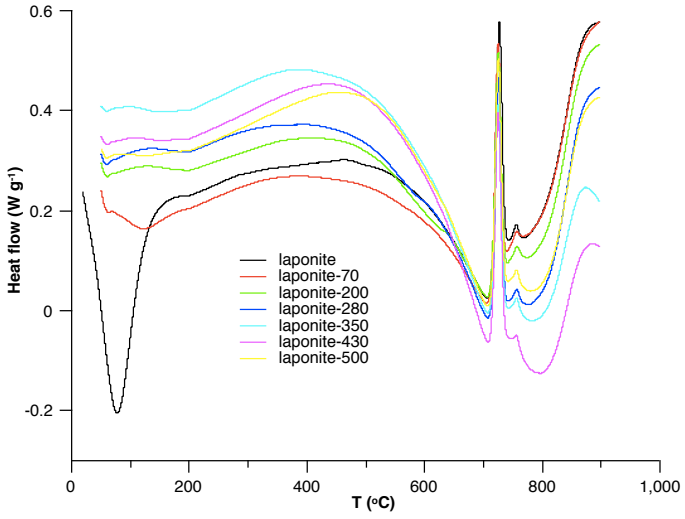

Figure 4.22: Heat flow for laponite and laponite-X by thermogravimetric analysis.

The weight loss for different pretreatment temperature of laponite and laponite-X are listed in Table 4.6. It can be seen that the weight loss of laponite mainly consistes of removal of water, *i.e.* 13.1%. Only 4.2% of weigh loss occurs during dehydroxylation. In the laponite-350, it is noted that the weight loss linked to dehydroxylation decrease to 2.8%. It means that the pretreatment at 350 °C leads to release the 1.4% of weight due to dehydroxylation. For all the samples, the weight loss between 650 and 800 is stable at around 2.5%. Compared with catalytic performance, we find that the quite significant variation of conversion does not occur for the important loss weight under 200°C, attributed to the loss of physisorbed water, but when the dehydroxylation happens.

Table 4.6: TGA measurements for laponite and laponite-X.

Catalyst	**Weight loss (%)**		
	50-200 °C[a]	**200-650 °C[b]**	**650-800 °C[c]**
laponite	13.1	4.2	2.4
laponite-70	2.2	3.9	2.5
laponite-200	0.3	3.8	2.4
laponite-280	0.2	3.4	2.4
laponite-350	0.2	2.8	2.5
laponite-430	0.3	2.0	2.5
laponite-500	0.5	1.4	2.6

[a] weight loss/mass of catalyst

[b, c] weight loss/pure mass, pure mass = mass of catalyst x (100% – weight loss below 200 °C)

Rehydration experiments are performed in a water saturated atmosphere in a dessicator on the sample of laponite-350 and the results in terms of AcOEt conversion and the TGA are shown in Table 4.7. 16 minutes exposure is enough to fully recover the global water content (50-200 °C) of the sample laponite. However, the weight loss from dehydroxylation (200-650 °C) is not fully recover, and the conversion remains 65.1%. The sample laponite-350 is then put in water saturated atmosphere for 42 days. It is shown that the weight loss from dehydroxylation succeeds to be fully recovered. Meanwhile, the conversion decreases to 53.6%, that is close to the conversion of initial laponite. It is noted that the laponite adsorbs a large amount of water (46.4%) after long time rehydration. In order to desorb this physically adsorbed water, the sample is dried in oven at 60 °C for one night. The sample lapoinite-350-R42d-dry shows the similar weight loss than laponite in the three ranges of temperature 50-200, 200-650 and 650-800 °C. It is interesting to note that the activity of laponite-350-R42d-dry is close to that of laponite and laponite-R42d, which again confirm that the influence of physically adsorbed water is not important. In order to check the stability of the material during these thermal pretreatment, nitrogen sorption analysis and X-ray diffraction are performed.

Table 4.7: TGA measurements and catalytic performances of rehydration samples.

Catalyst[a]	Weight loss (%)			AcOEt Conv. (%)
	50-200 °C	200-650 °C	650-800 °C	
laponite	13.1	4.2	2.4	48.8
laponite-350	0.2	2.8	2.5	66.4
laponite-350-R16m	12.9	3.5	2.5	65.1
laponite-350-R42d	46.4	4.2	2.6	53.6
laponite-350-R42d-dry	14.1	4.0	2.5	50.4

[a] As these samples have importantly different amount water, we weight different mass of catalyst for reaction test to make sure the pure mass (excluding water) of all samples are similar (around 13 mg). The rehydrated samples were noted as laponite-350-Rtu, t is the time of rehydration, u is the unit of time (m is min, h is hour, d is day).

4.6.2. Characterisation of laponite after pretreatment at different temperatures

4.6.2.1 Nitrogen sorption analysis

Nitrogen sorption measurements are performed to examine the porous nature of the laponite and laponite-X (before measurement, the samples are degassed at 60 ^{o}C for 22.5 h). Figure 4.23 and Figure 4.24 show the N_2 adsorption-desorption isotherm and the pore-size distribution of the samples, respectively. Isotherms of the laponite are identified as type IV with a H_2 hysteresis, which is characteristic of ink-bottle-like pores. After 350 °C pretreatment, as can be seen in Figure 4.23, the laponite-350 keeps the similar N_2 adsorption-desorption isotherm curve compared to laponite, while the adsorbed volume of laponite-500 decreases obviously. The BET specific surface areas of laponite and laponite-350 were determined and no significant difference was found (357 and 326 m^2 g^{-1} respectively), while that of laponite-500 decreases to 267 m^2 g^{-1} (Table 4.8). A similar phenomenon is also observed in pore volume. In addition, for all samples, the same narrow pore size distribution, derived from desorption data and calculated from the isotherm using the BJH model, was observed with an average pore diameter of 3.7 nm (Figure 4.24). In conclusion, from the BET gas sorption measurements, we can conclude that the 350 °C thermal pretreatment does not lead to the alteration of porous nature, but it is not the case with a treatment at 500 °C.

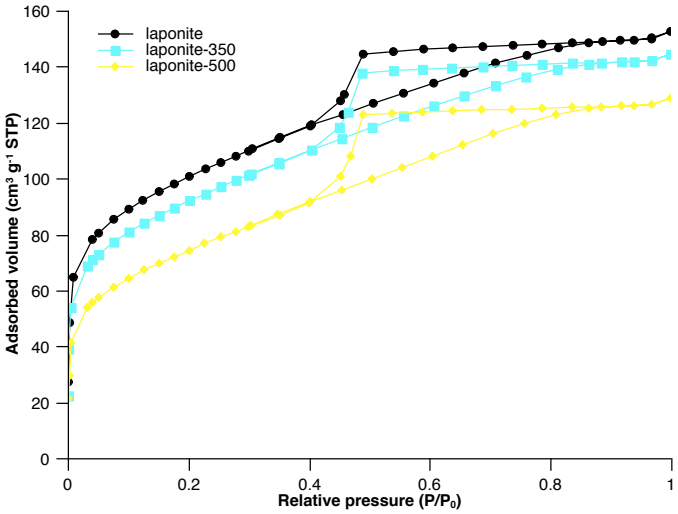

Figure 4.23: N_2 adsorption-desorption isotherms patterns of laponite and laponite-X.

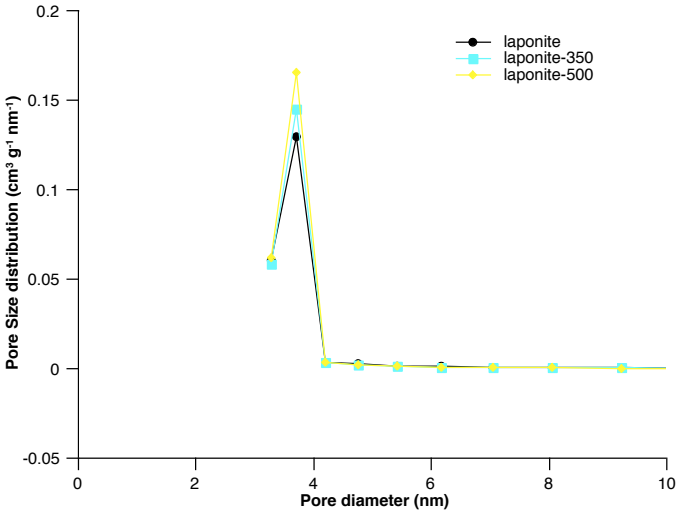

Figure 4.24: BJH pore size distributions for laponite and laponite-X.

Table 4.8: Specific surface area and pore volume of phyllosilicates.

Sample	**laponite**	**laponite-350**	**laponite-500**
Specific surface area (m^2 g^{-1})	357	326	267
Pore volume (cm^3 g^{-1})	0.23	0.22	0.19

4.6.2.2 X-ray diffraction analysis

XRD patterns of laponite and laponite-X are shown in Figure 4.25. They fit with the profiles of PDF 00-009-0031 which was identified as hectorite[11], but exhibits a somewhat broader XRD pattern to indicate low crystallinity and small particle size. From these XRD patterns, it is evidenced that the structure of laponite is not altered by thermal treatment.

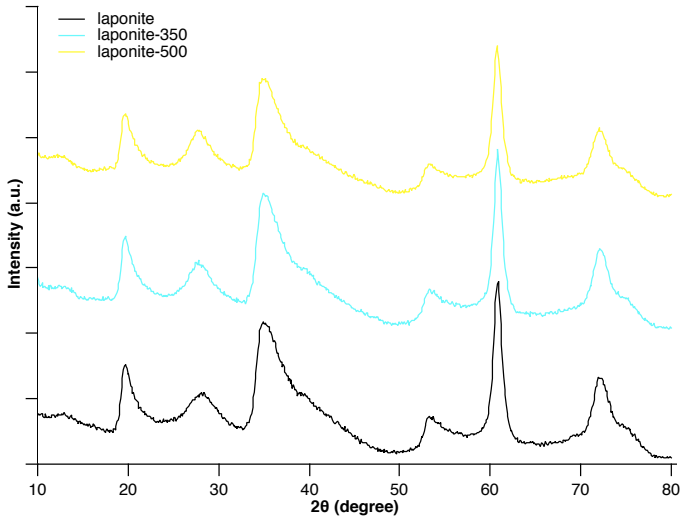

Figure 4.25: XRD patterns of laponite and laponite-X.

In conclusion, the thermal treatment has no effect on the crystalline structure of laponite. However, high temperature treatment leads to a decrease of specific surface area, which may explain that the activity decreases at high temperature treatment. The treatment at moderate temperature causes the dehydroxylation on the surface of laponite, which corresponds to the high activity. In order to know in detail the change on the surface, some other characterisation such as ^{1}H NMR, Infrared Spectroscopy with CO adsorption will have to be performed in the further studies.

4.7. Conclusion

In this chapter, we studied the transesterification of ethyl acetate with methanol on a series of phyllosilicates. The natural phyllosilicates such as montmorillonite and talc have no activity. Thanks to the preparation methods, talc and laponite with nano particle sizes are successfully synthesized and exhibit outstanding activity. XRD patterns give an evidence that nano talc and laponite have smaller crystallite sizes than talc. The results of N_2 sorption analysis fit well with the XRD results showing that nano talc and laponite have larger specific surface

area than that of talc. An interesting result is observed that a small part of laponite can form colloids in methanol, which is highly active. This highly active phase consists of small laponite particles and carbonates. The main role of the carbonate crystalline phase on the high activity is excluded and so the small particles with abounding OH are again confirmed to play a key role.

The kinetic study of transesterification reaction on laponite was performed and the reaction order in ethyl actate is 0.97 at low concentration. This result indicates that the transesterification reaction on laponite with mainly basic property obeys to the Eley-Rideal mechanism, which is contrast to the MSH with acido-basic properties that obey to the Langmuir-Hinshelwood mechanism. The role of thermal treatment on the reactivity of laponite is investigated and it is completely different from that of MSH. The conversion of ethyl acetate increases with the increase of treatment temperature from 200 to 350 ^{o}C. In case of MSH, water participates to acid sites formation and has a positive effect. Whereas, on laponite, it has a typical base catalyst behaviour, so water dissociation, like on MgO poisons the reactivity.

References

[1] S. Mukherjee, in *Sci. Clays*, Springer Netherlands, **2013**, pp. 23–32.

[2] S. Mukherjee, in *Sci. Clays*, Springer Netherlands, **2013**, pp. 3–22.

[3] S. Mukherjee, in *Sci. Clays*, Springer Netherlands, **2013**, pp. 33–45.

[4] L. P. Ramos, C. S. Cordeiro, M. A. F. Cesar-Oliveira, F. Wypych, S. Nakagaki, in *Bioenergy Res. Adv. Appl.*, Elsevier, **2014**, pp. 255–276.

[5] J. W. Gruner, *Z. Für Krist. - Cryst. Mater.* **1932**, *83*, 75–88.

[6] J. Breu, W. Seidl, A. Stoll, *Z. Für Anorg. Allg. Chem.* **2003**, *629*, 503–515.

[7] J. E. Post, D. L. Bish, P. J. Heaney, *Am. Mineral.* **2007**, *92*, 91–97.

[8] C. Le Roux, F. Martin, P. Micoud, A. Dumas, *Process for Preparing a Composition Comprising Synthetic Mineral Particles and Composition*, **2012**.

[9] J. W. Gruner, *Z. Für Krist. - Cryst. Mater.* **1934**, *88*, 412–419.

[10] I. S. Stemple, G. W. Brindley, *J. Am. Ceram. Soc.* **1960**, *43*, 34–42.

[11] G. Nagelschmidt, *Mineral. Mag.* **1938**, *25*, 140–155.

[12] P. Scherrer, in *Kolloidchem. Ein Lehrb.*, Springer Berlin Heidelberg, **1912**, pp. 387–409.

[13] A. L. Patterson, *Phys. Rev.* **1939**, *56*, 978–982.

[14] F. Dellisanti, G. Valdre, M. Mondonico, *Appl. Clay Sci.* **2009**, *42*, 398–404.

[15] M. Thommes, K. Kaneko, A. V. Neimark, J. P. Olivier, F. Rodriguez-Reinoso, J. Rouquerol, K. S. W. Sing, *Pure Appl. Chem.* **2015**, *87*, DOI 10.1515/pac-2014-1117.

[16] A. F. Zanette, R. A. Barella, S. B. C. Pergher, H. Treichel, D. Oliveira, M. A. Mazutti, E. A. Silva, J. V. Oliveira, *Renew. Energy* **2011**, *36*, 726–731.

[17] R. Ratti, S. Kaur, M. Vaultier, V. Singh, *Catal. Commun.* **2010**, *11*, 503–507.

[18] T. F. Dossin, M.-F. Reyniers, G. B. Marin, *Appl. Catal. B Environ.* **2006**, *62*, 35–45.

[19] M. J. Kim, S. M. Park, D. R. Chang, G. Seo, *Fuel Process. Technol.* **2010**, *91*, 618–624.

[20] Y. Xi, R. Davis, *J. Catal.* **2008**, *254*, 190–197.

[21] L. Lin, D. Cornu, M. Mounir Daou, C. Domingos, V. Herledan, J.-M. Krafft, G. Laugel, Y. Millot, H. Lauron-Pernot, *ChemCatChem* **2017**, *9*, 2399–2407.

[22] D. Cornu, H. Guesmi, G. Laugel, J.-M. Krafft, H. Lauron-Pernot, *Phys Chem Chem Phys* **2015**, *17*, 14168–14176.

[23] D. Nied, K. Enemark-Rasmussen, E. L'Hopital, J. Skibsted, B. Lothenbach, *Cem. Concr. Res.* **2016**, *79*, 323–332.

[24] L. Bippus, M. Jaber, B. Lebeau, *New J. Chem.* **2009**, *33*, 1116.

General Conclusion and Outlook

This thesis allowed us to deepen our knowledge of transesterification reaction on magnesium silicate based catalyst, by revealing the active phase, establishing the link between the acido-basic properties of a surface and its reactivity, and by studying the kinetics. The study focus on two typical kinds of magnesium silicate based catalysts, amorphous magnesium silicates such as Magnesol® with acido-basic sites and defective structure, and phyllosilicates such as laponite with mainly basic sites and crystalline structure. Key parameters influencing the catalytic reactivity of the two kinds of magnesium silicate were investigated. Moreover, different reaction mechanisms were proposed for the two catalysts based on the kinetic study and the role of thermal treatment on the reactivity were compared.

To study the key parameters of the reactivity of magnesium silicates, two magnesium silicates were synthesized by coprecipitation and sol-gel methods, then their catalytic performances were compared to the commercial magnesium silicate, i.e. Magnesol®. Coprecipitated magnesium silicate and the commercial catalyst Magnesol® were found very active in transesterification of ethyl acetate with methanol. It was demonstrated by ^{29}Si and ^{25}Mg-NMR, IR, X-ray fluorescence and X-ray photoelectron spectroscopies, together with XRD, that a magnesium silicate hydrate structure (MSH) is formed at the surface of the most active silicates, which appears to be structurally close to the talc but with defective silicate layers. This phase with acido-basic properties characterized by MBOH conversion, is able to activate together the alcohol (over base sites) and the ester (over acid sites). To go further, kinetic study was performed and the results are highly in agreement with the Langmuir-Hinshelwood mechanism considering the reaction between adsorbed methanol and adsorbed ethyl acetate on different kinds of sites as rate determining step. The reactivities of esters and alcohols vary with the carbon chain length confirm that transesterification reaction occurs between adsorbed reactants on the bifunctional catalysts.

Since the active MSH phase is highly hydroxylated, the role of adsorbed water on activity of the catalysts was further investigated. With the pretreatment temperature increasing and therefore water gradually removing from the catalyst, a decrease in conversion was observed. Calorimetry, *in situ* DRIFT spectroscopy, FTIR with CO adsorption, and ^{1}H NMR indicated the existence of two kinds of sites, that are the mild and strong Brønsted acid sites, created from the water coordinated to magnesium located on the edge of the clay-like particles

or in the defects located in the silicate layer. A link between the mild Brønsted acid sites formation and catalytic performance in transesterification reaction was established. The role of the mild Brønsted acid sites could be to stabilise methanol deprotonated by basic Mg-OH groups, activate ester or help the departure of the alkoxyl moiety.

Work is on-going to extend to phyllosilicates with similar but more ordered structures compared to MSH. These more ordered structures have little defects. However, thanks to the XRD and N_2 sorption analysis, we found that nano talc and laponite have small particle size and high specific surface area, and show promising activities. A novel phenomenon was observed that a small part of laponite can form colloid in methanol, of which the particle size is rather small and the activity for transesterification is very high. Thus, it is concluded that the edges of layer particles with abounding OH are a key parameter for the reactivity of phyllosilicates on transesterification reaction. Again, the kinetic study of transesterification reaction on laponite was performed. Based on the kinetic results and and considering the mainly basic property of laponite characterized by MBOH conversion, we proposed that the transesterification on laponite obeys to the Eley-Rideal mechanism assuming the reaction between adsorbed methanol and ethyl acetate in liquid as rate determining step. In agreement with the different reaction mechanisms on MSH and laponite, the role of thermal treatment on the reactivity is shown to be different: the conversion of ethyl acetate on laponite increases with the increase of treatment temperature from 200 to 350 ^{o}C. We saw that a Langmuir-Hinshelwood mechanism was occurring on MSH involving adsorption of ester on acid sites that are created by water adsorption. Thus desorption of water decreases the activity. On the reverse, an Eley-Rideal mechanism was obtained on laponite involving methanol adsorption on base sites, thus the water dissociation, like on MgO can poison the active sites.

Compared to the two distinct magnesium silicates, we can have a comprehensively understanding on the catalytic behaviours of relative catalysts. Firstly, based on our study, it can be understood that the magnesium silicate with weak basic properties exhibits high activity, as the acid sites work together with base sites on magnesium silicate that can improve the conversion. The role and the formation of acid sites was systematically clarified as involving in the adsorption of water. Laponite possesses mainly base sites and is highly active, more than MgO. It can be explained by the role of size particles that the edges with abounding OH contribute significantly to the activity. In conclusion, the link between acido-basic properties and reactivity for transesterification reaction, in some case considering other parameters such

as particle size, is well established. Moreover, the reaction mechanism on the two distinct catalysts were proposed and correspondingly, the active sites were revealed.

It has been reported that the properties of magnesium silicate synthesized by coprecipitation method can be varied depending on the preparation conditions[1,2]. For example, different feeding order can lead to different mole ratio of Mg/Si in magnesium silicate[1]. As the concentration of silicate species is highly dependent on the pH[3], the addition of NaOH into sodium silicate solution has effects on the chemical composition and particle size of MSH[2]. For the future work, the magnesium silicate could be synthesized at various conditions and the influence on catalytic performance for transesterification reaction should be studied.

In addition, the fundamentally study on this thesis, allows us to transfer the objective from model reaction to valuable molecules such as γ-valerolactone or triglycerides, where the chain length is changed. Although the influence of chain length has been studied on MSH, it would be interesting to be developed on laponite in the future work.

Moreover, the phyllosilicates are tunable materials, of which the surface properties can be easily modified. For example, the hydrophobicity can be modified by the loads of the sheet and the nature of the interlayer cation[4,5]. The nature of the anionic groups can also be modified by substituting the hydroxyl groups with fluorides[6]. Upon such modifications, the catalytic performance for transesterification reaction could be studied to go further in the identification of the parameters that can be adjusted to the nature of the reactant.

References

[1] F. Ciesielczyk, A. Krysztafkiewicz, T. Jesionowski, *J. Mater. Sci.* **2007**, *42*, 3831–3840.

[2] A. Krysztafkiewicz, L. K. Lipska, F. Ciesielczyk, T. Jesionowski, *Adv. Powder Technol.* **2004**, *15*, 549–565.

[3] Ulrich Schlottmann, *UNEP Publ.* **2004**, 11–13.

[4] B. Dazas, B. Lanson, A. Delville, J.-L. Robert, S. Komarneni, L. J. Michot, E. Ferrage, *J. Phys. Chem. C* **2015**, *119*, 4158–4172.

[5] E. S. Boek, P. V. Coveney, N. T. Skipper, *J. Am. Chem. Soc.* **1995**, *117*, 12608–12617.

[6] M. Jaber, S. Komarneni, C.-H. Zhou, in *Dev. Clay Sci.*, Elsevier, **2013**, pp. 223–241.

Appendices

Appendix I. Transesterification reaction

A certain amount of the catalyst was introduced in a Schlenk flask. Vacuum was then performed in the Schlenk through a vacuum manifold (10^{-3} Torr). Then nitrogen (Air liquide 99.99%) was introduced into the Schlenk (1 bar). Methanol (10 mL, Sigma Aldrich anhydrous 99.8%) as well as 1,4 dioxane (1 mL, Sigma Aldrich anhydrous 99.8%), as standard reference, were introduced through needles into the Schlenk. Then it was heated in an oil bath at 70 °C. With this kind of configuration, the temperature of the liquid phase inside the schlenk was kept at 60 °C. The introduction of ethyl acetate (AcOEt, 1 mL, Sigma Aldrich anhydrous 99.8%) determines the initial time of the reaction (t = 0 h). The molar ratio between the reactants was kept at 24.25. The ratios AcOEt/dioxane was checked at the beginning (t = 0 h) and after 5 hours of reaction (t = 5 h) by gas chromatography (Perichrom PR2100 equipped with a FID detector and a CP WAX 57 CB column. The parameters of gas chromatography was as follow: temperature of oven, 60 ^{o}C; carrier, N_2, 100 kPa; temperature of detector, 260 ^{o}C; temperature of injector, 200 ^{o}C). To perform these analyses a few drops of the reaction mixture were drawn from the Schlenk and diluted in 2 mL of 1-propanol (Sigma Aldrich, ACS reagent). The only detected products were methyl acetate and ethanol.

Appendix II. Acido-basic properties study: MBOH conversion

The MBOH conversion test is carried out in gas phase at atmospheric pressure, with gas chromatographic analysis. Figure 1 shows the experimental setup used.

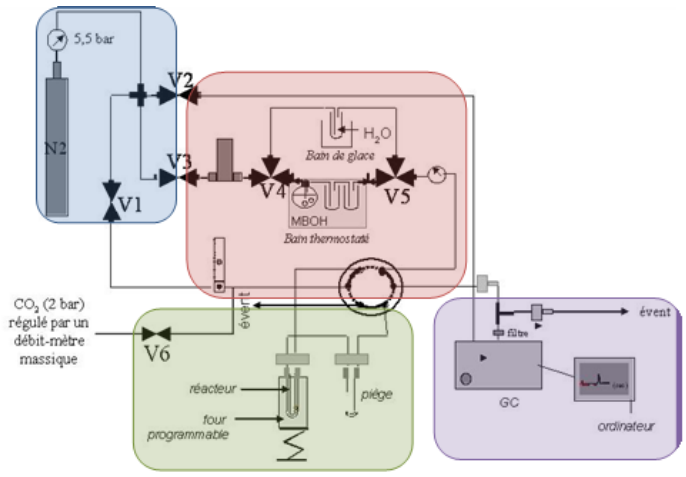

Figure 1: Apparatus for the MBOH test

It consists of a thermal pretreatment circuit and a reaction circuit, made in 1/8" diameter stainless steel tube. Four zones can be distinguished in these circuits:

- In blue: The gas supply area supplies the entire system. Nitrogen (Nitrogen U, purity> 99.99%, Air Liquide) is used both as a pretreatment gas, reagent diluent and eluent for chromatographic analysis.

- In red: The gas distribution zone supplies the sample pretreatment circuit and the feedback circuit through which the MBOH is routed to the sample. The pretreatment gas and diluent of the MBOH are delivered by a ball flow meter and a mass flow meter, respectively. At the outlet of the flow meter, the gas from the reaction path is sent to a saturator, immersed in a cryostat, containing the MBOH stored at a temperature of 293 K, *i.e.* with a saturating vapor pressure of 1.73 kPa. A six-way valve then connects either the pretreatment circuit, or the reaction circuit, to the reactor containing the sample to be tested.

- In green: The reaction zone consists of a U-shaped quartz reactor equipped with a sintered porosity 1 and 10 mm in diameter, on which the catalyst sample is deposited. The reactor is installed so that the gas passes through the sample.

- In purple: The analysis zone detects the gases leaving the reactor during the reaction. The analysis of the products is carried out every 9 minutes by a Perichrom PR2100 gas chromatograph equipped with a tetracyanoethyl pentaerythyrol column on chromosorb P and a FID detector. The chromatography column is maintained at 120 ° C.

The MBOH tests were performed in this apparatus: 40 mg of catalyst are introduced for each measurement. The heat treatments are carried out in a vertical tubular furnace under a flow of nitrogen at 20 mL min^{-1} at 350 ^{o}C. The reactant feed was composed of MBOH diluted by bubbling nitrogen (50 mL min^{-1} through a Brooks gas mass flow controller) in liquid MBOH maintained at 20 ^{o}C. The diluted MBOH flow (partial pressure of 1.73 kPa) was then allowed to pass through the catalyst. Reaction temperature was set to 160 ^{o}C

Appendix III. X-ray Diffraction (XRD)

X-ray diffraction involves measuring the diffraction angles of an incident beam of X-rays by the crystalline planes, which act as a lattice. The interferences between rays diffracted by neighbouring lattice planes are constructive if the difference of step which characterizes

them is worth a whole number of times the wavelength λ of the monochromatic incident beam[1]. The Bragg relation $2d_{hkl}\sin\theta = n\lambda$ is then verified (n is the order of the diffraction (number integer), d_{hkl} is the inter-reticular distance between the planes (hkl) diffracting the incident wave, and the diffraction angle). During the measurement, λ is kept constant, so that varying the diffraction angle makes it possible to measure inter-reticular distances.

The powder analysis method involves placing a polycrystalline sample in the monochromatic X-ray beam. In this case, there are always crystallites whose orientation obeys the Bragg's law for a plane (hkl), at the origin of a series of diffraction cones. The diffracted intensity is collected in a plane containing the incident ray, and the maxima observed are characteristic of the crystal structure.

The diffractograms are recorded on a diffractometer (D8 Bruker) with Cu-Kα radiation (1.5418 Å; 30 kV and 30 mA) and a Ni filter from 2θ of 10.0° to 80.0° (step size 0.02°). The powder after grinding is flattened in the central cavity of a pyrex disc. Crystalline phase identification was based on comparison with standard powder XRD files published by the International Center for Diffraction Data (ICDD).

Appendix IV. X-ray spectroscopies

i. X-ray Fluorescence spectroscopy (XRF)

The Mg/Si ratios of the materials were determined using a SPECTRO XEPOS spectrometer equipped with a 50-Watt end-window X-ray tube to excite the samples. The detection system consists of a 10 mm^2 Si-drift detector (SDD) with Peltier cooling and a spectral resolution of less than 155 eV at Mn Kα is achieved. Measurements were conducted in a He gas atmosphere.

ii. X-ray Photoelectron Spectroscopy (XPS)

The principle of XPS consists in analysing, the kinetic energy of the electrons resulting from the ionization of the elements of a solid irradiated by a monochromatic X-ray beam. The measurement of the kinetic energy Ec of the photoelectrons and the knowledge of the irradiation energy hν makes it possible to go back directly to the energy of binding of the electrons by the energy conservation relation. This technique therefore gives direct access to the electronic structure of the various constitutive elements of the material.

The low mean free path values of the photoelectrons in the solids make XPS a surface analysis technique. In the range of kinetic energy used (less than 1400 eV), the information obtained comes from a thickness of material well below 10 nm. This technique mainly informs on the relative proportions of the elements present in the first atomic layers and on their oxidation state.

XPS analysis were performed using a PHOIBOS 100 X-ray photoelectron spectrometer from SPECS GmbH (Berlin, Germany) with a monochromated Al Kα X-ray source (hν = 1486.6 eV) operating at P = 1 × 10−10 Torr or less. Spectra were obtained with a 50 eV pass energy for the survey scan and 10 eV pass energy for the C1s, O1s, Si2p, and Mg2p regions. Auger peaks were recorded during XPS data acquisition and the Auger parameters were then calculated with respect to the kinetic energy of the X-ray source. Element peak intensities were corrected by Scofield factors. The spectra were fitted using Casa XPS v.2.3.15 Software (Casa Software Ltd.) and applying a Gaussian/Lorentzian ratio G/L equal to 70/30.

Appendix V. Diffuse Reflectance Infrared Fourier Transform Spectroscopy (DRIFTS)

i. Infrared and diffuse reflection

Reflectance spectroscopy is a technique for investigating the spectral composition of radiation reflected by a surface. In the case of an ideally matt surface, this reflection is said to be diffuse (as opposed to specular reflection in the case of polished surfaces). Diffuse reflection can be considered as the result of multiple reflections, refractions and diffractions on a set of particles whose faces are randomly inclined. For isolated particles whose size is of the same order of magnitude as the wavelength, a diffusion of light takes place, the distribution of which follows for spherical particles the theory of Mie dispersion.

The absolute diffuse reflectance is defined for a single crystal as Eq. 1:

$$R_\infty = \frac{J}{I_0} \qquad \text{Eq. 1}$$

Where I_0 is the incident intensity and J is the intensity diffused in all directions of space.

The theory of Kubelka-Munk[2] is the simplified theory of the most general diffuse reflection in the case of powders. Assuming an isotropic distribution of light scattering, the

absence of any specular reflection, the random distribution of particle size (assumed to be very small in comparison with the sample thickness), we can define the Kubelka-Munk function as Eq. 2:

$$f(R_\infty) = \frac{(1 - R_\infty)^2}{2R_\infty} \qquad \text{Eq. 2}$$

Which has the same properties as the absorbance in the case of transmission IR (Beer-Lambert law). A quantitative exploitation of the DRIFTS spectra can then be envisaged.

ii. Experimental implementation

DRIFTS experiment was performed using a Vertex70 Bruker spectrometer with a DRIFTS cell as shown in Figure 2. For the data presented in Chapter 2, the sample compartment of the cell was filled with the as-prepared sample (~20 mg), which was first heated in situ under Ar flow (20 $cm^3.min^{-1}$) up to 140 ^oC (5 $^oC\ min^{-1}$) for 1 h. A first spectrum was taken at this temperature. The sample was then pretreated to 350 ^oC (5 $^oC\ min^{-1}$) for 1 h and then cooled down under Ar to 140 ^oC. The second spectrum was taken after this pretreatment. For the data presented in Chapter 3, the sample compartment of the cell was filled with the as-prepared sample (~20 mg), which was first heated *in situ* under Ar flow (20 $cm^3.min^{-1}$) up to 50 °C (5 °C min^{-1}) for 2 h. A first spectrum was taken at this temperature. The sample was then pretreated at 70 °C (5 °C min^{-1}) for 2 h and then the second spectrum was taken at 70 °C. The spectra of samples pretreatment at 90, 110 and 140 °C respectively, were then taken in the same way. All spectra are recorded *in situ* and were converted into Kubelka–Munk units after subtraction of the spectrum recorded on the dehydrated KBr sample (Fluka, purity > 99.5%).

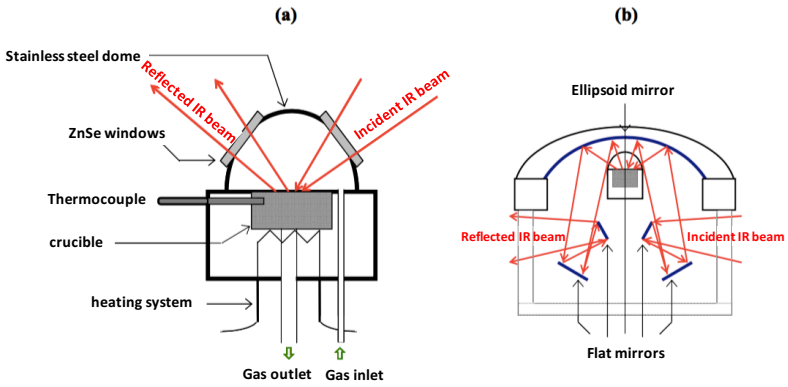

Figure 2: DRIFTS measuring cell: (a) stainless steel cell and crucible sample holder; (B) a cavity in which the cell is included, enabling the sample to be irradiated and the scattered signal to be collected.

Appendix VI. Fourier Transform Infrared spectroscopy (FTIR) measurement of adsorbed CO

FTIR spectra of adsorbed CO were collected on a Bruker Vertex 70 spectrometer using a MCT detector (resolution 2 cm^{-1}, 64 scans per spectrum). The assembly is consisting of three parts: evacuation and gas system, IR measuring cell, and the spectrometer (Figure 3). The IR measuring cell as shown in Figure 4, allows one to raise or lower the sample vertically between the two sections of the cell: the upper oven section in which thermal treatment takes place and the lower section equipped with a perpendicular body mounted with CaF_2 windows, cooled to liquid nitrogen temperature, where measurements are made.

The sample was pressed into self-supported wafers of 21.1 mg, diameter 16 mm. The wafer was first heated *in situ* at 70, 90, 140 and 350 °C, respectively, for 2 h under a flow of Ar (20 mL min^{-1}), before being evacuated (5 x 10^{-6} Torr) for 1 h. The wafer was then moved to the lower part of the cell, which was cooled down to temperature of liquid nitrogen. CO was successively added (up to 1 Torr of CO). The difference spectra were obtained by subtracting the spectra of the pretreated sample (before increments of CO) recorded at the liquid nitrogen temperature from those recorded after successive increments of CO.

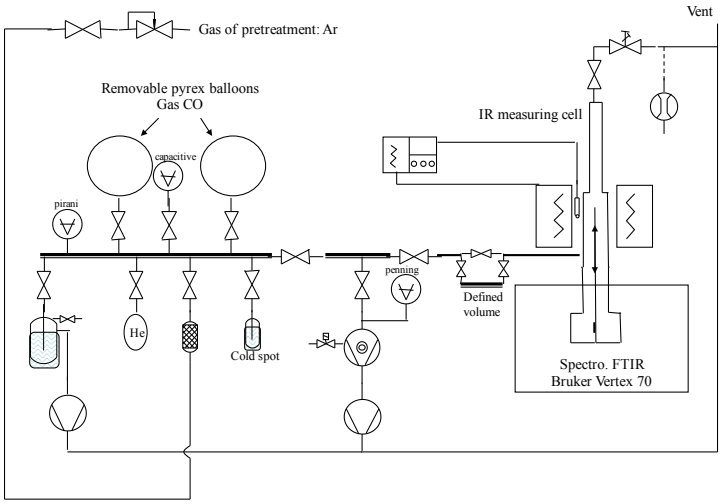

Figure 3: Assembly for transmission FTIR measurement of adsorbed CO.

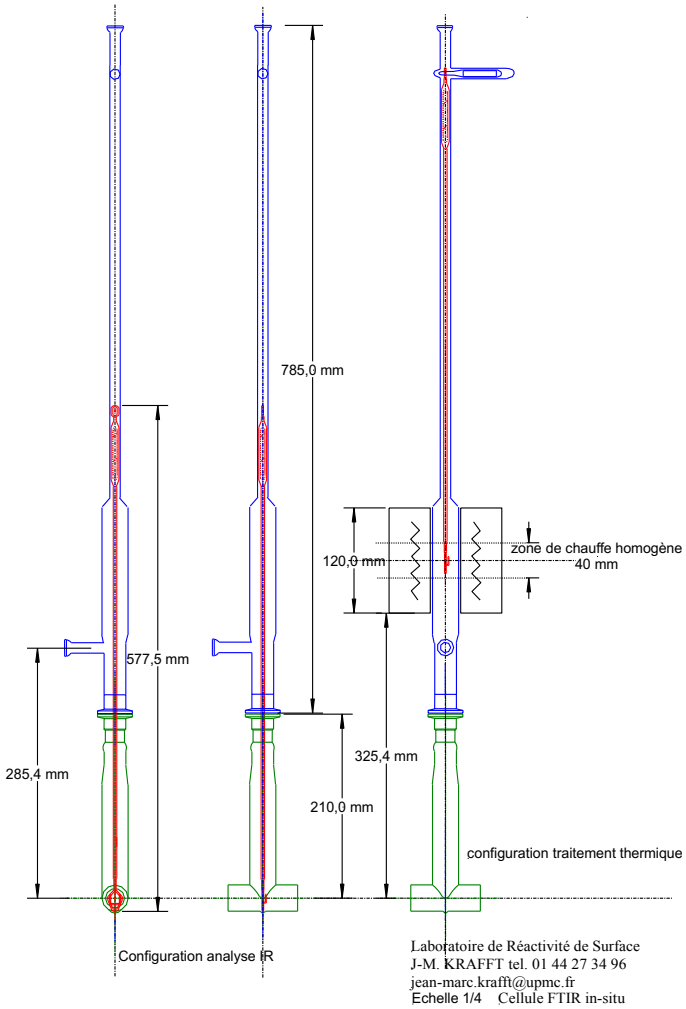

Figure 4: *In situ* infrared cell for Transmission FTIR measurement of adsorbed CO.

Appendix VII. Measurement of specific surfaces

i. Principle

The description of the adsorption isotherms in the case of multilayer formation was carried out by Brunauer, Emmett and Teller. In the hypothesis of surface sites all equivalent (same force for interaction) and adsorption in multilayers according to a process similar to that of gas condensation, the writing of equality of velocities of adsorption and desorption makes it possible to arrive at the linearized form of the BET equation (Eq. 3):

$$\frac{P}{q(P^* - P)} = \frac{1}{q_m C} + \frac{C-1}{q_m C}\frac{P}{P^*} \qquad \text{Eq. 3}$$

Where P^* is the saturating vapour pressure of the gas, C is a characteristic constant of the adsorption and condensation equilibria, q is the quantity of adsorbed gas and q_m is quantity necessary for the formation of a monolayer. These constants can be determined by the linear regression of the equation BET, by varying the pressure P. If the adsorbed gas molecule occupies the area s on the surface, the area A of the solid (m^2) is deduced by Eq. 4:

$$A = q_m N_A s \qquad \text{Eq. 4}$$

Here N_A is the Avogadro constant.

The method of Barrett, Joyner, and Halenda is a procedure for calculating pore size distributions from experimental isotherms using the Kelvin model of pore filling. It applies only to the mesopore and small macropore size range.

ii. Procedure

N_2 adsorption–desorption isotherms were obtained at 77 K on a Micromeritics ASAP 2020 instrument. Prior to measurement, the samples were degassed under vacuum at a certain temperature (the normal temperature is 300 ^oC, otherwise it is presented with the measurement results). The Brunauer–Emmett–Teller (BET) surface areas were calculated from the BET equation for a relative pressure (P/P_0) range between 0.05 and 0.25.

Appendix VIII. Thermogravimetric analysis

Thermogravimetric analysis were carried out on a STD Q600 apparatus from TA® instruments under 20 mL min^{-1} of N_2 with a ramp rate of 5 °C min^{-1} up to 400 °C or 900 °C.

Appendix IX. Calorimetry

Heat of adsorption measurements were conducted on SETARAM Calvet Calorimeter C80 at 30 °C. 0.15 g of sample was loaded into the sample cell (Membrane Mixing Cell), then a tube with a telfon membrane at the bottom was set up at the top of sample cell, and then 0.38 mmol. of ethyl acetate was added into the tube. After the temperature of sample and the heat energy are stable, the measurement was started by breaking the telfon membrane with a stirrer bar so the sample and ethyl acetate mixed. The stirring rate was kept at 1500 rpm.

Appendix X. Nuclear Magnetic Resonance (NMR) study

^{29}Si MAS NMR spectra were recorded with a Bruker Avance500 spectrometer at 99.4 MHz in 7 mm zirconia rotors. The chemical shifts of silicon were measured by reference to tetramethylsilane (TMS). ^{29}Si DPMAS NMR spectra were obtained at 7 kHz spinning speed, 3 μs excitation pulse and 10 s recycle delay. 3-(trimethylsilyl)-1-propanosulfonic sodium salt was used for setting the Hartmann-Hahn conditions in ^{29}Si CPMAS NMR experiments. The proton π/2 pulse duration, the contact time and recycle delay were 3.1 μs, 5 ms and 5 s, respectively. ^{25}Mg NMR spectra were performed with a Bruker Avance700 spectrometer at 42.8 MHz and with a 5 mm static probe.

For WURST-QCPMG sequence[3], WURST-80 pulse shapes was used with a 45 μs WURST pulse length, a sweep width of 500 kHz and a RF power of 9.5 kHz. The echo delay was set at 0.5 ms and 30 echoes were collected. The spikelet spectrum was obtained by direct Fourier transform of the echo-train. The reconstructed spectrum was produced by Fourier transform of sum of the individual echoes. Chemical shifts of magnesium were measured by reference to $MgCl_2$ (δ = 0 ppm). The simulation of the NMR spectra were performed using the DMFit program[4].

All the ^{1}H MAS NMR spectra were recorded at room temperature using a Bruker Advance spectrometer operating in a static field of 11.7 T. The resonance frequency of ^{1}H were

500.16 MHz. The ^{1}H chemical shifts were referenced to external standards of tetra-methylsilane (TMS). ^{1}H MAS NMR spectra are performed with a 90° pulse duration of 2.8 μs, a recycle delay of 5 s, and a scan number of 32. The MAS equipment for rotation was carefully cleaned with ethanol then dried to avoid spurious proton signals. From two successive experiments performed in the same recording conditions and using the same empty or filled rotor, the probe and rotor signals were subtracted from the total FID.

Appendix XI. Scanning Electron Microscopy (SEM)

SEM images were recorded with a Hitachi SU-70 field emission gun scanning electron microscope. The samples were fixed on an alumina SEM support with a carbon adhesive tape and were observed without metallization. An in-lens secondary electron detector (SE-Upper) was used to characterize our samples. The accelerating voltage was 1 kV, and the working distance was around 4 mm.

References

[1] W. H. Bragg, *J. Chem. Soc. Trans.* **1916**, *109*, 252–269.

[2] P. Kubelka, *JOSA* **1948**, *38*, 448–457.

[3] L. A. O'Dell, R. W. Schurko, *Chem. Phys. Lett.* **2008**, *464*, 97–102.

[4] D. Massiot, F. Fayon, M. Capron, I. King, S. Le Calvé, B. Alonso, J.-O. Durand, B. Bujoli, Z. Gan, G. Hoatson, *Magn. Reson. Chem.* **2002**, *40*, 70–76.

List of Figures

List of Tables